PhD in ENERGY

Dipartimento di Ingegneria

SSD ING-IND/33 Sistemi Elettrici per l'Energia

Innovative Methods and Control Strategies for Frequency Support in Power Systems

PhD Candidate: Antony Vasile

Tutor: Prof. Gaetano Zizzo

PhD Course Coordinator: Prof. Eleonora Riva Sanseverino

Cycle XXXVI

2022/2023

PANORMITANÆ STVDIORVM VNIVERSITATIS SIGILLVM

Table of Contents

List of Figures

List of Tables

Acronyms

AC	Alternate Current
ARERA	Regulatory Authority for Energy, Networks, and Environment (Italy)
aFFR	Automatic Frequency Restoration Reserve
BESS	Battery Energy Storage System
CE	Continental Europe
COP	Conference of Parties
DC	Direct Current
DG	Distributed Generation
DSO	Distribution System Operator
ENTSO-E	European Network of Transmission System Operators for Electricity
EV	Electric Vehicle
EU	European Union
FCR	Frequency Containment Reserve
GFL	Grid Following
GFM	Grid Forming
GHG	Green-House Gases
HV	High Voltage
HVAC	High Voltage Alternate Current
HVDC	High Voltage Direct Current
IEA	International Energy Agency
IGBT	Insulated Gate Bipolar Transistors
LCC	Line Commutated Converter
LCOE	Levelized Cost Of Energy
MV	Medium Voltage
mFFR	Manual Frequency Restoration Reserve
OG	Over Generation
PCC	Point of Common Coupling
PLL	Phased-Lock Loop
RES	Renewable Energy Source

RSE	Ricerca Sistema Energetico
SA	Synchronous Area
SFR	Synchronous Rotation Frame
SI	Synthetic Inertia
SOC	State Of Charge
STATCOM	Static Synchronous Compensator
TL	Tyrrhenian Link
TL-E	Tyrrhenian Link East
TL-W	Tyrrhenian Link West
TSO	Transmission System Operator
TYNDP	Ten Years Network Development Plan
UCTE	Union for the Coordination of Transmission of Electricity
UNFCCC	United Nations Framework Convention on Climate Change
VSC	Voltage Source Converter
VSM	Virtual Synchronous Machine
V1H	Vehicle-to-Home
V2G	Vehicle-to-Grid

Candidate declaration

The undersigned Antony Vasile declares that this thesis submitted for the final examination to obtain the degree of PhD is the product of personal and original work. All sources consulted in the realization of the same are cited in the appropriate "References" section; part of the thesis has been published as scientific articles in journals and conference proceedings; please consult the section "Author's publications list".

Palermo, 01/02/2024 Antony Vasile

Preface

Until about twenty years ago, the electrical system was linear, with generation on one side, consumption on the other. Climate change and the need to decarbonize the energy system have led national governments to increasingly invest in policies that would favour the installation of both utility and small-scale Renewable Energy Sources (RES). This has brought in recent years to a shift in the previous generation/consumption paradigm, putting a severe burden on grid operators whose task of maintaining a safe and reliable grid has remained unchanged. In addition to this, RES power plants undermine grid resiliency as they provide a weak (and sometimes null) contribution to the regulation of the power system. In order to achieve a complete decarbonization, it is essential to integrate renewable sources into the power grid control system through innovative and efficient regulation solutions.

This research work presents the study, implementation and impact evaluation of some control techniques for frequency support. These techniques involve the control of power electronics converters in different scenarios in order to assess the effect of new and innovative regulation solutions on both interconnected systems and weak or isolated grids. The structure of the thesis reflects the intentions of investigation and research on frequency control: Chapter 1 contextualizes the work within the scope of the electric power systems research for the energy transition, briefly analyzing the European regulatory process that promoted the integration of renewable sources into the frequency regulation system. In Chapter 2, the main features of the current frequency regulation system are presented, with particular reference to the entire European synchronous area and to what, in the near future, could be the new regulation services to be included in national network codes. Starting from the third chapter, the original studies conducted on the topic are presented and divided based on a criterion of size and robustness of the analyzed systems: Chapter 3 presents studies conducted on the Continental Europe Synchronous Area, while Chapter 4 covers those related to weak systems and isolated microgrids. Finally, Chapter 5 has been entirely dedicated to the studies conducted on the Sicilian power grid. These studies are a part of a broad-spectrum ongoing project with the main partner

being the Italian research institute "*Ricerca Sistema Energetico*" (RSE) that has been financed by the Research Fund for the Italian Electrical System under the Three-Year Research Plan 2022-2024 (DM MITE n. 337, 15.09.2022), in compliance with the Decree of April 16th, 2018. Given its important strategic position at the centre of the Mediterranean Sea, Sicily arouses great interest among all stakeholders in the power system. In the coming years, it will be involved in new renewable installations and various network enhancement projects. Among the latter, the Tyrrhenian Link project stands out as a flagship development, involving a dual HVDC connection with Sardinia and Campania, utilizing VSC converters. Among the contributions to the research provided by this thesis, it is worth mentioning the simulation of Grid-Forming control of the Tyrrhenian Link converters for frequency support, with highly positive result both in conditions of connection with Continental Europe and during islanded operation.

The theoretical development, the simulation analysis and the implementations were conducted at the Engineering Department of University of Palermo (Italy) from November 2020 to October 2023. A part of the research was carried out in Malta during the six months visiting period at University of Malta, from November 2022 to April 2023. The results demonstrate how the regulating contribution of inverter-based sources will play a crucial role in the future electric power grid, suggesting the urgent need to standardize this contribution in national and international grid codes in order to provide explicit guidelines to manufacturers, producers, grid operators, and investors.

Chapter 1

1. Introduction

In the last decades the urgency of addressing global environmental challenges has become increasingly evident. As humanity deals with issues such as climate change, resource depletion, biodiversity loss, and social inequality, the concept of sustainable development has emerged as a guiding principle for ensuring a harmonious coexistence between human societies and the natural environment. According to the definition proposed in the report "*Our Common Future*" published in 1987 by the World Commission on the Environment and Development (Bruntland Commission) of the United Nations Environment Programme, sustainable development consists in «the satisfaction of the needs of the present generation without compromising the ability of future generations to fulfil their own» [1]. The transition of electrical systems plays a crucial role in achieving sustainable development and clean energy goals. Indeed, the energy production sector is the one with the greatest impact in terms of CO2 emissions: as reported by the International Energy Agency (IEA) in its report "CO_2 Emissions in 2022" [2] , the power sector was responsible for about 42% of global emissions in 2022, with the all-time record of 14.6 Gt and an increase of 1.8% compared with 2021, Figure 1. Despite the constant growth in the last two decades, the installation of new Renewable Energy Source (RES) power plants is of fundamental importance in order to reduce emissions and contain the increase in global average temperature.

To achieve this ambitious goal, national Governments and international organizations are engaging in the promotion of programs and laws aimed at promoting the ecological transition with short-, medium- and long-term objectives. In this scenario, all actors in the power system are involved in the transition process, whether to facilitate the integration of renewables or to ensure efficient but most importantly reliable operation of the grid.

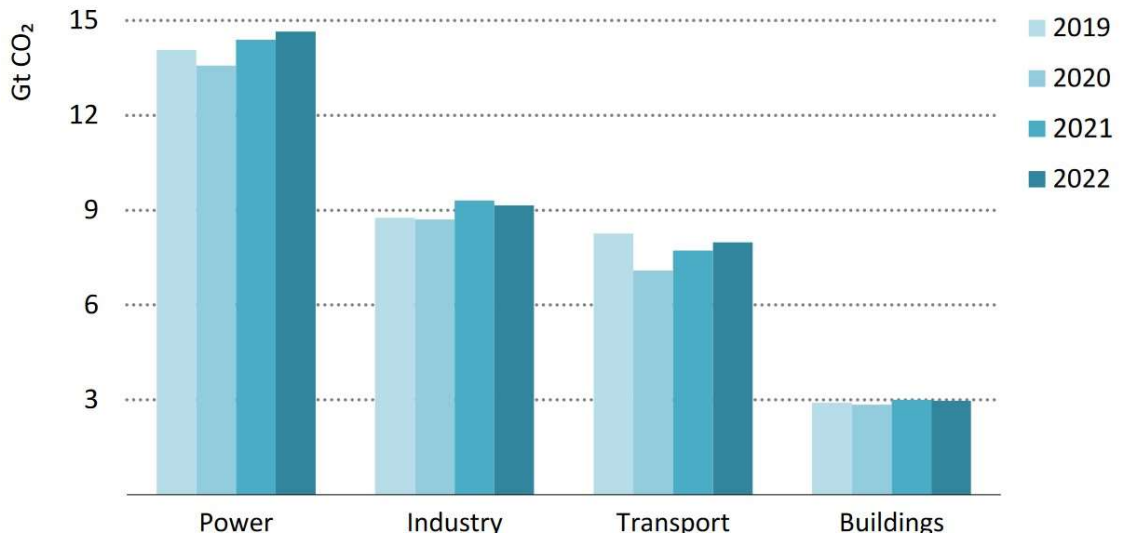

Figure 1. Global CO2 emissions by sector, 2019-2022 [2]

1.1 Policies for Climate Change and RES Integration

The world began to discuss seriously about climate change and interventions to mitigate the anthropic footprint on the planet only starting from the 90s. The first treaty calling on nations to reduce Green-House Gases (GHG) was signed in Rio de Janeiro in 1992 and is known as United Nations Framework Convention on Climate Change (UNFCCC)[3]. Although of a voluntary nature and not binding from a legal point of view, the treaty focused attention on an issue that would become fundamental in the political choices of all the countries of the world in the years to come. The first document binding the signatory countries to an effective reduction of climate-altering emissions was in 1997 with the ratification of the famous Kyoto Protocol [4]. The Protocol imposed two target thresholds, a 5% reduction in emissions compared to 1990 to be achieved between 2008 and 2010, and a further 18% reduction by 2020. Although contested and sometimes abandoned by some important countries, the Protocol has given rise to climate legislation as a central theme of developed countries' policies. Since that historic conference, various Conferences of Parties (COP) have followed one another, i.e., annual meetings of the signatory countries of the UNFCCC to verify the objectives achieved and update future objectives. Among these, another important milestone on the road to decarbonisation was COP 21, held in Paris

on 12 December 2015, in which the Paris Agreement was signed [5]. The Agreement, adopted by 55 countries responsible for more than 55% of global emissions, have the main goal to hold the increase in the global average temperature «to well below 2°C above pre-industrial levels and pursue efforts to limit the temperature increase to 1.5°C above pre-industrial levels». From the perspective of operational strategies for emission reduction, the European Green Deal [6] came into effect in 2019. It is a set of political initiatives proposed by the European Commission with the overarching goal of achieving climate neutrality in Europe by 2050. The overall goal of the European Green Deal is to make the European Union the first "climate-neutral" continent by 2050. The objectives cover various sectors, including construction, biodiversity, energy, transportation, and food. The plan also involves potential carbon taxes for countries that do not reduce their greenhouse gas emissions at the same pace as others. To date, the proposals and initiatives in the implementation phase constitute the "Fit for 55" package [7]. The package of proposals aims at providing a coherent and balanced framework for reaching the EU's climate objectives ensuring a just and socially fair transition, maintaining innovation and competitiveness of EU industry and underpinning the EU's position as leading the way in the global fight against climate change. Among the innovative strategies adopted, there are plans for an emissions trading system, a climate social fund, and a radical change in the energy sector, both in terms of energy production and final consumption, as well as in the transportation sector concerning emission reduction and the use of sustainable fuels.

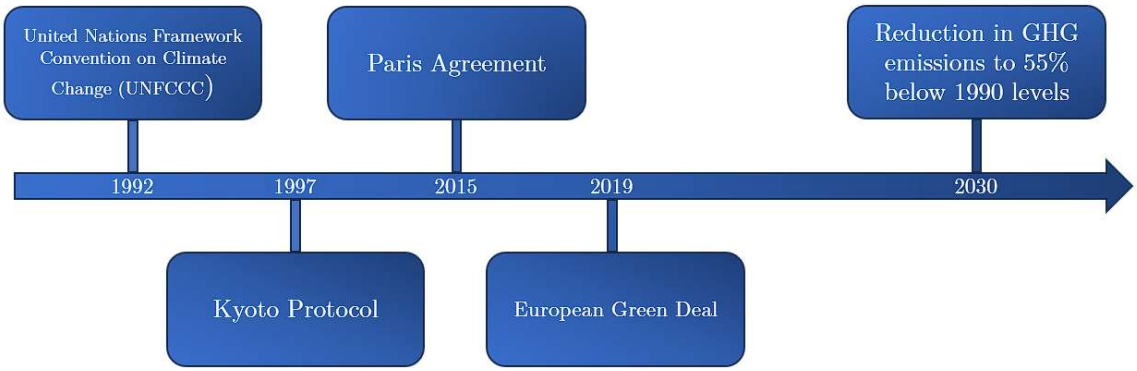

Figure 2 Major Policies for Climate Change, a chronological view.

1.2 Distributed Generation: Current State and Future Trends

The decarbonization of the electricity system plays a fundamental role in achieving the climate objectives by 2030 and 2050. The main source of emissions is precisely the generation of electricity, which has been based, since the early developments of the infrastructure, on the combustion of fossil fuels and the use of rotating electrical machines. The system thus constituted was of a pyramid type, with production concentrated in large generation centres and consumption distributed throughout the territory; in between, there was the transmission and distribution network that ensured the transport of energy where it was most needed. The system conceived in this way, virtually unchanged since its establishment, has been called into question since the early 2000s, with the development of new technologies for power generation from alternative and renewable sources. Unlike traditional power plants, the new generators were significantly smaller in size, located closer to consumers, and installed according to different technical and economic logics. The concept of centralized generation was about to change, and a new way of understanding the power system was gaining more and more ground.

Distributed Generation (DG) is a term coined precisely to underline the paradigm shift compared to the past centralized generation system, it is used in the energy and power generation industry to describe the decentralized production of electricity at or near the point of consumption [8]-[9]. DG systems can range from small-scale renewable energy installations, such as solar panels and wind turbines on residential rooftops, to larger commercial and industrial facilities that generate power for local consumption. The primary goal of DG is to improve energy efficiency, enhance grid reliability, and reduce transmission and distribution losses: by generating electricity closer to the point of consumption, DG systems reduce the energy losses that typically occur during long-distance transmission and distribution, they often incorporates RES like solar, wind, and biomass, thus contributing to a cleaner and more sustainable energy mix. By reducing the need for extensive transmission and distribution infrastructure, DG can help lower the overall costs of electricity delivery, benefiting both consumers and utilities, for some users, furthermore, these systems offer a degree of energy independence by

allowing them to generate their own power, potentially reducing reliance on the grid and mitigating exposure to electricity price fluctuations. Despite its advantages, DG also presents challenges, particularly related to grid integration, regulatory frameworks, and system balancing. Coordinating numerous small-scale generators can be complex, and the intermittent nature of certain renewable energy sources can create stability issues in the grid.

According to the International Renewable Energy Agency (IRENA) in its report "*Renewable Energy Statistics 2023*" [10][11] approximately 3381 GW of renewable energy generation capacity is installed worldwide, showing a 215.8% increase compared to 2013. Positive trends in installations are recorded worldwide, but there are significant differences among the regions. Leading the ranking is Asia, with 1637 GW installed, accounting for a global share of 48.41%. Out of these, China alone has 1086 GW, which is more than the entire Europe (706 GW), confirming a technological trend where the Chinese economy plays a central role in component production. In North America, it accounts for a solid 14.52%, which decreases to 7.86% in South America and is as low as 0.52% in Central America. Africa and Oceania contribute similarly, while the Middle East region closes the ranking with 0.86%. Table 1 presents data related to installed capacities divided by continent. It is evident that the most developed countries lead this particular ranking, benefiting from a strong economy and policies focused on climate and energy transition. Smaller economies, on the other hand, likely suffer due to a lack of targeted investments and general poverty conditions, while the Middle East, being a major oil player, still appears hesitant towards renewables, most likely seen as a competitor primarily in economic terms.

Table 1 Total renewable capacity per continent [10]

	2013 [GW]	**2022 [GW]**	**Increment [%]**	**Global Share [%]**
World	1567	3381	+115,8	100
Africa	31	59	+90,3	1,74
Asia	554	1637	+195,5	48,41
Eurasia	81	119	+46	3,51
Middle East	15	29	+93	0,86
Europe	419	706	+68	20,87
North America	273	491	+79	14,52
Central America	10	18	+80	0,52
South America	161	266	+65	7,86
Oceania	24	58	+141	1,71

The energy transition is a process that can be said to have just begun and will see its maximum development in the coming decades. In order to achieve the climate goals set in place, it is estimated that by 2050, the average renewable energy share for major economic powers should be no less than 60% for final energy consumption and approximately 50% for the transportation sector [11]. The massive increase in renewable energy installations poses a significant challenge for Transmission System Operators (TSOs) and Distribution System Operators (DSOs) in all countries around the world. The power system's regulation, in fact, is well-suited for more traditional generation, based on rotating machines with parameters that can be controlled for energy production. The power electronic components, crucial for interfacing renewable generators with the electrical grid, combined with the unpredictability of the primary source, have the potential to challenge the very paradigms of the system, which was designed to ensure increasingly higher quality and continuity of service. In this context, it is crucial to evaluate, in a first phase, new control strategies for renewable sources to provide regulation services that are comparable, or even superior, to those of traditional generation. After defining performance and minimum requirements, it will be necessary to regulate these new services both in terms of network regulations and codes, as well as in terms of economic compensation for providers. It is precisely in this direction that the recommendations of international entities responsible for defining priorities for the future grid are heading.

1.3 Need for New Regulation Solutions: the role of ENTSO-E

To ensure the operational security of the power system, it is essential that its frequency remains within a predetermined range and doesn't deviate significantly from the design frequency. When the frequency strays too far from its nominal value, protective mechanisms are triggered to safeguard machinery and maintain the functionality of the power system. Synchronous generators play a crucial role in helping the power system to withstand frequency fluctuations. All rotating machines contribute by virtue of their kinetic energy. However, as RES power plants replace traditional ones, the system's ability to resist these frequency changes diminishes. Many RES plants, especially PV and wind plants, consist of generating units connected to the grid via power electronic converters. These

converters are typically controlled in a manner that makes the operation of these power plants independent of the system frequency, consequently reducing the system's inertia. The reduction of inertia is considered the main challenge that grid operators will have to face during the energy transition process. This is evident from numerous reports produced by the "European Network of Transmission System Operators for Electricity," known by the acronym ENTSO-E [12]. This association comprises 43 TSOs from 36 European countries, and its objectives revolve around developing an efficient electrical system and energy market that combine sustainability and innovation while ensuring a secure and reliable power supply to consumers. ENTSO-E pursues these objectives by promoting collaboration among TSOs, developing European network development plans (TYNDPs), providing guiding principles for coordinating R&D activities. All of this is done in collaboration with other European institutions and organizations, as well as various stakeholders in the energy sector.

System inertia is a crucial factor for maintaining the frequency stability of the electrical power system. It dictates how quickly the frequency changes when there's a sudden mismatch between power supply and demand, such as the sudden loss of a large MW power source or an increase in demand. However, inertia is a parameter that is difficult to define strictly numerically, as it is a global parameter of the system and, at the same time, varies from generator to generator. The main reference for addressing the issue of calculating or, more precisely, estimating inertia is the ENTSO-E report "Future System Inertia" [13], which, despite focusing on a specific project, outlines the methodologies for calculating and measuring the overall system inertia. Among the conclusions of the report, it was highlighted that, depending on the needs of the system, it is recommended to investigate possible measures to compensate for situations with low system kinetic energy. Furthermore, it was emphasized the need to carefully evaluate the performance of these measures in order to integrate them properly into the electricity markets.

Following this, a report tiTL-Ed "Need for Synthetic Inertia for Frequency Regulation" was published in 2018 [14]. The purpose of the report was to offer guidance regarding Synthetic Inertia (SI) considerations when deciding on national parameters and whether to adhere to non-mandatory requirements. It's worth noting that the necessity for SI is typically lower when the relevant TSO is dealing with a limited presence of RES. The difficulty of maintaining frequency

stability significantly rises as the total system inertia decreases at the Synchronous Area (SA) level. In exceptional cases, during rare system divisions, some TSOs that usually rely on sufficient inertia from other parts of the SA might face a shortage of inertia for a brief critical period. If there's insufficient inertia available after a system split, this could pose a major challenge in preventing an immediate system collapse. The necessity for SI is especially relevant in smaller synchronous areas with a significant presence of non-synchronous generation, which typically have lower overall system inertia and more pronounced frequency fluctuations (such as small islands). It may also be essential in larger synchronous areas to prevent a complete system collapse during a system split and subsequent islanded operation. From a system operations perspective, it becomes critical that all generators and HVDC systems can offer SI and receive rapid support from appropriate demand units. Nonetheless, it is highlighted that the subject of SI requires additional research and development efforts. This is coupled with the need for manufacturers to enhance the technical aspects to align with the system's requirements.

The theme of enhancing the system's inertia has remained and continues to be central, to the extent that it has led ENTSO-E to produce a comprehensive guide for defining inertia and all related aspects [15]. This includes basic definitions, the current state of measurement technologies, and potential future developments. Beginning with theoretical discussions and followed by practical methodologies for assessing system inertia, and concluding with dynamic model calculation outcomes, the report seeks to provide power system engineers with guidance on the essential factors and tools necessary to achieve a comprehensive understanding of power system operation in relation to system inertia. In the same document, it also discusses the main connections between the increase in renewable generation and other issues not necessarily related to frequency, such as the reduction in short-circuit power or the increase in the frequency and intensity of voltage deeps.

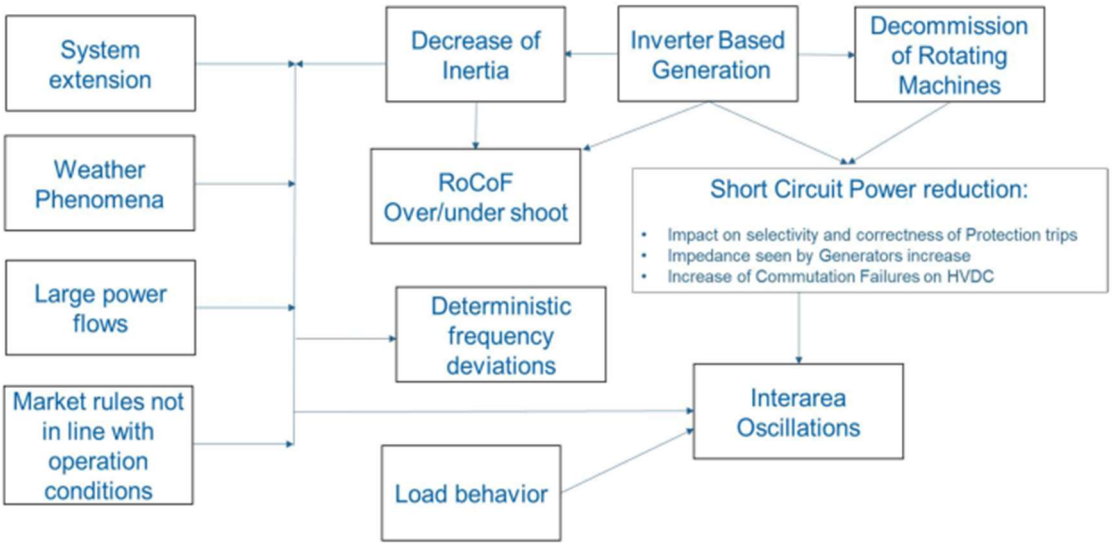

Figure 3 Map of interaction between system conditions and electric phenomena [15]

According to ENTSO-E, there are essentially four ways to deal with an inertia deficit:

- Taking the risk;
- Reducing transit;
- Speeding up the control;
- Increasing of system inertia;

The term "taking the risk" refers to refraining from any measures to address the inertia deficiency. This approach is relevant when dealing with out-of-range contingencies (i.e., no transient stability issues) that impact only relatively small portions of the system. In such instances, the out-of-range contingency may result in a localized blackout, followed by a rapid reenergization with support from the stable backbone of the main grid. "Reducing transit" refers to the practice of minimizing power transfers across the AC-grid to maintain imbalances within manageable limits following a system split. However, this kind of approach has effects on the market, so it has to be involved when all the other solutions are not available. “Speed up the control” involves new regulation solutions such ad SI or Battery Energy Storage Systems (BESSs) for deployment of primary reserves. In order to fully exploit their potential, these solutions need a medium-long term period of develop since they require new investment in technology, new power plants, new measurement systems and, very important, an evolution of grid codes and electricity markets. At last, the term "Increasing inertia" refers to the action

of enhancing the system's inertia, which can be accomplished through measures taken by TSOs. In the medium term, TSOs can install synchronous condensers with increased inertia or innovative E-STATCOM (Energy Static Synchronous Compensator) systems with storage capability. However, considering the rapid advancements in grid-forming control technologies, these control methods are likely to become equivalent solutions to synchronous condensers.

Several key challenges have been identified, and directly linked to these challenges, various key enablers have also been proposed. TSOs have to manage the unprecedented growth in grid complexity, the future European energy system will be even more dependent on the power system, and thus, more susceptible to its growing risks and threats. To address the new threat landscape, an enhanced resilience design will be necessary [16].

Chapter 2

2. Power System Frequency Control

In an electric power system, the active power must be balanced between generation and consumption. If the amount of power generated is not equal to the amount of power consumed, a frequency deviation will occur. A disturbance in the balance of power generation and consumption can cause the system frequency to deviate from its target value. This must be addressed to prevent outages or, in the worst case, a system collapse. The system frequency is directly linked to the speed of rotating generators connected to the grid and it is a measure of the pre-mentioned balance: an increase in demand will cause a decrease of the frequency and vice-versa. It is the duty of the frequency control system to restore the electrical balance, returning thus the frequency back to the nominal value.

This thesis focuses on assessing by simulations the impacts of innovative services for providing frequency regulation. In order to introduce the various case studies and simulations, this chapter presents the traditional frequency control strategies in electrical power grids. It will be explained the basic mechanism that enables the automatic frequency regulation in traditional generators, both for zone control and interconnected areas. Subsequently, the regulatory framework regarding frequency limits imposed on active users will be introduced, with a focus on the control methodologies currently in place to ensure these limits are not exceeded. Finally, after a brief overview of the market sessions for procuring reserves for frequency control, a short review of innovative regulation services currently under study by both the scientific community and this thesis work will be proposed.

2.1 Generalities on Frequency Control

The synchronous grid of Continental Europe, formerly known as the UCTE (Union for the Coordination of Transmission of Electricity) grid, holds the distinction of being the largest synchronous electrical grid in the world based on connected power. This grid operates as a unified, phase-locked system with a frequency of 50 Hz. It provides electrical power to more than 400 million customers across 24 countries, encompassing a significant portion of the European

Union. The operation of power generation units and the management of loads connected to the UCTE network require careful control and monitoring to ensure the secure and reliable operation of synchronous areas. Load-frequency control, technical reserves, and their associated control performances play a vital role in enabling TSOs to conduct their daily operational activities effectively.

In the UCTE synchronous area, control actions and reserves are structured hierarchically, consisting of control areas, control blocks, and the synchronous area, all managed by two coordination centres, Figure 4 [17].

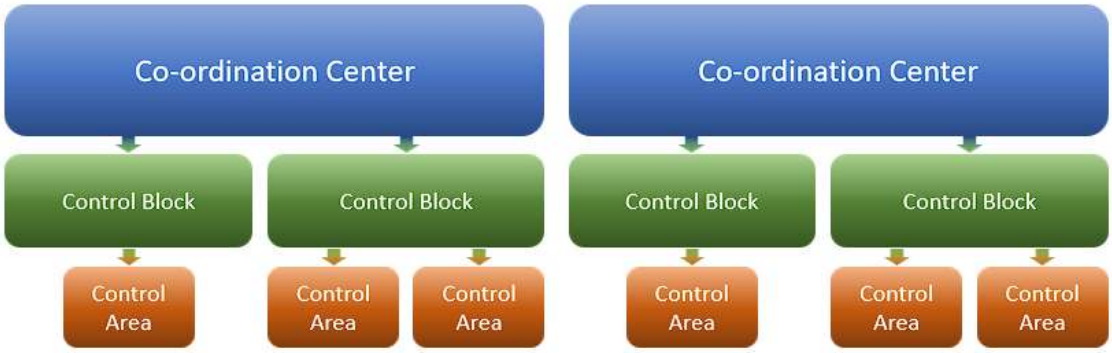

Figure 4 Hierarchical control structure of UCTE Synchronous Area composed of Control Areas, Control Blocks, and Co-ordination Centres [17].

Control actions are executed in a series of sequential steps, each possessing unique attributes and properties, all interdependent on one another (Figure 5):

- Primary Control occurs within seconds through a collaborative effort from all participating parties;
- Secondary Control takes over from Primary Control within a matter of minutes, with activation exclusively managed by the responsible TSOs.
- Tertiary Control initially complements and eventually replaces Secondary Control by adjusting generation schedules. Its implementation is carried out by the responsible TSOs.
- Time Control collectively corrects long-term global time deviations in synchronous time and involves the joint effort of all parties and TSOs.

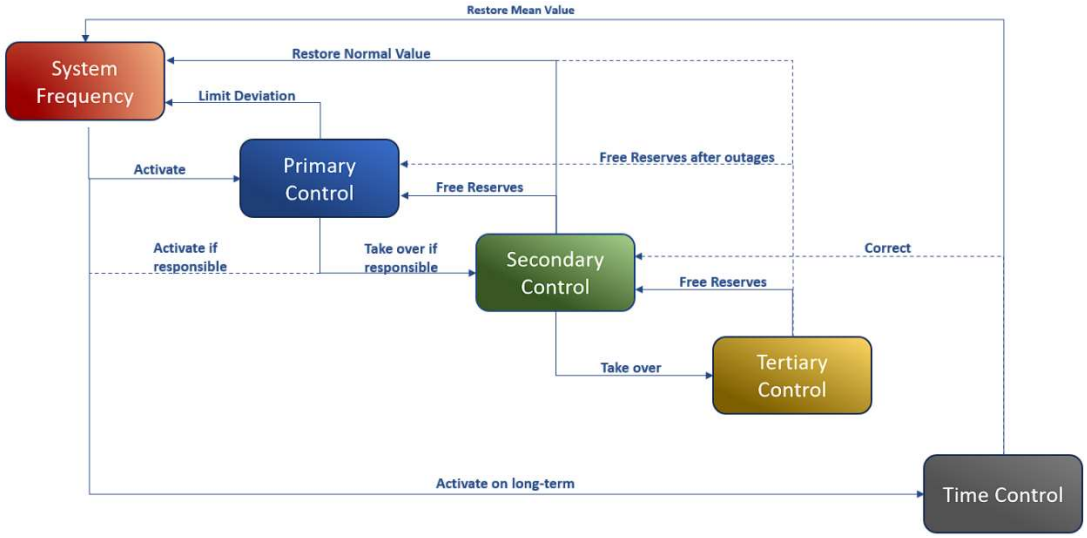

Figure 5 Complete Scheme for Frequency Control [17].

The first limitation to the frequency deviation is naturally provided by the inertia of the rotating generators connected to the system. This inertial response is of fundamental importance in maintaining system stability, as it prevents sudden changes that could trigger the untimely activation of frequency protection measures, leading to the disconnection of generators. The frequency control system presents a dead band, typically ±20 mHz, to ensure insensitivity to minor disturbances. If an event occurs that causes a frequency deviation greater than this value, the control system intervenes, initially limiting the frequency excursion and subsequently restoring it to its nominal value.

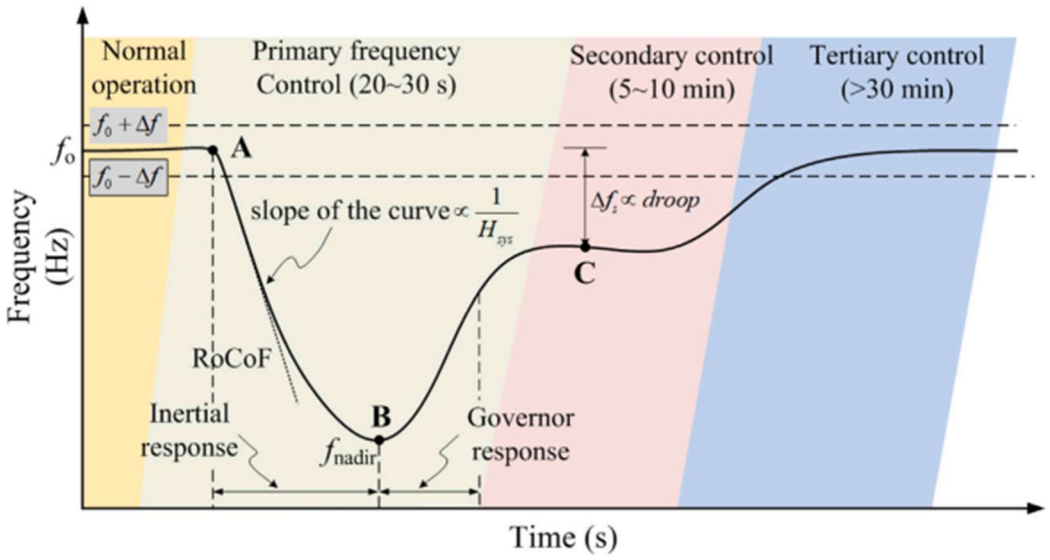

Figure 6 Sequential activation of the frequency control after a frequency event [17].

2.1.1 Primary Control

Primary control is the first line of defence in maintaining the balance between generation and consumption in a synchronous area (Please refer to Appendix 1 for basic principles of primary control). It is done by all interconnected TSOs, to ensure the operational reliability of the power system. Primary control stabilizes the system frequency at a stationary value after a disturbance or incident within seconds but does not restore the frequency and power exchanges to their reference values. Regulating units will then automatically perform primary control to re-establish the balance between demand and generation.

A fundamental characteristic of generators is the *droop* σ, generally expressed as:

$$\sigma = \frac{f_M - f_0}{f_N} \quad ; \quad \sigma\% = \frac{f_M - f_0}{f_N} \cdot 100 \tag{2. 1}$$

With f_0 the initial frequency, f_M the maximum frequency and f_N the nominal frequency. As a function of the active power, the droop can be expressed as:

$$\sigma = \frac{\frac{\Delta f}{f_N}}{\frac{\Delta P}{P_M}} \tag{2. 2}$$

Where Δf is the frequency variation at steady state, ΔP is the injected power variation at steady state and P_M the maximum power provided by the generator. A generator's contribution to network disturbance correction primarily depends on the generator's droop and its primary control reserve. The figure below illustrates variations in the power output of two generators, a and b, which have different droop characteristics but possess identical primary control reserves, under equilibrium conditions. If a minor disturbance occurs with a frequency offset less than ∆fb, the generator with the smaller droop controller, which is generator a, will provide a greater contribution to correcting the disturbance compared to generator b, which has the larger droop. The frequency offset (∆fa) at which the primary control reserve of generator a is exhausted (i.e., where the power output reaches its maximum value, Pmax) will be smaller than that of generator b (∆fb), even when both generators have identical primary control reserves. During a

major disturbance (where the frequency offset exceeds ∆fb), both generators will contribute equally to primary control under quasi-steady-state conditions.

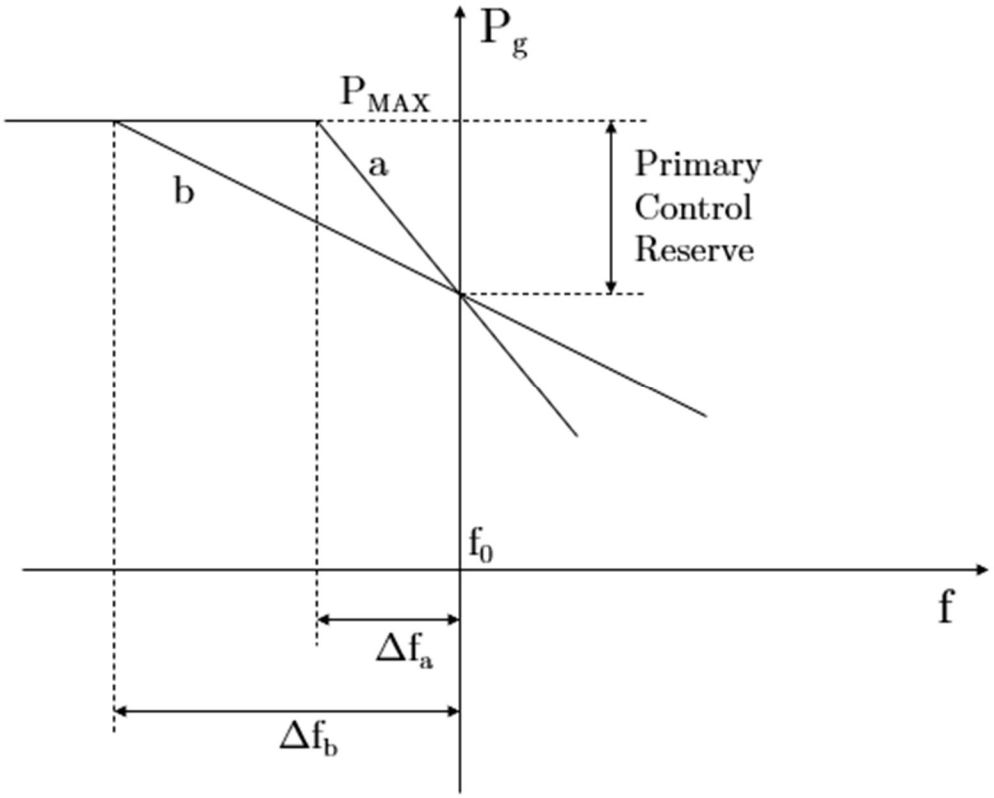

Figure 7 Power output of two generators with different droops.

Another important parameter is the "*primary control energy*" E_P, expressed as:

$$E_P = E_i + E_R$$

(2. 3)

With E_i and E_R respectively the "*load regulating energy*" and "*regulating energy of the machine*".

$$E_R = \frac{P_M}{\sigma \cdot f_N} \quad ; \quad E_i = \frac{\Delta P_C}{\Delta f}$$

(2. 4)

These two parameters define the degrees of regulation provided by the load (E_i), which absorbs different power as the frequency changes, and by the generator regulation (E_R), which is adjusted to support the grid in case of power imbalance. These "energies", under suitable assumptions, can be extended to the entire control area, essentially maintaining the same form.

Different disturbances or random fluctuations that disrupt the balance between generation and demand can lead to a frequency deviation, triggering the response of the primary controller of the generating sets involved in primary control at any given moment. All of this occurs when the insensitivity zone, which should not exceed a maximum of ±10 mHz, is surpassed. The proportional nature of primary control, along with the collaborative efforts of all interconnection partners, ensures the swift restoration of equilibrium between power generation and consumption, thereby guaranteeing that the system frequency remains within acceptable limits. If the frequency exceeds these permissible limits, additional measures beyond the scope of primary control, such as automatic load shedding, become necessary and are implemented to maintain interconnected operation. The deviation in the system frequency triggers a response from the primary controllers of all generators under primary control within a matter of seconds. These controllers adjust the power output of the generators until a balance between power generation and consumption is restored. Once this balance is regained, the system frequency stabilizes and remains at a quasi-steady-state value Δf_{stat}. The magnitude of the frequency deviation f_{nad} is called "*frequency nadir*" (or simply *nadir*) and depends mainly on:

- the magnitude and evolution of the disturbance that impacts the equilibrium between power generation and consumption over time;
- the kinetic energy of rotating machines in the system;
- the number of generators under primary control, the primary control reserve, and its allocation among these generators;
- the dynamic characteristics of loads;
- the dynamic characteristics of loads.

The quasi-steady-state frequency deviation Δf_{stat} is determined by the disturbance's magnitude and the network power frequency characteristic, which is primarily influenced by the following factors:

- the droop characteristics of all generators that are under primary control within the synchronous area;
- the sensitivity of consumption to changes in system frequency.

Having known the active power disturbance ΔP_D and the primary regulating energy value E_P, it is possible to derive the steady state frequency by the equation:

$$\Delta f_{stat} = -\frac{\Delta P_D}{E_P}$$

(2. 5)

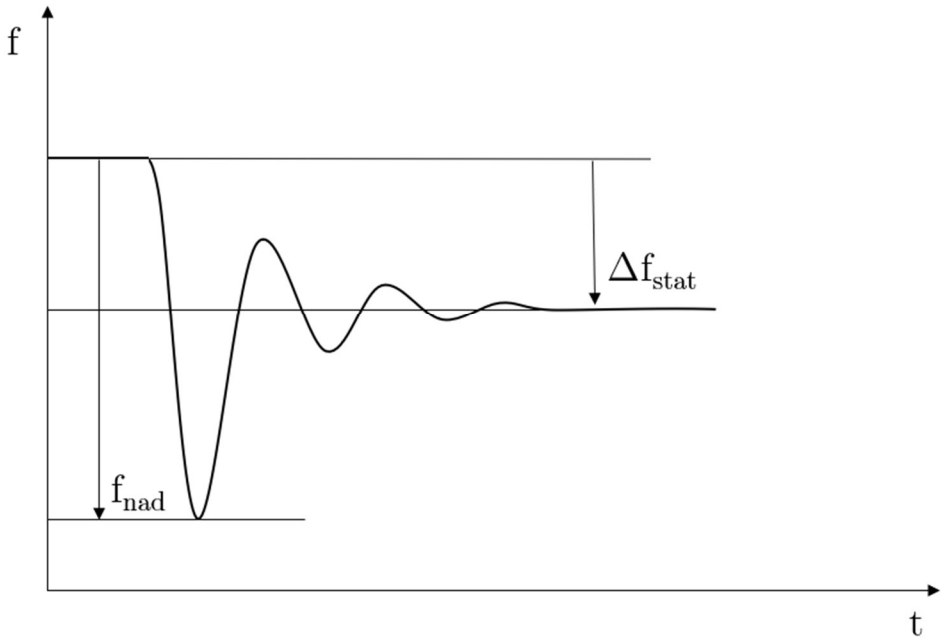

Figure 8 Generic representation of an under-frequency transient

During Primary control it is of fundamental importance the "*Principle of Joint Action*": each TSO is obligated to participate in correcting disturbances based on their respective contribution coefficient to primary control. These contribution coefficients, denoted as C_i, are routinely computed for each Control Area/Block or interconnection partner/TSO using the following formula:

$$C_i = \frac{E_i}{E_u}$$

(2. 6)

where E_i is the electricity generated in the *i-th* Control Area and E_u the total electricity production in all the Control Areas of the Synchronous Area.

2.1.2 Target Performance and Reference Incident

The conditions for the target efficiency of primary control are based upon the following considerations:

- the concurrent failure of two power plant units, or the outage of a line section or busbar;
- past experiences have demonstrated that incidents resulting in an even more substantial power loss are exceedingly uncommon;
- overreacting to such incidents by deploying excessive control power may result in the overloading of the transmission system.

The design hypothesis is founded on conservative parameters, which incorporate a safety margin in estimated values. As a result, it is likely that even more severe incidents could be managed in practice without resorting to load shedding. The maximum instantaneous power deviation between generation and demand in the un-split synchronous area (by the sudden loss of generation capacity or load-shedding / loss of load) to be handled by primary control is defined "*reference incident*". In the UCTE synchronous area, the reference incident is set at 3000 MW, taking into account operational considerations related to system reliability, as well as the scale of loads and generation units.

Transitioning from normal operation in the interconnected network, a sudden 3000 MW loss of generating capacity should be compensated for by primary control alone, eliminating the necessity for customer load shedding in response to a frequency deviation. Moreover, considering the self-regulating impact of the system load at a rate of 1%/Hz, the absolute frequency nadir should not exceed 180 mHz. Similarly, a sudden total load shedding of 3000 MW should not result in a frequency deviation exceeding 180 mHz.

2.1.3 Primary Control Reserve

In case of severe imbalances, it is necessary to have reserve regulating power that further limits the frequency deviation. This reserve is defined as "*primary control reserve*" and it is distributed among the interconnected systems. Considering what stated before, the total primary control reserve for the entire synchronous area, denoted as P_{pu}, is determined by the UCTE based on the specific conditions

of the grid. In particular, the overall primary control reserve is dimensioned in order to be at least equal to the reference incident, $P_{pu} = 3000\ MW$. The shares, P_{pi}, allocated to the control areas are determined by multiplying the calculated overall reserve by the contribution coefficients C_i of the respective control areas:

$$P_{pi} = P_{pu} C_i$$

(2. 7)

The complete primary control reserve is engaged when there is a quasi-steady-state frequency deviation of -200 mHz or more. Similarly, if there is a frequency deviation of +200 mHz or more, power generation must be reduced by the equivalent of the entire primary control reserve. To limit the utilization of the primary control reserve to unplanned power imbalances, the system frequency should not consistently go beyond or drop below a range of ±20 mHz for extended durations during normal, undisturbed conditions.

2.1.4 System Inertia

While the adoption of renewable energy sources for electricity generation helps reduce greenhouse gas emissions, their integration into the power grid can lead to grid destabilization and an increased risk of instability. In a traditional power system, electricity generation is primarily accomplished by alternators. These rotating machines respond to load variations by counteracting them, thus preserving electrical balance, at least during the initial moments.

In an electrical system equipped with rotating generators, an imbalance between the load and the generator output results in a frequency fluctuation. This concept is mathematically represented by the swing equation [18][19]:

$$P_{gen} - P_{load} = J\omega_g \frac{d\omega_g}{dt}$$

(2. 8)

where P_{gen} is the generated power, Pl_{oad} is the load power (including losses), J is the inertia moment and ω_g is the generator angular speed [rad/s]. Power system inertia is the capacity of the system to withstand frequency fluctuations, primarily attributed to the kinetic energy of the rotating masses within the system. The power system's inertia constant, denoted as H, is calculated as the kinetic energy

of the generators normalized to the apparent power S_g generated by all the connected generators in the system:

$$H = \frac{J\omega_g^2}{2S_g}$$

(2. 9)

By conducting dimensional analysis, it becomes evident that the inertia constant of the machine possesses the dimensions of time. This can be interpreted as *the duration for which the energy stored in the rotating masses can provide power to the load at a level equivalent to the nominal apparent power of the generator.*

Beginning with the inertia of a single machine, it's feasible to determine the total inertia of all synchronous machines connected to the same grid by computing a weighted average of the inertia constants of all generators, assessed in proportion to their rated power:

$$H_{syn} = \frac{\sum_{i=1}^{n} S_{gi} H_i}{S_{syn}}$$

(2. 10)

where H_{syn} is the total system inertia, S_{gi} is the rated power of the *i-th* generator, H_i is the inertia of the *i-th* generator and S_{syn} is the total rated power of the system. When the expression for H_{sys} is substituted into equation (2. 8), we obtain:

$$\frac{2H_{syn}}{f}\frac{df}{dt} = \frac{P_{gen} - P_{load}}{S_{syn}}$$

(2. 11)

The term $\boldsymbol{\frac{df}{dt}}$ represents the Rate of Change of Frequency (RoCoF) of the system. A system with higher inertia constants of the generators will possess greater overall inertia, making it more robust during significant disturbances and imbalances. Various generators have distinct inertia constants based on their energy source and conversion technology. Renewable energy sources, for instance, are connected to the grid through electronic converters that lack rotating masses. Consequently, the kinetic energy associated with them is zero, leading to a zero inertia constant. To account for the impact of inverter-based generators, the system's inertia, H_{sys}, can be redefined as:

$$H_{sys} = \frac{\sum_{i=1}^{n} S_{gi} H_i}{P_{load}}$$

(2. 12)

where P_{load} is the power requested by the load [15].

When there is a substantial integration of inverter-based energy sources, the overall system inertia decreases. As a result of this reduction in inertia, the system becomes more susceptible to power imbalances, which can lead to concerns regarding stability and reliability. The same converters responsible for connecting RES can, if properly controlled, provide a significant regulating contribution to the grid. Numerous studies in the literature evaluate the effectiveness of these systems, and the work of this thesis aligns with the research focus on innovation in the field of frequency regulation using innovative methods and strategies.

2.2 State of the art in the field of frequency regulation innovation

Innovations in power system frequency control are primarily motivated by the necessity to adjust to evolving energy landscapes, including the integration of renewable energy sources and the changing behaviours of consumers. These advancements are crucial for ensuring the stability and reliability of electrical grids and, at the same time, to reduce environmental footprints and improving overall grid efficiency. Scientific research has, especially in recent years, tackled the search for new flexibility solutions, considering technologies and energy sources that were not previously considered for these purposes in traditional systems. Given the large volume of articles and case studies considered, several authors have produced review articles to summarize this topic and gather all the information related to the state of the art in the field. For the purpose of the entire thesis research, and particularly for the writing of this section, some well-known articles published with some time intervals between them have been considered. These articles span from 2018 to 2022, the reason behind this choice is to track the chronological development of publications on this topic, in order to chart a path that can provide insights into the most effective and implementable methods considered in the near future. In [20] authors identify four different categories of Load-Frequency Control approaches, such as:

- classical control approaches focus on designing proportional-integral-derivative (PID) controllers;
- modern control approaches including optimal control method, sliding mode control schemes, and adaptive control systems;
- intelligent control schemes, such as fuzzy control systems;
- soft computing-based approaches for controllers' parameter tuning.

For each of these groups, the advantages and disadvantages are highlighted, and various research gaps are identified. These research gaps are considered worthy of further investigation, such as enhancing control system robustness or proposing new methods to improve system performance, among others.

In [21], the authors mention various frequency regulation techniques, this time focusing on specific methods of providing the service, such as demand-side response, vehicle-to-grid, or virtual power plants. Among the conclusions, it is also emphasized that controls need to be designed for increasingly high rates of change of frequency (RoCoF). However, it's noted that with a faster response, there comes an increased number of oscillations, potentially leading to instability.

If the frequency regulation issue is already significant in large, interconnected areas, it becomes even more pronounced in low-resilience systems. In [22], the authors indeed focus on this type of system, analysing the regulating contribution of Type-3 and Type-4 wind generators. Two major regulation components are identified in relation to the duration of the provided service and the required energy:

- *Temporary Energy Reserves:* high-power services for short amount of time (synthetic inertia, droop control, fast power reserve)
- *Persistent Energy Reserves:* low-power services for long amount of time (de-loading control)

Among the fundamental points of discussion raised by the authors, the most significant one concerns the availability of the service, understood as the producibility at the time of delivery. The existing control strategies highly depend on the operating point of wind turbines: in integrated energy systems, wind turbines are unable to provide frequency response when the wind speed is exceptionally low. In such scenarios, battery energy storage systems, energy

conversion, and other ancillary services become viable alternatives. These options can offer a basic, but acceptable, response and help offset the power deficiency resulting from a frequency event.

In conclusion, in this brief review of the literature, in [23], the authors conducted a review of nearly 500 articles in order to fully identify the state of the art in the field of frequency regulation and anticipate future developments and prospects. The authors distinguish themselves from previous reviews by considering a possible frequency regulation by distribution networks and advanced load forecasting techniques. From what emerges from the study conducted, the use of innovative strategies primarily based on renewable sources (and thus on the use of converters) should be seen not only as a potential problem for the grid but as an alternative system operation with a lower environmental impact. However, even in this case, it is highlighted that the randomness of the primary source is the main barrier to the widespread adoption of this type of service in national electricity markets.

2.3 The map of ancillary services in Europe

From a regulatory perspective, Europe is undergoing a significant change to ensure the integration of new flexibility resources into the electricity market. This is evident from a study published by SmartEn in 2022 [24], which outlines the current state in terms of services and opportunities offered by various states to integrate new forms of ancillary services. For the purposes of this thesis, the focus is on frequency services, but it is essential to note that renewable sources will also play a crucial role in other areas of regulation, such as voltage regulation or congestion resolution. In general, there has been some enhancement in the domain of ancillary services. However, considering the ongoing energy crisis and the substantial demand for balancing electricity that the energy system will face due to increased electrification and the expanded use of renewable energy sources (RES), the current efforts appear to be inadequate for attaining the EU decarbonization goals in a cost-effective manner while involving all engaged consumers. The most significant impediments are associated with the incomplete execution of the 2019 Electricity Market Design. This includes issues such as the introduction of the aggregator role in national legislation, as stipulated by Article

17 of the Electricity Directive (EU) 2019/944 [25], as well as the presence of high minimum bid sizes and overly strict technical prerequisites. Some countries impose even more substantial barriers for Demand Side Flexibility (DSF), as exemplified by Spain, Romania, Greece, and Portugal. On the other hand, some countries, including France, the United Kingdom, and Germany, are at the forefront of this field. They have long incorporated some of the most innovative flexibility solutions into the market, which are subjects of study by the scientific community. Special mention is made of Italy: the national TSO, Terna S.p.a., has launched a series of pilot projects since 2018 aimed at evaluating the feasibility and potential impact of various regulation technologies and services. In this thesis, some of these projects have been studied and will be presented in the following chapters. Returning to the European map, SmartEn has categorized different countries with a score related to the progress status of ancillary services. Specifically, they considered the following indicators:

- Access to ancillary services;
- Participation requirements;
- Market composition;
- Data transparency;
- Upcoming legislative changes;

In reference to the first point, they also present subcategories regarding the specific service under consideration, namely:

- Frequency Containment Reserve (FCR)
- Automatic Frequency Restoration Reserve (aFRR)
- Manual Frequency Restoration Reserve (mFRR)

The scoring system involves a progressive assignment from 0 to 4, where the maximum represents the highest accessibility to the market, the minimum number of barriers, a diverse composition of the energy mix, maximum transparency on data, and significant legislative changes in the field, while the 0 represent the absence of the service or completely inaccessibility for distributed resources (storage, RES, demand response). The following table provides a summary of the scores of the various examined states. It is worth to note that

the last row of the table presents an average calculation of the different indicators in order to provide an overall picture of the European condition.

Table 2 Score summary of European Countries for ancillary services access to distributed resources.

PR: Participation Requirements; MC: Market Composition; DT: Data Transparency; ULC: Upcoming Legislative Changes

Country	**Overall**	**FCR**	**aFRR**	**mFRR**	**PR**	**MC**	**DT**	**ULC**
Austria	2	2	2	2	1	1	1	2
Belgium	3.5	3	3	3	3	3	4	3
Denmark	3	4	3	2	3	1	2	2
Estonia	2	0	0	2	2	1	4	2
Finland	3	4	2	2	3	3	4	3
France	3	4	1	3	3	3	4	2
Germany	2	4	3	3	2	1	2	1
Great Britain	2	2	0	2	2	1	3	3
Greece	1	1	1	1	1	0	2	2
Hungary	3	3	3	3	3	2	2	2
Ireland	2	2	2	2	1	1	2	3
Italy	2	0	2	3	1	3	2	2
Latvia	1	0	0	2	1	0	1	2
Netherlands	3	4	4	2	3	2	1	2
Poland	1	1	1	0	0	1	1	2
Portugal	1	0	1	1	1	1	2	2
Romania	1	0	2	2	1	0	1	2
Slovenia	4	4	4	4	4	3	3	3
Spain	2	0	2	2	1	0	3	3
Sweden	2	3	2	2	3	2	2	4
Switzerland	2	4	2	2	3	1	1	2
Europe	2.17	2.14	1.90	2.14	2.00	1.43	2.24	2.33

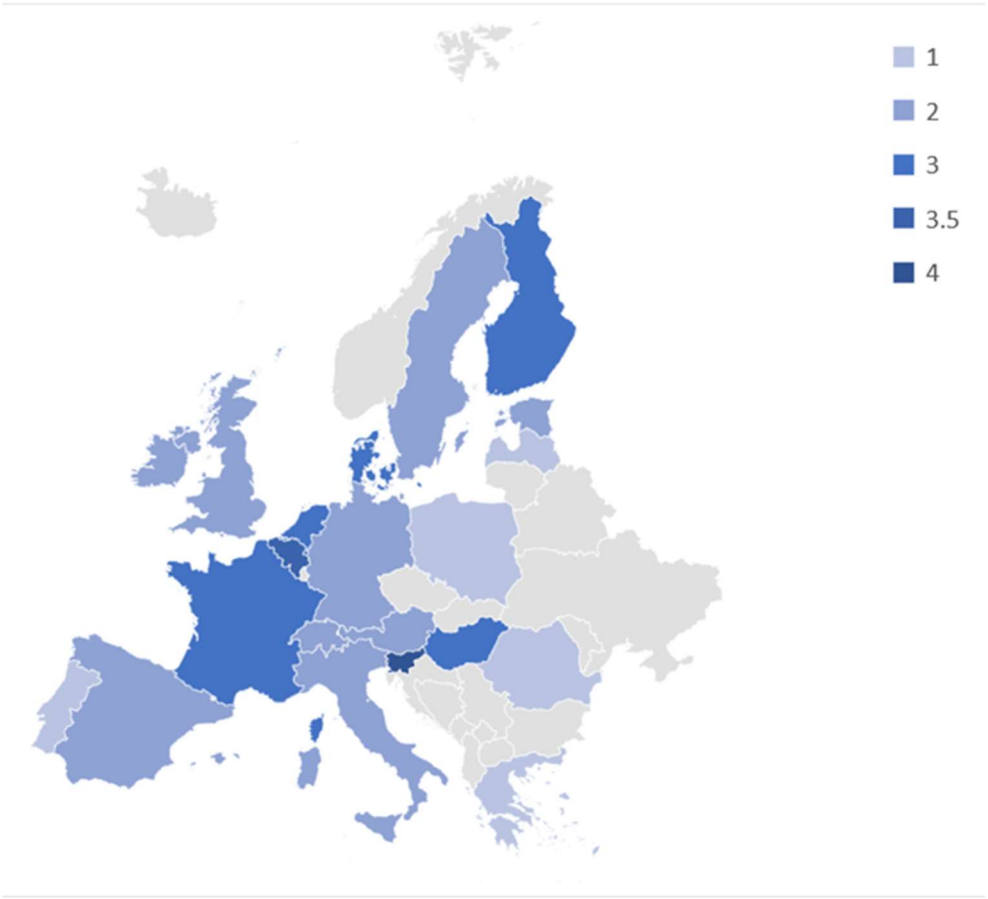

Figure 9 Map of ancillary services in Europe according to SmartEN score [24].

What emerges from the conducted analysis is a favourable inclination of European countries to open their markets to new market players, with a particular focus on distributed generation. The most virtuous country is Slovenia, while among the less inclined towards these new solutions (at least for the moment) are Greece, Lithuania, Poland, and Portugal. Notably, these countries are situated in geographic areas on the edges of the European synchronous area. This condition could potentially imply lower grid resilience, leading these countries to be more cautious about introducing flexibility services whose effectiveness and reliability have not been thoroughly tested. The weak point among those analyzed at the European level appears to be the market composition. It is clear that the provision of ancillary services is still the prerogative of traditional sources, especially in some countries where regulatory barriers prevent the entry of new sources. From a regulatory perspective, there is a clear and growing trend towards innovation, indicating that what is currently considered pioneering and cutting-edge will become an integral part of grid codes in the years to come.

This paragraph concludes the introductory section of the thesis and provides all the necessary information for the comprehension of the studies collected in the following chapters. The macro-theme of climate change has been introduced, emphasizing the need to decarbonize the electrical system and comply with regulatory requirements. Subsequently, the concept of electrical system resilience was introduced, focusing on the decrease of this parameter in relation to the penetration of renewable sources in the energy mix, with specific reference to frequency regulation. After describing the traditional regulation model and its underlying physics, a review work was presented, providing an overview of innovative frequency regulation methods and the state of European regulatory framework on ancillary services. In the next chapter, original studies conducted to evaluate the effectiveness of various frequency regulation techniques and models in numerous case studies are presented. Chapter 3 will present the studies that consider extended and interconnected systems, while in Chapter 4, the studies related to low-resilience networks will be analyzed, typically systems found on Mediterranean islands connected via a single link or, in some cases, operated as frequency islands. Finally, in Chapter 5, all the studies related to the Sicilian power grid are concentrated. This grid has been the subject of numerous investigations during the last year of activity. These recent studies were conducted in collaboration with various research institutes, including the Italian organizations "Ricerca Sistema Energetico (RSE)" and "ENEA."

Chapter 3

3. Frequency Control Strategies for Interconnected Power Grids

Frequency control services are essential for maintaining grid stability and ensuring the reliable delivery of electricity in interconnected power grids. These services involve a combination of automated control systems, communication networks, and the coordinated efforts of power generators, grid operators, and other stakeholders to respond swiftly and effectively to changes in frequency. As already presented in the previous chapters, frequency regulation is, in most cases, the prerogative of traditional generation systems. The regulations regarding this matter vary greatly among European countries. In some cases, services are open to various energy sources and system actors, while in others, certain actors are excluded from the market and certain services are mandatory. To respond promptly to the ongoing changes in the electrical system, several European countries have started various pilot projects to assess the impact of new technologies in the system, evaluating their technical effectiveness and economic feasibility. For example, Italy has been experimenting with various pilot projects since 2017, including the one called Fast Reserve Unit (FRU). For the purposes of this thesis, studies have been conducted on this project, initially considering alternative control methods for the units to provide synthetic inertia, and later, proposing the dissemination of various FRUs throughout the European grid.

3.1 Fast Reserve Unit

3.1.1 Generalities of the project

On November 20, 2019, the Italian TSO Terna released a document for public consultation concerning a pilot project for delivering an ultra-fast frequency regulation service called "Fast Reserve" (FR). The ultra-rapid frequency regulation service represents one of the solutions to address the emerging requirements resulting from the development of the electric power system. The Fast Reserve Units aim to counteract the gradual extension of the response time associated with primary frequency regulation due to the phase-out of coal-based

power generation [26]-[27]. This ancillary service is expected to enhance grid frequency stability while working in conjunction with existing ancillary services like primary reserve. The consultation period concluded on January 24, 2020, and the regulation was approved on June 3, 2020, through resolution 200/2020/R/eel by the Italian Regulatory Authority for Energy, Networks, and Environment (ARERA) [28]. After receiving approval from the Authority, Frequently Asked Questions (FAQs) were published in September and November, along with a document that provided estimated hours of availability for the year 2021, which was released on November 6, 2020, [29]. An auction for the allocation of available capacity was conducted on December 10, 2020. The total available qualified power was 230 MW, to be distributed across the country. The auction saw substantial participation, with 53 operators and 117 Fast Reserve Units, resulting in a total qualified power value of approximately 1327.3 MW, exceeding six times the available qualified power, [30]. Seventeen operators were assigned, and they represented a total of 23 plants. This active involvement illustrates the significant interest of market operators in this new regulatory service, in addition to Terna's initiative to establish a flexibility service based on storage systems.

Specifically, the definition of an FRU is given by Article 2.1 of the regulations: "*Fast Reserve Units are individual devices connected directly or indirectly to the public network or aggregates of devices that meet the technical requirements set out in Article 3 of the present regulation. Such devices may be*:

a. stand-alone generating units;
b. generating units sharing the point of connection to the public grid with one or more consumption units other than ancillary services and/or storage facilities;
c. consumption units, except for those units providing interruptibility service;
d. storage plants, as defined according to ARERA Resolution 574/ 20 [31], both "stand-alone" and combined with generation units and/or consumption units."

For what concerns precision, two conditions must be respected:

- Dynamic accuracy: in case of frequency deviations sufficiently large to activate the service, the power exchange must be within a defined area in

the Δ P - t plane. In particular, a maximum overshoot of 5 % with respect to the steady-state value is allowed during the transient, while a maximum error of $\pm$ 1 % from the setpoint is allowed at steady-state.

- Static accuracy: 1 s after the frequency deviation that caused the service activation, and in the absence of further changes, the actual power exchanged with the grid must be in a tolerance range of $\pm$ 1 % of the qualified power from the expected value.

The Qualified Power P_q (i.e. the power available for regulation purposes) had to be not below 5 MW and not over 25 MW, but in the following auctions the minimum Qualified Power was set to 1 MW. In any case, the FRU must be able to receive and manage the pilot set-point sent by Terna, in addiction it has to maintain sufficient energy capacity to allow a stable exchange with the grid of a power value at least equal to the Qualified Power, in injection or absorption, for at least 15 minutes continuously.

3.1.2 Simulink Implementation of the Fast Reserve Unit

The provision of the power must be in accordance with the power-frequency adjustment curve in Figure 10, with activation without intentional delay and in any case within 1 second after the event which determined the activation of the service. In the absence of further frequency errors, it is requested to maintain the power value activated for at least 30 s continuously and then reducing the activated power in 5 minutes. The contribution offered by a Fast Reserve Unit (FRU) is similar to the primary control provided by a static power converter, which scientific literature characterizes as Fast or Enhanced Frequency Regulation. As a result, the generation or consumption of power at the Point of Common Coupling (PCC) of the FRU is achieved by employing a control scheme featuring a proportional regulator, as depicted in Figure 11. In this scheme:

- K_droop is the gain of the proportional regulator;
- DPc is the power variation at the PCC provided by the FRU system.

The technical specifications for the Italian Fast Reserve Units (FRU) include the following features: an intentional dead band for the first activation (threshold #1) and an additional threshold (threshold #2) known as the saturation band. Beyond this saturation band, it is required to ensure the consumption/production of

power for as long as the frequency deviation surpasses the threshold and within the time frame allowed by the stored energy.

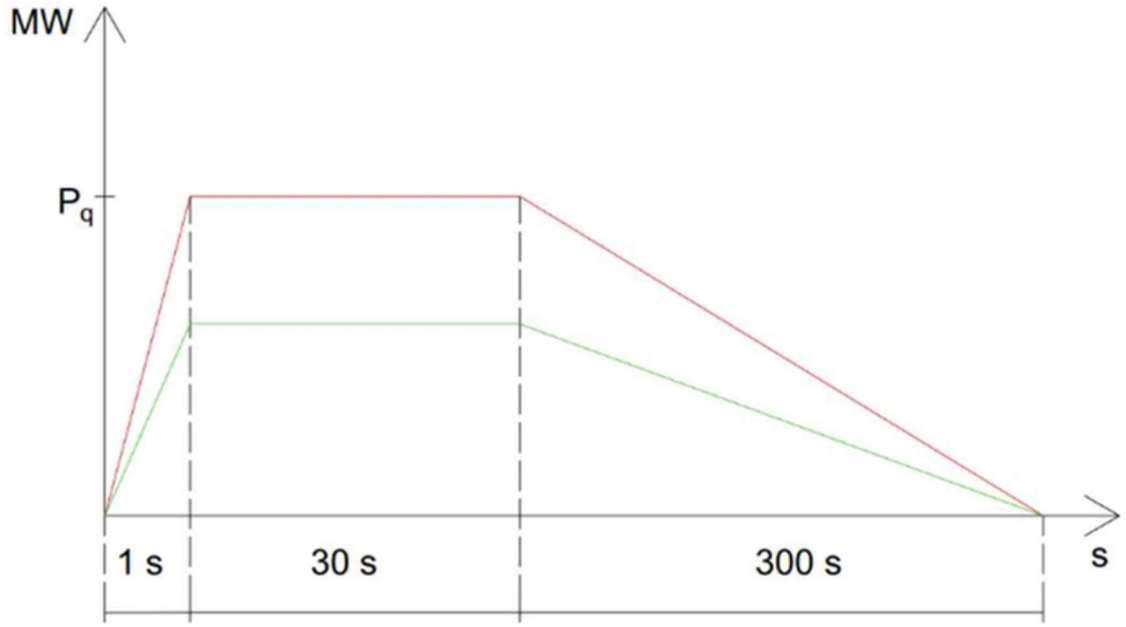

Figure 10 Power-frequency curve requested to the FRUs.

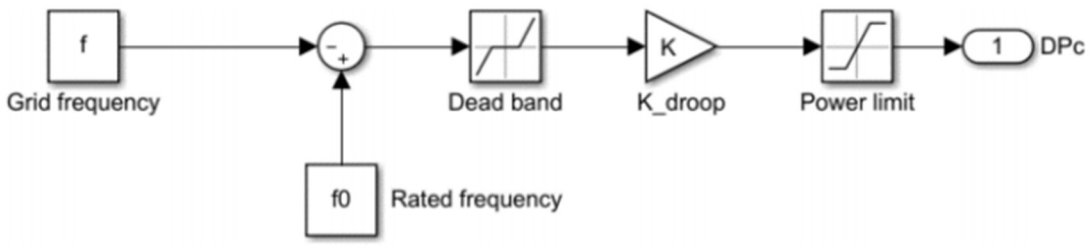

Figure 11 Implementation in Matlab/Simulink of the control scheme for fast frequency regulation

According to Terna's conditions reported in Figure 10, the adopted adjustable parameters are the following ones:

- Dead band of first activation $f_{db} = \pm$ (0 ÷ 500) mHz;
- Saturation band $f_{sat} = \pm$ (f_{db} ÷ 1000) mHz;
- Maximum power of the single Unit $P_q = 5 \div 25$ MW;
- Proportional gain: $K_{droop} = P_{MAX}$ / (f_{sat} - f_{db}).

If suitably controlled, the same units can be used also for providing synthetic inertia, contributing to the Rate of Change of Frequency (RoCoF) containment in the first moments of a disturbance.

3.1.3 Virtual Inertia Control

The same converters used in Renewable Energy Sources (RES) plants can also make a significant contribution to system inertia. When appropriately controlled, a converter can offer a response that closely resembles that of a traditional alternator. This "virtual" regulation is known as Synthetic Inertia (it is also commonly referred to as artificial, emulated, or virtual inertia). In the scientific literature, various Synthetic Inertia (SI) configurations are available [32], each distinct in terms of mathematical models, control algorithms, performance characteristics, and applications. For the conducted study, the approach proposed in [33] was adopted. The proposed control scheme belongs to the "frequency-power response based" models, as it performs a continuous control on the network frequency by calculating the power contribution to be delivered.

The power consumed/produced for the SI service at the PCC is then expressed as:

$$\Delta P_{SI} = \begin{cases} -K_{in} \cdot f \cdot \dfrac{df}{dt} \forall \left|\dfrac{df}{dt}\right| < RoCof_{MAX} \\ -P_{MAX} \cdot sign\left(\dfrac{df}{dt}\right) \forall \left|\dfrac{df}{dt}\right| \geq RoCof_{MAX} \end{cases}$$

(3. 1)

where K_{in} is the SI parameter responsible for the active power provision. By examining the aforementioned relationship, it becomes evident that once the frequency returns to its new steady-state value following the disturbance, the SI control no longer triggers any response from the FRU since *df/dt* is equal to zero. This distinguishes SI control from fast primary regulation, which continues to operate beyond the frequency transient, as it depends on the frequency error. One method to determine the value of K_{in} is to consider the maximum acceptable RoCoF [34]. By setting a condition that when the RoCoF reaches a specified fraction, $k_{\%}$, of the maximum acceptable RoCoF value, $RoCoF_{MAX}$, the FRU response should be equal to the maximum power, P_{MAX}. In this case, K_{in} can be calculated as:

$$K_{in} = \frac{P_{MAX}}{f_0 \cdot k_{\%} \cdot RoCof_{MAX}}$$

(3. 2)

The inertia of the FRUs H_{FRU} with SI is obtained as done in [34]:

$$H_{FRU} = \frac{K_{in} \cdot f_0}{2 \cdot P_{MAX}} \tag{3. 3}$$

Considering the overall inertia equation and adding the FRU contribution, it can be obtained:

$$H_{sys} = \frac{\sum S_{gi} \cdot H_i + P_{MAX} \cdot H_{FRU}}{P_{load}} \tag{3. 4}$$

where H_{sys} is the inertia of the power system with the contribution of the FRU.

3.2 Simulation of the Continental Europe Synchronous Area with FRU and SI

In the literature, various models are employed to simulate frequency dynamics, and the choice depends on the specific objectives of the study. In this study, a standard transfer function model of a single-area power system is utilized. This model is typically chosen when investigating the effects of various technologies on primary frequency regulation. The model is represented in Figure 12 with all the blocks which simulate the presence of FRUs with the SI control described in the previous paragraphs (for a basic overview on primary regulation, please see Appendix 1).

The variables that characterize the scheme are, in order:

- T1, T2, T3, Td: power plants time constants (s);
- Er: generators power-frequency characteristic (MW/Hz);
- DPd: disturbance (MW);
- Ei: loads power-frequency characteristic (MW/Hz);
- Ti: time constant of the system (s);
- Df: frequency error (Hz);
- f0: rated frequency (Hz).

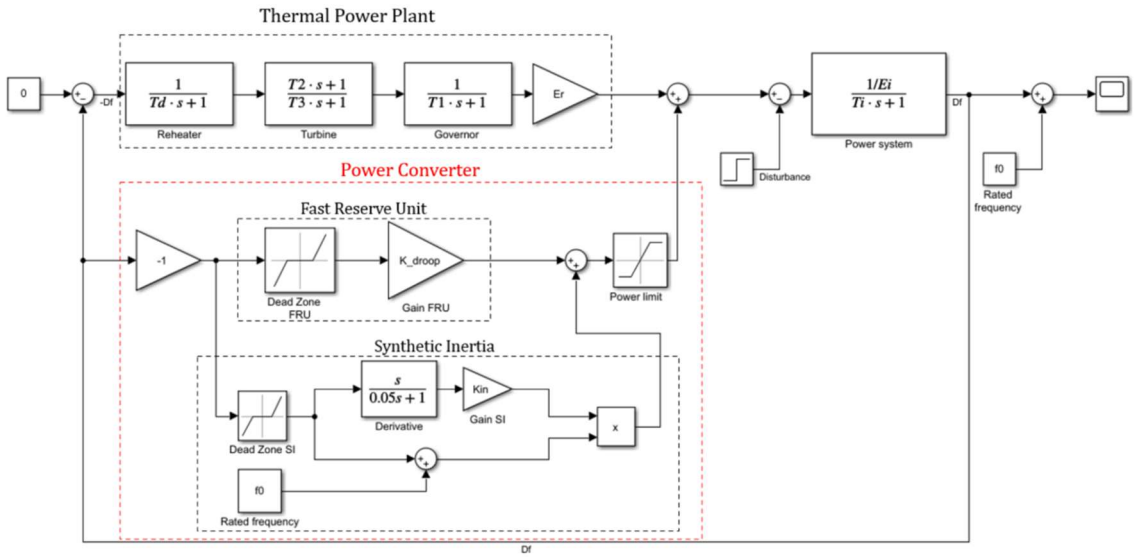

Figure 12 Implementation in Matlab/Simulink of the primary regulation control including FRUs and SI

The time constant of the system, denoted as 'T_i,' dictates the frequency transient and is determined by the system's inertia according to the following relationship:

$$T_i = 2 \cdot H_{sys} \tag{3. 5}$$

This formula illustrates the direct impact of inertia: higher inertia values result in longer time constants for the system, which in turn lead to better responses to power disturbances. When inertia is low, for the same disturbance, frequency oscillations are more pronounced, and the system might not have sufficient time to respond before the instantaneous frequency triggers protection mechanisms and leads to the disconnection of generators.

The novelty of this study lies in its exploration of the repercussions of extensive FRUs deployment in the CE synchronous area, as well as in contemplating the potential synergy of their actions with SI control. One of the key strengths of this analysis consists in the incorporation of a comprehensive model for the CE area, relying on the ENTSO-E Initial Dynamic Model [35] and energy projections that lead to a realistic representation of the dynamic behavior of the European power system. In this work, the presence of Fast Reserve Units (FRUs) connected to the CE synchronous grid in two distinct scenarios is simulated. The first scenario is the base scenario associated with the year 2020, and the second scenario pertains to the future, specifically 2040. These scenarios are founded on ENTSO-E

projections for both load and generation. In the following sub-section the model is implemented with or without the contribution of FRUs in four scenarios:

- Base scenario 2020;
- Future scenario 2040, traditional (without FRU);
- Future scenario 2040, with FRU;
- Future scenario 2040, with FRU and additional SI.

3.2.1 Current base scenario 2020 and future base scenario 2040, traditional primary regulation

The study starts with the dynamic simulation of the CE grid focusing on the Reference Incident, which is presumed to involve a 3000 MW disturbance. This simulation solely relies on traditional primary frequency regulation. The system data is derived from the Initial Dynamic Model provided by ENTSO-E , a model that has been employed in numerous studies to investigate primary frequency control within the CE synchronous area [36][37]. The purpose of these simulations is to assess the frequency dynamics under the RES penetration anticipated for 2040, as outlined by ENTSO-E. This evaluation is conducted under the premise of an imbalance equal to that in the Reference Incident. All relevant data used in the simulations are presented in Table 1. The initial frequency is conventionally set to the rated frequency. The data for both the 2020 and 2040 scenarios are based on information obtained from ENTSO-E documents [38]-[41].

Table 3 Data for the simulations of the 2020 and 2040 base scenarios.

Parameters	**Base Scenario 2020**	**Base Scenario**
Initial load P0	317000 MW	363000 MW
Initial Frequency f0	50 Hz	50 Hz
Rated apparent power of the generators in	462450 MVA	167500 MVA
System inertia Hs	3.71 s	1.71 s
Load regulating factor D	0.01	0.01
Load power frequency characteristic Ei	3170 MW/Hz	3630 MW/Hz
Generators power frequency characteristic	30830 MW/Hz	11167 MW/Hz
Time constant of the system Ti	21.65 s	6.84 s
Generators start time constant Td	0.05 s	0.05 s
Governor time constant T1	0.5 s	0.5 s
Turbine derivative time constant T2	4 s	4 s
Turbine delay time constant T3	9 s	9 s
Disturbance DPd	3000 MW	3000 MW

Fig. 3 shows the frequency dynamics in the analyzed cases. In the 2020 Base Scenario the frequency nadir is equal to f_{nad} = 49.87 Hz and the steady-state frequency is f_{stat} = 49.91 Hz. In the 2040 Base Scenario instead it can be seen that the parameters related to the frequency are worse: the frequency nadir is f_{nad} = 49.72 Hz while the value at steady state is f_{stat} = 49.79 Hz. Even if these values may seem comparable to those in the 2020 scenario, it has to be noticed that the steady-state frequency reaches values below 49.80 Hz, considered an attention threshold by ENTSO-E in case of a disturbance equal to the Reference Incident.

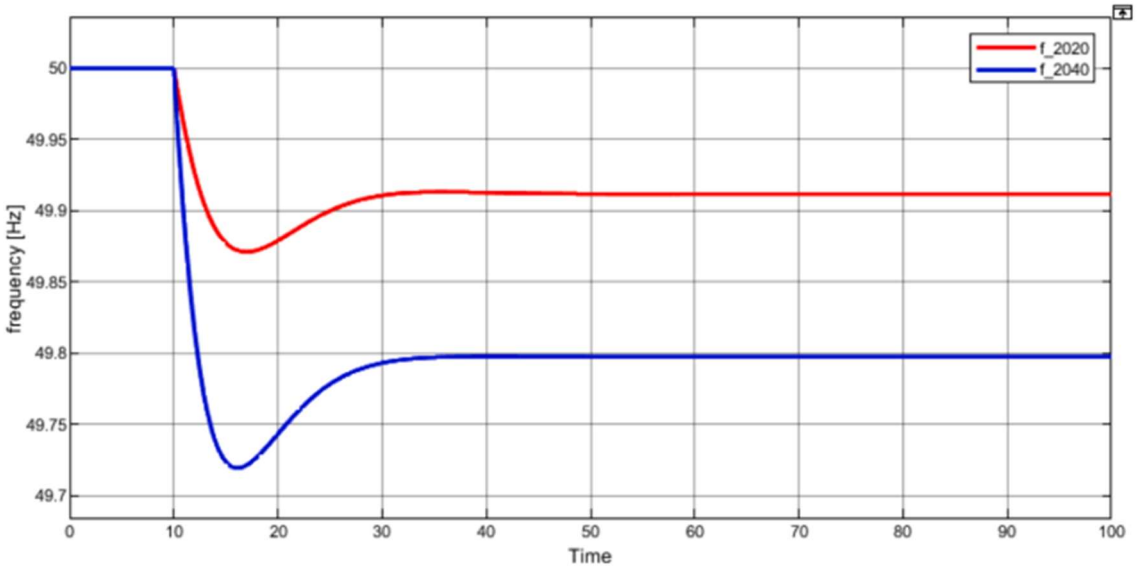

Figure 13 Frequency trend in 2020 base scenario (red line) and in 2040 base scenario (blue line).

Following the initial evaluation that focused exclusively on traditional primary regulation, two additional simulations are presented to assess the impact of the control actions described earlier within the 2040 scenario:

1. Primary regulation with FRU support;

2. Primary regulation with FRU support along with supplementary SI control.

3.2.2 Primary regulation with fast Reserve Unit and additional synthetic inertia control in the 2040 scenario

In this scenario, the Qualified Power of the FRUs was determined using a proportion similar to what Terna used in the first auction of the pilot project. To

compensate for the loss of 6.6 GW of coal power plants, an equivalent Qualified Power for the FRUs was set at 230 MW. Based on projections and applying the same proportion, considering the decommissioning of 134 GW of fossil generation in 2040, the equivalent Qualified Power for FRUs is established as 4060 MW. As for the activation and saturation thresholds, the former is set at 20 mHz, and the latter is set at 500 mHz. The Inertia Parameter K_{in} is assumed to be 20 MW·s/Hz².

The support provided by the FRUs enhances both dynamic and steady-state frequency parameters. Simulations demonstrate that the frequency nadir is now at $f_{nad} = 49.79$ Hz, while the steady-state frequency is at $f_{stat} = 49.84$ Hz. Although there is some difference from the frequency parameters in the base scenario of 2020, the integration of FRUs into the regulation chain results in a safer and more reliable management of the synchronous area.

The inclusion of the SI control allows the system to be supported from the point of view of the inertia with an improvement in RoCoF and nadir. Using the equation from the previous paragraph, the FRU inertia is computed and is equal to H_{FRU} =6.16 s. The implementation of SI leads to improvements in the frequency transient, with the frequency nadir at $f_{nad} = 49.80$ Hz. Figure 14 displays the frequency trend in this final simulation in comparison to the other scenarios. It's evident that the curve's slope with SI is more gradual compared to the other cases.

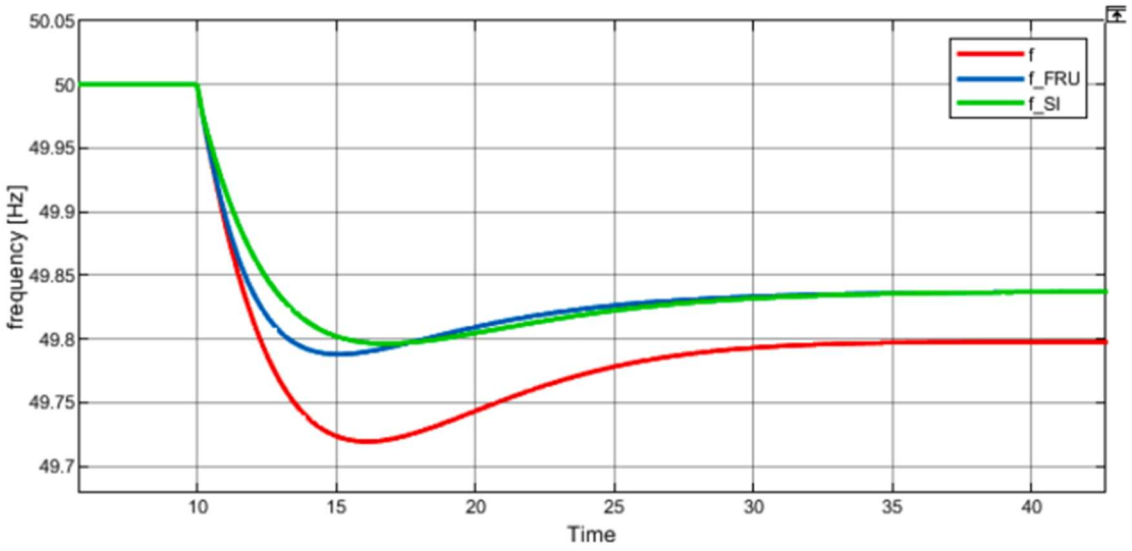

Figure 14 Frequency trends comparison in 2040 scenarios: traditional primary regulation (red line), primary regulation with FRU (blue line), primary regulation with FRU and SI (green line)

The discussion of the total rated power of FRUs is noteworthy. As depicted in Figure 14, the transient behavior of the system is significantly enhanced by the presence of FRUs in the system. The simulation results demonstrate that, based on the assumptions outlined in the preceding sections, activating around 4000 MW of FRUs in 2040 is adequate to achieve nearly the same steady-state performance as observed in 2020 for the reference incident of 3000 MW. While FRUs represent one solution for fortifying the power system and its resilience against major disturbances, what's particularly evident is that the required installed power amounts to only 0.34% of the current total installed power in the Continental Europe (CE) region [42]. Thanks to FRUs, all parameters characterizing the transient behavior of the Continental Europe (CE) area are significantly improved compared to the 2040 scenario with only traditional power plants. As evident in Figure 4, the action of FRUs reduces the steady-state frequency error by approximately 24% and the frequency nadir by about 25%, compared to the scenario without FRUs (Future scenario 2040, traditional). The results are even more positive when Synthetic Inertia (SI) control is considered (Future scenario 2040, FRU + SI). In this case, the action of FRUs reduces the Rate of Change of Frequency (RoCoF) by about 4% (from -0.121 to -0.116 Hz/s) and the frequency nadir by around 29% compared to the scenario without FRUs. The provision of SI, however, does not influence the steady-state frequency due to the intrinsic characteristics of the SI control. The system inertia, calculated using equation (3. 4), increases from 1.71 s to 1.78 s due to the contribution of FRUs. The contribution of FRUs to system inertia is modest since PMAX represents only a small percentage of the size of the synchronous generators in the area. In theory, to achieve the same inertia as in the base scenario, K_{in} should be set to 581 MWs/Hz^2, according to equations (3. 3) and (3. 4), with $H_{FRU} = 179$ s. By fixing $H_{sys,\ SI}$ in equation (3. 4) and increasing P_{MAX}, H_{FRU} decreases.

3.2.3 Proposals for the Dissemination of FRUs in the European Synchronous Area

The question of how to distribute the total rated power of Fast Reserve Units (FRUs) among the Continental Europe (CE) countries for the 2040 scenario is an interesting one. This paper proposes two feasible criteria:

1. **Proportional to Decommissioned Coal Plants**: The first criterion suggests that the rated power to be installed in each country is proportional to the rated power of the coal plants that will be decommissioned in that country. This criterion aligns with the strategy employed in the Italian FR program.
2. **Contribution Factors to Frequency Containment Reserve**: The second criterion involves dividing the total rated capacity according to the contribution factors of each country to the frequency containment reserve. These factors are computed in 154[38], as indicated by European regulation [43]-[45].

The results of applying the two criteria, considering the production and consumption data from [42] and the announced decommissioned coal plant capacity from the European Coal Plant Database [46], are presented in Table 4.

It is immediately evident that the two criteria yield significantly different results. Associating FRU installation with the decommissioning of coal plants implies that the total FRU capacity must be provided by only 12 out of the 26 considered countries. On the other hand, applying the second criterion ensures that all Continental Europe countries participate in the FRU service provision. Examining the results in Table 4, according to the first criterion, most of the FRU rated power should be installed in Germany and Poland, as they currently experience a greater capacity decommissioning from coal plants. In contrast, the second criterion suggests a greater contribution from France, Germany, Italy, Spain, and Turkey, as these countries have the highest contribution factors.

Table 4 FRU rated power to be installed in each country according to the two sizing criteria.

	Criterion 1		Criterion 2	
Country	Coal plant capacity announced to retire [MW]	FRU rated power [MW]	Contribution factor	FRU rated power [MW]
Albania	-	-	0.26	11
Austria	-	-	2.55	104
Bosnia and Herzegovina	-	-	0.44	18
Belgium	-	-	3.04	123
Bulgaria	-	-	1.34	54
Switzerland	-	-	2.34	95
Czech Republic	960	58	2.37	96
Germany	39471	2378	17.49	710
Denmark	1180	71	1.25	51
Spain	672	40	8.93	363
France	1919	116	18.16	738
Greece	2525	152	1.85	75
Croatia	-	-	0.66	27
Hungary	884	53	1.53	62
Italy	1980	119	11.58	470
Luxembourg	-	-	0.25	10
Montenegro	-	-	0.12	5
North Macedonia	-	-	0.24	10
Netherlands	4458	269	4.21	171
Poland	12894	777	5.54	225
Portugal	-	-	1.81	74
Romania	-	-	2.09	85
Serbia	-	-	1.39	56
Slovenia	419	25	0.53	22
Slovakia	44	3	1.09	44
Turkey	-	-	8.91	362

The conducted simulations clearly show that even with a minimal deployment of FRUs in the CE grid, the reliability and stability of the system are improved, especially in scenarios with a high penetration of inverter-based generation systems. Beyond aiding in RES integration, the contribution of FRUs could prove valuable in controlling frequency drifts during exceptional operating conditions of the grid. One of the most critical events that the electrical system might encounter is the separation into different frequency islands due to faults and malfunctions. The occurrence of a system split event can sometimes be more critical than the reference incident itself. Therefore, it is worth to analyze how FRU or equivalent devices can provide support to the grid during such an occurrence.

3.3 Simulation of the Continental Europe System Split and potential FRU contribution

On January 8th, 2021, a tripping of a 400 kV busbar coupler in the Croatian network triggered a sequence of overcurrents, leading to the split of the Continental Europe (CE) system into two areas [47]. The countries of the CE system were divided into two areas as follows:

North-West Area:

- Portugal, Spain, France, Italy, Switzerland, Luxembourg, Belgium, the Netherlands, Germany, Denmark, Austria, Slovenia, Czech Republic, Poland, Slovakia, and Hungary.

- Total load: 317 GW

- Rated power of the generators: 434 GVA

- Total power frequency characteristic: 28.75 GW/Hz

South-East Area:

- Croatia, Romania, Bosnia Herzegovina, Serbia, Montenegro, North Macedonia, Albania, Bulgaria, Greece, and Turkey.

- Total load: 65 GW

- Rated power of the generators: 89 GVA

- Total power frequency characteristic: 5.89 GW/Hz

The system split resulted in an equivalent deficit of power in the North-West area and an excess of power in the South-East area, amounting to approximately 6.3 GW. To evaluate the potential impact of having FRUs deployed throughout the entire CE synchronous area during such an event, simulations were conducted using the models presented in previous section. The theoretical distribution of FRUs, as per "Criterion 2" (Table 4), was utilized for these simulations. Criterion 2 was chosen because it involves the participation of all European countries in fast frequency regulation, unlike criterion 1, where FRUs are installed only in some countries. The model of the system with the two areas is depicted in Figure

15. To simulate the split, two disturbances were applied to the two areas in Figure 15. The magnitude of the disturbances was calculated based on the data and information published by ENTSO-E [47]. Specifically, the disturbances were determined as the difference between the total power imbalance caused by the split (-6.3 GW) and the total load disconnected as a defensive action (1.7 GW in the North-West area and 5.1 GW in the South-East area). This calculation resulted in a net value of -4.6 GW for the North-West area and 1.2 GW in the South-East area. For this specific simulation, FRUs without the support of synthetic inertia were used to model the split, simulating the current operation of FRUs only. The system parameters were set based on the study in [48]. According to the division of CE countries into the two areas described earlier, the distribution of FRU qualified power was as follows:

- Qualified Power of FRUs in the North-West area: 3327 MW
- Qualified Power of FRUs in the South-East area: 703 MW

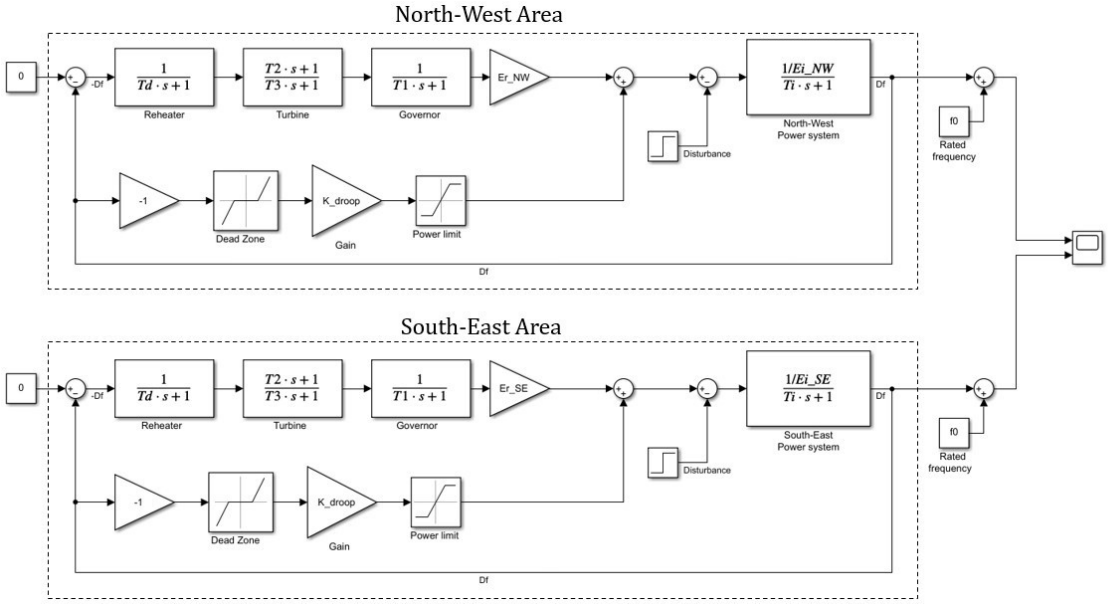

Figure 15 Implementation in Matlab/Simulink of the primary regulation control with FRUs during the system split.

Figure 16 illustrates the simulated frequency trends in the two areas following the split. As discussed in [48], the differences from the real trends during the system split in January are attributed to not implementing the action of the defence mechanisms that were activated during the split. Nevertheless, the steady-state values of the frequency and the timing of the frequency evolution in the two areas

are equivalent to those actually measured after the separation of the synchronous area. Figure 17 displays the frequency trends in the same system that would have occurred, under the same hypotheses, in the presence of FRUs. The contribution of fast frequency regulation results in smaller steady-state deviations in both areas, confirming the effectiveness of this control action. Table 5 summarizes the steady-state values of the frequency. It is noteworthy that, although the SE area contains a lower amount of fast reserve capacity, the effects of FRUs intervention on the frequency steady-state deviation and nadir are more evident. This is attributed to the smaller power-frequency characteristic of the SE part compared to the NW part. Indeed, the impact of the FRUs will be higher in the case of a relatively weak area with a lower power-frequency characteristic provided by traditional generators.

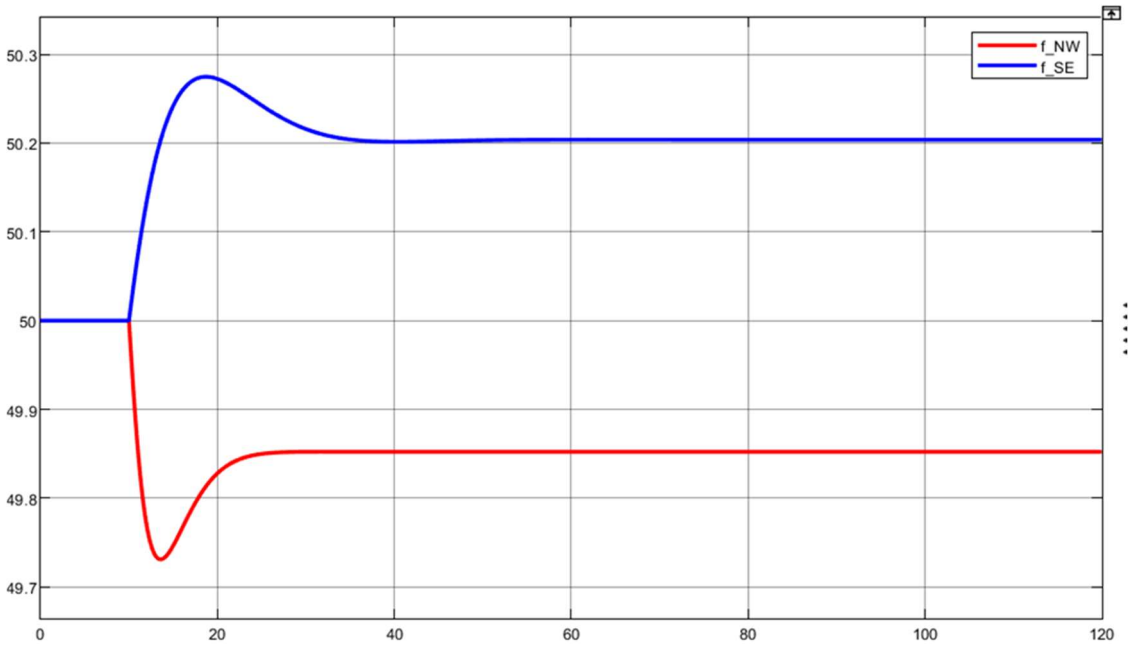

Figure 16 Frequency trends in the two areas after the split without FRUs.

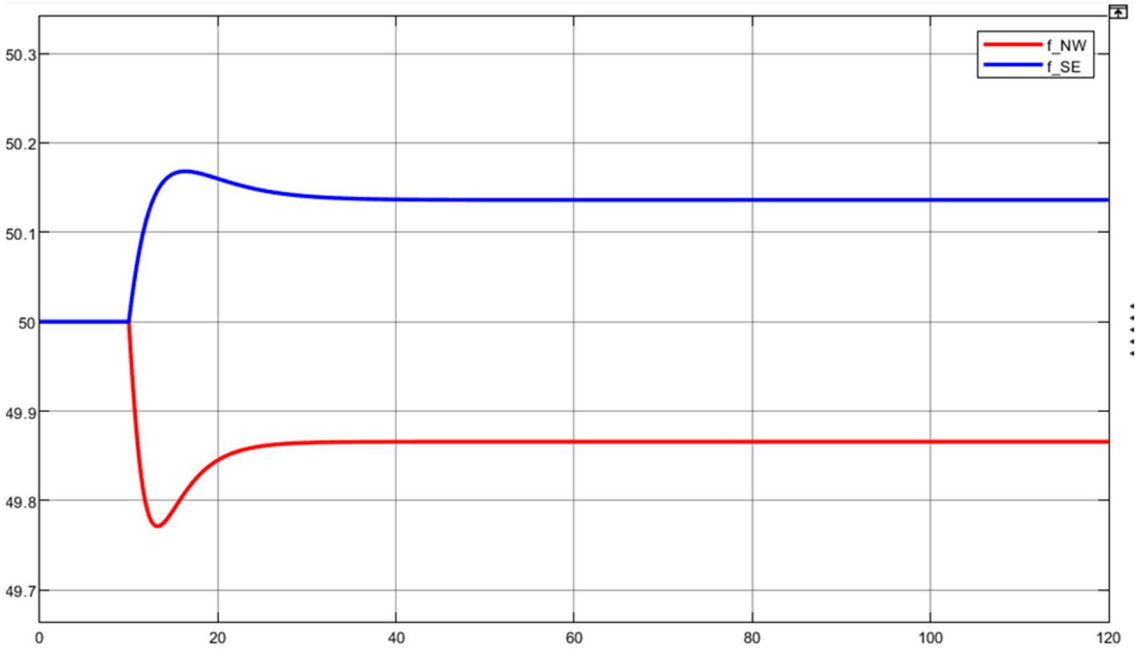

Figure 17 Frequency trends in the two areas after the split with FRUs.

Table 5 Frequency at steady state after the split for the analyzed cases.

Scenario	f_{stat} [Hz]	f_{nad} [Hz]
NW Area without FRUs	49.85	49.74
SE Area without FRUs	50.20	50.27
NW Area with FRUs	49.87	49.78
SE Area with FRUs	50.13	50.17

3.3.1 Summary of the results and final considerations

This chapter presented the results of a simulation study on the application of battery storage systems in a Fast Reserve Unit (FRU) configuration with an additional control for providing synthetic inertia (SI) in the CE synchronous area. For the European power system, studies and analyses concerning inertial response and frequency dynamics are particularly relevant, especially in view of events that can affect the stability and safe operation of the system, such as the split that occurred in January 2021 and the consequent severe frequency transients. The simulations, comparing the current scenario with a future scenario (2040) characterized by a higher penetration of renewable energy sources (RES) and lower inertia, have shown the advantages of the spread of FRUs throughout Europe. In particular, the study illustrates how frequency parameters in 2040 can become comparable to the current ones with only 4000 MW of FRUs, highlighting the strategic importance of an FR service in future electric power systems.

Continuing with the criteria established by the Italian FRU pilot project, the total power (4000 MW) can be divided among 160 to 800 installations with a rated power between 5 MW and 25 MW. These installations can be connected to both Medium Voltage (MV) and High Voltage (HV) nodes of the power system without causing difficult-to-solve power flow issues. Additionally, the units can be independent plants or electric storage units associated with renewable energy sources (RES)-based plants, such as hydro power plants, wind or PV plants. These units are typically managed for various purposes like energy arbitrage and peak shaving. They can be locally controlled to provide Fast Reserve (FR) and Synthetic Inertia (SI) services as soon as the frequency falls outside the dead band of the controller. In terms of territorial occupation, the parameter for these installations is approximately 8–13 kW/m^2, considering the area for auxiliary services, internal pathways, and excluding the HV/MV station. Therefore, finding free areas for installing FRUs close to HV/HV or HV/MV stations does not pose a significant issue for the widespread adoption of these systems.

In conclusion, it is intended to emphasize the significance of investing in grid-scale storage for frequency support, particularly considering the expected reduction in primary reserve in the coming decades. The study's results underscore the importance of resolving these issues promptly for the future stability and resilience of power systems.

Chapter 4

4. Frequency Control Strategies for Weak and Isolated Microgrids

Frequency control is fundamental for a secure operation of weak grids which are more susceptible to disturbances and challenging to restore to normal operating conditions. During the three-year doctoral program, several studies have been conducted regarding weakly interconnected systems and, in some cases, isolated power grids. The reasons for this research lie both in the geographical characterization of the Italian territory, particularly Sicily, and in the expertise that the electrical systems research group at the University of Palermo has developed over the years, thanks also to numerous research projects carried out directly on the islands and their power generation and distribution grids. In this chapter, various frequency control techniques are analyzed for two real case studies: the island of Favignana and the Country of Malta.

4.1 The Island of Favignana

Favignana is a small Italian island situated in the Egadi Archipelago, which also includes Levanzo and Marettimo. It is positioned approximately 7 km off the western coast of Sicily, between the cities of Trapani and Marsala (Figure 2). The island covers a surface area of around 19.8 km^2 and features a coastline that is 33 km long, characterized by numerous indentations. The topography of the island includes a small mountain chain running from north to south, reaching its highest point at 314 m above sea level. Favignana has a regular population of approximately 3,400 residents. However, during the summer months, the island experiences a significant increase in population due to its popularity as a tourist destination.

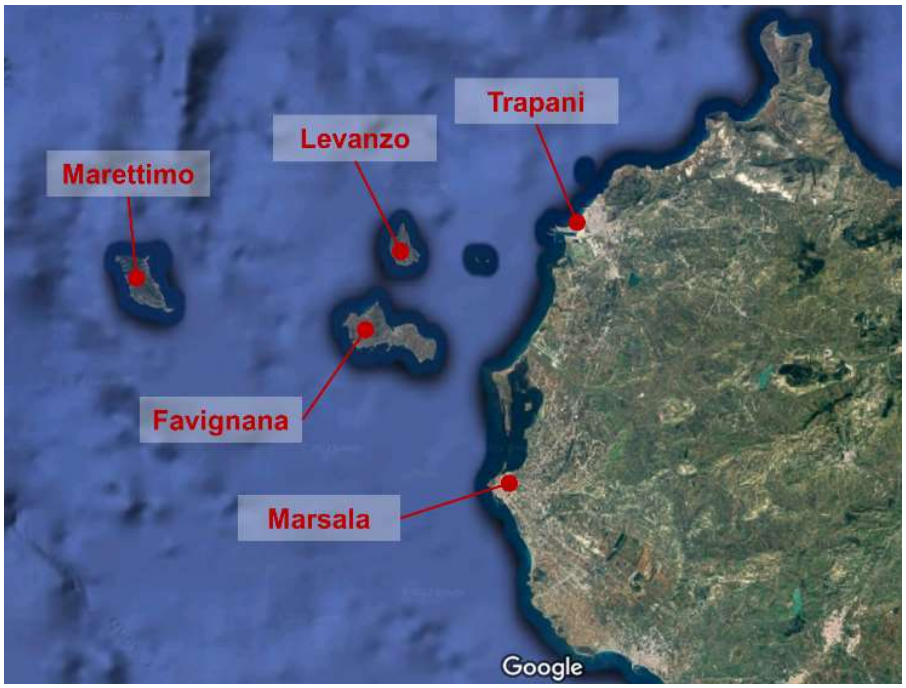

Figure 18 Location of the island of Favignana, Sicily (IT)

The study related to the reactive analysis of the island's electrical system was divided into three distinct phases:

1. **Definition of the Optimal Energy Mix**: in this phase, the design of an energy mix with a high penetration of renewables that is economically sustainable in terms of the Levelized Cost of Electricity (LCOE) was carried out. The impact on network stability was then assessed.

2. **Feasibility Study for the Transition to Electric Mobility**: in the second phase, a technical study was conducted. Based on projections of the development and dissemination of Electric Vehicles (EVs) on the island, this study aimed to evaluate the loading factor of lines and transformers. This evaluation provided information regarding the possibility of introducing new loads without substantial interventions on the island's electrical network.

3. **Frequency Regulation via Vehicle-to-Grid (V2G)**: in the final phase, the hypothesis was made to provide primary regulation services through electric vehicles and to determine the minimum number of charging stations that could allow the installation of 1 MW of photovoltaic capacity without compromising the stability conditions of the network.

4.1.1 Assessing Optimal Energy Mix and Stability in the Island of Favignana

The primary objective of this phase is to evaluate the operational status of a small electrical grid. Two scenarios are being compared: the current situation where the entire energy demand is met by conventional diesel engines, and an alternative scenario that involves incorporating wind turbines, solar photovoltaic panels, and sea wave energy converters. The design of the energy mix is determined by minimizing the Levelized Cost of Electricity (LCOE) for the entire energy mix, as outlined in prior studies [49][50]. About the climatic conditions, precipitations are concentrated during winter. The temperature ranges between 10.5 °C in winter and 30.6°C in summer. A similar trend is associated to the solar radiation, as reported in Figure 19. In contrast, the peak sea wave potential occurs primarily during winter. Regarding wind speed, Table 1 furnishes the parameters of the Weibull distribution for each month at a height of 10 meters above the ground.

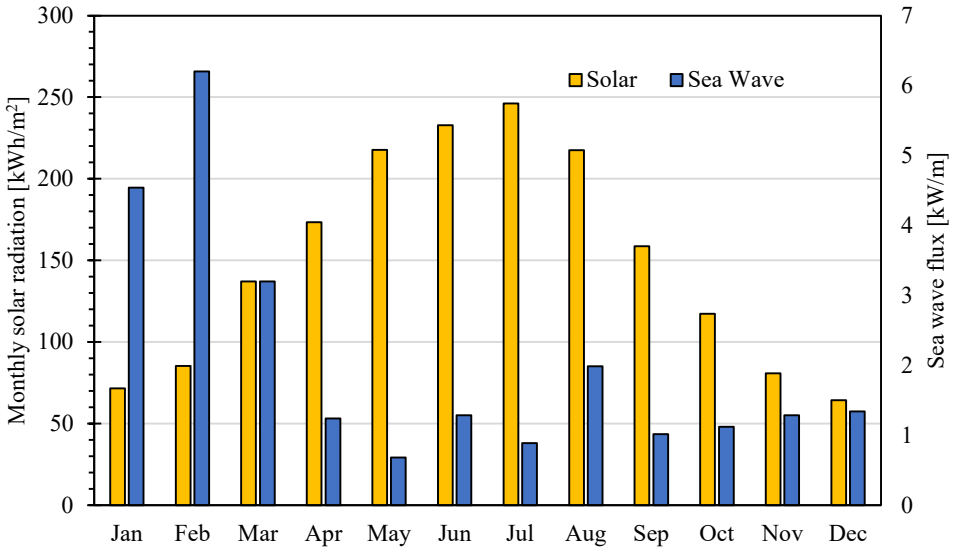

Figure 19 Monthly solar radiation and average sea wave flux in Favignana.

Table 6 Weibull distribution parameters for the sea wave potential in Favignana.

Month	λ [m]	α [-]	Month	λ [m]	α [-]
Jan	6.8	2.1	Jul	4.4	2.2
Feb	7.2	2.3	Aug	4.6	2.3
Mar	6.9	2.1	Sep	5.0	2.1
Apr	5.9	2.1	Oct	5.4	2.0
May	5.4	2.1	Nov	6.3	1.9
Jun	4.7	2.2	Dec	6.7	2.2

The touristic nature of the site largely influences the energy demand. As shown in Figure 20, the peak of the power demand achieves 5 MW in August at 20:00, while the minimal demand is measured in winter (0.75 MW at 2:00). The graph reveals also that the power demand in August could be almost four times higher than in winter.

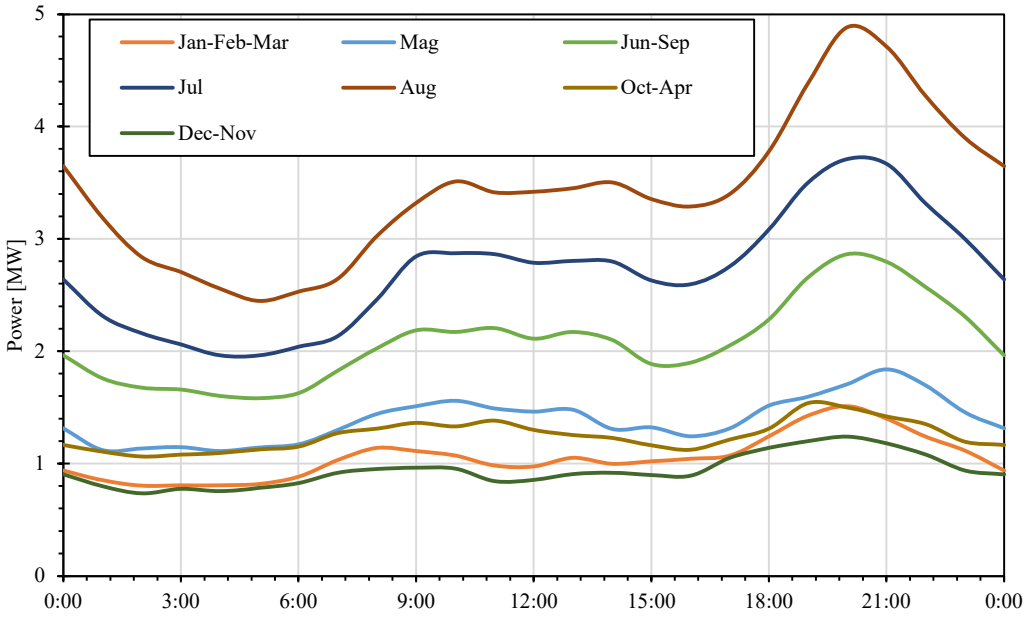

Figure 20 Load diagram in reference days, data provided per month.

In terms of the electrical infrastructure, Favignana is powered by a fleet of seven diesel generators, each with a rated power ranging from 1290 kVA to 1800 kVA, resulting in a total diesel generation capacity of 12.0 MVA. The power grid comprises three primary 20 kV lines connected to the power plant and 41 MV/LV substations. The central area of the island, housing accommodation facilities and tourist attractions, is the focal point for most of the load and substations. This setup reflects the island's tourism-driven economy and shapes the energy

distribution pattern, taking into account the positioning of distribution equipment.

The determination of the optimal energy mix is based on the minimization of the Levelized Cost Of Energy (LCOE). It is a metric used in the energy industry to assess the cost of generating electricity from a particular source over the entire lifetime of a power plant. The LCOE is expressed as the cost per unit of electricity (usually per megawatt-hour, MWh) and is used to compare the competitiveness of different energy technologies. In this study, the LCOE of the entire Energy Mix (LCOEM) is defined by (4. 1), while X expresses the conditions to be fulfilled for the optimization:

$$LCOEM = \frac{\sum_{i=1}^{20} E_f c_f \left(\frac{1+\varepsilon}{1+\tau}\right)^i + C_{r,0} + \sum_{i=1}^{20} \frac{C_{r,A} + C_{f,A}}{(1+\tau)^i}}{\sum_{i=1}^{20} \frac{E_d}{(1+\tau)^i}}$$

(4. 1)

$$\begin{cases} E_f = E_d - \left(P_{sw}e_{sw} + P_w e_w + P_{pv}e_{pv}\right) \\ C_{r,0} = P_{sw}c_{sw,0} + P_w c_{w,0} + P_{pv}c_{pv,0} + P_{inv}c_{inv,0} + Q_{bat}c_{bat,0} \\ C_{r,A} = P_{sw}c_{sw,A} + P_w c_{w,A} + P_{pv}c_{pv,A} + P_{inv}c_{inv,A} + Q_{bat}c_{bat,A} \end{cases}$$

(4. 2)

The proposed combination of renewable energy sources comprises three elements: solar photovoltaic panels (*pv*), wind turbines (*w*), and sea wave energy converters (*sw*). The plan incorporates the utilization of the current fossil fuel plant (*f*) and explores the potential integration of an energy storage system, consisting of an inverter (*inv*) and a chemical battery (*bat*).

Other variables in (4. 1) and (4. 2) include:

- E_d, representing the annual electrical energy demand.
- E_f, denoting the annual energy supplied by fossil fuels.
- c_f, the unitary operative cost for producing electricity from fuels.
- $C_{(r,0)}$ and $C_{(r,A)}$, representing respectively the initial investment (*0*) for the renewable energy sources mix (*r*) and the annual operation and maintenance costs (*A*).
- $C_{(f,A)}$, indicating the annual maintenance cost for the existing power plant.

- The parameter ε, signifying the inflation rate specific to the energy sector.
- τ, representing the interest index.

This comprehensive framework aims to assess the economic and operational aspects of the proposed renewable energy mix, considering various costs, demands, and inflationary factors in the energy sector. Equation (4. 1) serves as a tool for evaluating the financial implications and sustainability of this energy strategy. To standardize economic and energy metrics, total power values for each energy source are employed as scaling factors. Equation (4. 3) defines the annual specific energy production e_{pv} generated by photovoltaic panels. This calculation considers monthly solar radiation $I_{T,i}$, the surface area of the PV plant S_{pv}, and the average efficiency η_{pv}. Additionally, $P_{pv,rated}$ represents the rated power of the photovoltaic plant. This formula provides a quantitative measure of the energy output from the photovoltaic system over the course of a year, considering relevant parameters such as solar radiation, surface area, efficiency, and rated power.

$$e_{pv} = \frac{1}{P_{pv,rated}} \sum_{i=1}^{12} I_{T,i} S_{pv} \eta_{pv}$$

(4. 3)

For wind turbines, determining the annual specific energy production e_w involves considering the wind speed distribution in a discretized manner. This distribution is characterized by periods $t_{j,i}$ during which a specific wind speed class v_j is measured. The term $\psi\langle v_j \rangle$ represents the power output function associated with the chosen wind turbine. This function encapsulates the relationship between wind speed and the power produced by the wind turbine. By incorporating information about wind speed distribution and the power output function, the formula for e_w aims to quantify the energy generated by the wind turbine over the course of a year.

$$e_w = \frac{1}{P_{w,rated}} \sum_{i=1}^{12} \sum_{j=1}^{n} \psi\langle v_j \rangle \, t_{j,i}$$

(4. 4)

Concerning sea wave energy, Equation (4. 4), the assessment relies on the monthly average wave energy flux φ_i . This parameter characterizes the mechanical power

of waves per unit of wave front. The formula takes into account additional factors including the diameter (d_C) of the wave energy conversion device, its average energy efficiency (η_{sw}), and the number of hours in the i-th month ($t_{h,i}$). Together, these variables contribute to the determination of the energy output from sea wave sources, providing a comprehensive evaluation based on wave energy flux, device characteristics, efficiency, and monthly time duration.

$$e_{sw} = \frac{1}{P_{sw,rated}} \sum_{i=1}^{12} \varphi_i d_C \eta_{sw} t_{h,i}$$

The total installed power for each renewable energy source is evaluated according to Eq. (4. 5), by assuming a rated power for each technology:

$$P_{sw} = n_{sw} P_{sw,rated}$$
$$P_{pv} = n_{pv} P_{pv,rated}$$
$$P_w = n_w P_{w,rated}$$

(4. 5)

Therefore, the parameters n_{sw}, n_{pv}, and n_w (representing the number of devices for each renewable source) serve as the unknown variables in the optimization problem, specifically in the minimization of Equation 1. The optimization aims to find the values of these parameters that minimize the overall cost while meeting the specified energy demands and constraints.

The subsequent constraints are introduced to guide the optimization process:

- Each source must produce at least 0.5% of the total annual production from RES, in order to justify the introduction of this technology in the energy blend.
- The numbers of installable power plants are limited, by considering environmental constraints.

In this phase, the determination of the size of the energy storage system involves conducting an hourly analysis of the mismatch between the energy demand and the potential production from renewable energy sources (RES). Specifically, the rated power of the inverter is calculated using Equation (4. 6):

$$P_{inv} = 1.1 \max\left[P_{sw}\langle t_{i,j}\rangle + P_{pv}\langle t_{i,j}\rangle + P_w\langle t_{i,j}\rangle - P_d\langle t_{i,j}\rangle\right]$$

(4. 6)

This condition sets a requirement that the inverter must be capable of handling the maximum power imbalance between the production from renewable energy sources (RES) and the local energy demand. Additionally, a 10% margin is included to prevent excessive stress on the inverter. This ensures that the inverter has the capacity to efficiently manage and balance the power variations between RES production and local demand, with a safety margin to account for fluctuations and uncertainties. Regarding the sizing of the energy storage system, the calculation involves identifying the day with the maximum energy imbalance between the uncontrollable renewable energy sources (RES) production and the local energy demand. This is determined using Equation 7:

$$Q_{bat} = 1.3 \max \sum_{j=1}^{24} \left[P_{sw}\langle t_{i,j} \rangle + P_{pv}\langle t_{i,j} \rangle + P_{w}\langle t_{i,j} \rangle - P_{d}\langle t_{i,j} \rangle \right] 1h$$

An increase of 30% is considered for the sizing of batteries. The hourly analysis is performed by considering the climatic data for several years, for each reference day per month, and evaluating the most stressful condition.

The algorithm was implemented for the given case study, resulting in a proposed energy mix that achieves a renewable energy sources (RES) production covering 49.83% of the local energy demand. Key parameters are detailed in Table 2. Concerning the energy storage system, the inverter necessitates a rated power of 14.26 kW, paired with a chemical battery having a capacity of 16.85 kWh. The Levelized Cost of Electricity from the Mix (LCOEM) is calculated to be 274.65 €/MWh, compared to the current diesel price set at 311.77 €.

Table 7 Results of the optimization process and energy mix assessment.

Parameter	Solar	Wind	Sea wave
Unit cost [€/kW]	980.10	1212.57	5020.00
O&M cost [€/kW-y]	12.15	42.12	75.00
Rated power [kW]	3.3	60	40
Number of devices	130	9	7
Total power [kW]	429	540	280
Annual prod. [MWh]	772.97	6056.98	225.17

Performing traditional primary control simulations with the optimized energy mix is a prudent step to ensure the stability and reliability of the power grid. Simulations are carried out on days where the RES/Load ratio is particularly challenging. Critical hours on typical monthly days will be identified, and a disturbance equal to a 5% load loss will be simulated. The primary objectives of these simulations are as follows:

1. **Verification of Power Grid Stability:** assess the stability of the power grid under challenging conditions, considering the optimized energy mix.
2. **Technical Feasibility Check:** evaluate the technical feasibility of the proposed energy mix during critical hours.
3. **Adjustments if Necessary:** if the simulations reveal instabilities or challenges that compromise the reliability of the power grid, consider modifying the energy mix.

The contribution of diesel generators was determined by analyzing hourly typical daily demand profiles for each month throughout the year. This assessment considered three distinct renewable scenarios, characterized by minimum, medium, and maximum shares of renewable energy sources (RES). The contribution of diesel generators was computed on an hourly basis, representing the disparity between the actual demand and the generated renewable energy across the three scenarios. The hourly rate of renewable is calculated as:

$$RES\% = \left(1 - \frac{Diesel}{Demand}\right) * 100 \qquad (4.\ 7)$$

This value is essential for determining the system's inertia. The analysis prioritizes the most challenging scenario for the system, specifically the instance with maximum renewable energy production and the highest proportion of energy supplied by renewable sources (RES). Table 3 outlines the crucial time slots corresponding to this defined critical condition.

Table 8 Summary of critical slots identified.

S.A: average Summer RES/Load ratio	32.9 %
W.A: average Winter RES/Load ratio	62.8 %
S.Max: maximum Summer RES/Load ratio	64.5% (April, 2.00 p.m.)
W.Max: maximum Winter RES/Load ratio	101.6 % (January, 4.00 a.m.)
S.min: minimum Summer RES/Load ratio	4.0 % (August, 10.00 p.m.)
W.min: minimum Winter RES/Load ratio	% (October, 10.00 p.m.)

The conclusions drawn from the analysis are as follows:

- Critical hours are predominantly concentrated in the winter period (October-March). This phenomenon is not solely attributed to lower renewable production during the summer months (April-September), which actually reaches its peak. Instead, it is primarily influenced by higher energy demand during the winter, driven by the tourist nature of the island.
- Under the assumption of maximizing renewable production to meet demand, winter periods exhibit very high percentages of the RES/Load ratio. Notably, there are instances of the ratio exceeding 100 percent, indicating that renewable production surpasses the energy demand. A peak of over 100 percent is observed at 4 a.m. on a typical day in January.
- In contrast to the winter pattern, the RES/Demand ratio in the summer poses no significant concerns. Most summer months, except for spring, remain below the 60% threshold, indicating a relatively comfortable margin between renewable energy production and the island's energy demand.

The primary control simulations are specifically conducted utilizing the classical Linearized single bus area model for frequency control [18] (See Appendix 1). The assessment of system inertia follows the guidelines provided by ENTSO-E [15], employing the already presented equation (2. 12).

As for diesel generators, an inertia value of $H_{diesel} = 1.5\ s$ is assumed, while for PV generators the assumed inertia is $H_{PV} = 0\ s$. Table 9 presents the simulation parameters and the frequency indicators - frequency nadir, Rate of Change of Frequency (RoCoF) and steady-state frequency - related to the critical time slots shown in Table 8.

Table 9 Simulation results for identified critical timeframes.

Timeframe	**S.A**	**S.Max**	**S.min**	**W.A**	**W.Max**	**W.min**
Load [kW]	2177	1160	3512	1046	792	1332
ES coverage [%]	32.9	64.5	4.0	62.8	101.6	19.2
System Inertia [s]	1.01	0.53	1.44	0.56	0.00	1.21
Frequency nadir [Hz]	51.01	51.66	50.70	51.6	52.4	50.84
RoCoF t=0 [Hz/s]	1.50	5.00	0.75	4.75	$\rightarrow\infty$	1.00
Steady-state frequency	50.15	50.26	50.10	50.25	52.4	50.13

The simulation results highlight a notable risk of system instability during the winter period, and the RoCoF emerges as the parameter of greatest concern. The data presented in the tables indicate pronounced frequency drifts in the winter months, with an average RoCoF value of 4.75 Hz/s. This elevated RoCoF poses a significant risk, as it suggests rapid and potentially disruptive changes in system frequency. The concern is that such pronounced frequency drifts can trigger maximum and minimum frequency protections to activate before the effects of primary control can take effect. This situation may lead to the disconnection of generators, triggering a cascade of events and potentially resulting in blackouts. he extreme case labelled as "*W.Max*," where full load coverage is attempted from renewable sources with zero system inertia, is indeed emblematic. While this condition is theoretical, as conventional technologies cannot entirely power the load through inverter-based resources, the information derived from it indicates that, under economic optimum conditions, there are instances where the optimal energy mix may not guarantee safe grid operations. This finding implies that, to ensure the reliable operation of the power system, there might be a need to curtail some renewable generation in favour of conventional generation. This curtailment is necessary to address the lack of system inertia, which is crucial for maintaining frequency stability. However, such curtailment can lead to economic losses and higher CO2 emissions, presenting a trade-off between economic efficiency and system reliability. Indeed, increasing the energy capacity of storage systems to store excess energy during periods of excessively low system inertia is a plausible solution. This strategy helps mitigate the challenges posed by the extreme case with zero system inertia, allowing for the accumulation of surplus renewable energy during favourable conditions for later use when needed. Additionally, the use of technologies for providing regulation services from converters can play a crucial role. These technologies, often associated with advanced control systems,

can dynamically adjust the output of converters to help regulate frequency and maintain grid stability. By incorporating such regulation services, it's possible to enhance the reliability of the power system without compromising the presented model or the economic efficiency of the overall system.

4.1.2 Feasibility Study for the Transition to Electric Mobility

The second phase of the study aims to evaluate the technical impact of EVs in the existing power grid of the island. In the upcoming years, a significant proliferation of electric vehicles and an equal number of charging stations is expected on the island. This development could pose serious challenges, if not compromise, the existing infrastructure on the island, especially transformers, lines, and substations. The study was conducted using the specialized software NEPLAN, which allowed for assessments of potential power flows that would affect the network in the case of a massive and rapid integration of electric vehicles. As previously noted, Favignana relies on a fleet of seven diesel generators with rated powers ranging from 1300 kW to 1800 kW for its power supply. The power grid is composed of three 20 kV lines originating from the power plant and includes 41 MV/LV substations (32 belonging to the DSO and 9 to private users). Among the three main lines, Line 1 is the longest and most extensive, covering the entire island, while Lines 2 and 3 are shorter, primarily feeding the city centre. The configuration of the three main lines, substations, and the location of the diesel power plant can be observed in Figure 21 Favignana MV power grid.Figure 21.

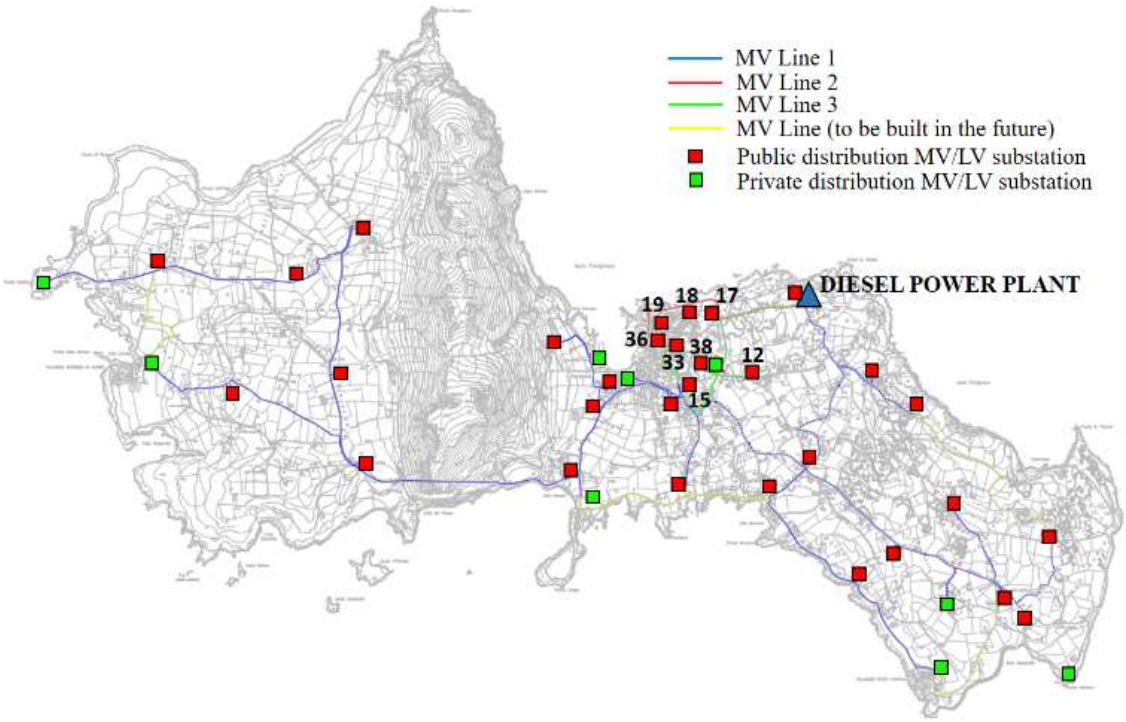

Figure 21 Favignana MV power grid.

The analyzed scenario assesses the impact of EVs on the island's power grid as they consume power for recharging through home charging stations. The initial phase of the analysis involves sizing the variables, including the number of charging stations and assumptions about the size of the car fleet. Based on demographic statistics from 2016, Favignana has approximately 2500 households (with a resident population of 4292 individuals). According to data from the Automobile Club of Italy, there were 2446 vehicles in Favignana as of December 2016. Assuming a 20% penetration rate for Electric Vehicles (EVs), the presence of 500 EVs is considered. According to [51], which provides information about the number of EVs by segment according to the Italian market trend, the analysis considered only cars belonging to small/medium size market segments, distributed as follows:

- 100 Smart fortwo (20%),
- 150 Renault Zoe (30%),
- 200 Nissan Leaf (45%),
- 50 Nissan Leaf e+ (10%).

Table 10 shows the main features of the vehicles considered. The analysis considered a battery efficiency of 0.9 and an average daily distance covered of 20

km for each vehicle (given that there are a total of 50 km of streets on the island) to evaluate the average daily energy consumed.

Table 10 Features of the considered vehicles.

Vehicle Model	BatteryCapacity[kWh]	Consumption range [kWh/km]	Battery efficiency	Average daily distance [km]	Average daily energy consumed [kWh/day]
Smart	17.6	0.11	0.9	20	2.44
Renault	52	0.165	0.9	20	3.66
Nissan	40	0.148	0.9	20	3.28
Nissan	63	0.161	0.9	20	3.57

The analysis considered two single-phase AC recharging modes with constant charging until completion:

- Slow charge: Power consumption of 2.3 kW, suitable for domestic users with a 3 kW contract.
- Fast charge: Constant power consumption of 3.4 kW.

To safeguard the useful life of the vehicle battery and ensure a minimum emergency autonomy to the user, a State Of Charge (SOC) between 30% and 80% was considered for each charging and discharging cycle. Therefore, the available battery capacity is 50% of that shown in Table 10. Table 11 summarizes these considerations for the whole fleet of vehicles and for both charging modes.

Table 11 Hypotheses for EV fleet simulation.

Vehicle Model	N. of vehicles	Available capacity [kWh]	Consumption time [day]	Car to charge (each day)	Charging time [h]	
					Slow charge (2,3kW)	Fast charge (3,4kW)
Smart Fortwo	100	8.8	3.6	27.7	5.1	3.4
Renault Zoe	150	26	7	21.1	15	10.2
Nissan Leaf	200	20	6	32	11.6	7.8
Nissan Leaf e+	50	3.5	8.8	5.6	18.2	12.3

Three scenarios are considered for each charging mode:

1 100 % of the vehicles start charging at 18:30 (when get home after work).
2 100% of the vehicles start charging at midnight (assuming a minimum of persuasion with incentives to charge at night).
3 charging during the day in three blocks:
   3.1 : 33% from 10:00;
   3.2 : 33% from 13:30;
   3.3 : 33% from 17:00.

Since users are concentrated in the city centre of the island, with the load evenly distributed among substations 17, 18, 19, 33, 36 (fed by Line 2) and 12, 15, 38 (fed by Line 3), the following Table 12 depicts the additional load required at each of these substations for the three scenarios mentioned and the two charge modes considered.

Table 12 Extra load for each substation per charging mode.

	Slow Charge mode				**Fast Charge mode**			
Scenario 1	18:30-23:30	23:30-5:30	5:30-9:30	9:30-12:30	18:30-22:00	22:00-2:30	2:30-4:30	4:30-6:30
Scenario 2	24:00-5:00	5:00-11:00	11:00-15:00	15:00-18:00	24:00-3:30	3:30-8:00	8:00-10:00	10:00-12:00
Extra load [kW]	18,97	12,93	5,82	1,3	28,05	19,12	8,6	1,9
Scenario 3.1	10:00-15:00	15:00-21:00	21:00-1:00	1:00-4:00	10:00-13:30	13:30-18:00	18:00-20:00	20:00-22:00
Scenario 3.2	13:30-18:30	18:30-24:30	24:30-5:30	5:30-8:30	13:30-17:00	17:00-21:30	21:30-23:30	23:30-1:30
Scenario 3.3	17:30-22:30	22:30-4:30	4:30-8:30	8:30-11:30	17:30-21:00	21:00-1:30	1:30-3:30	3:30-5:30
Extra load [kW]	6.26	4.26	1.92	0.42	9.25	6.31	2.84	0.63

To account for the significant load variations between winter and summer, attributed to the substantial increase in population during the summer holidays (population growth of more than 10 times), the simulations were conducted for both a summer scenario (high load) and a winter scenario (low load). While load variations are moderate in most of the examined substations, some substations

experience a notable increase in power demand. In particular, the worst-case scenario is the simultaneous charging of all vehicles at 18:30 (Scenario 1). In order to evaluate the impact of the charging infrastructure on the island's electrical system, this worst-case scenario is addressed, as the other cases represent less stress on the grid and its components. Figures 22 to 25 show the load diagrams of the most impacted substations (C17 and C38) and the main power plant. The reported cases, referred to as Scenario 1, include winter - slow charge, winter - fast charge, summer - slow charge, and summer - fast charge.

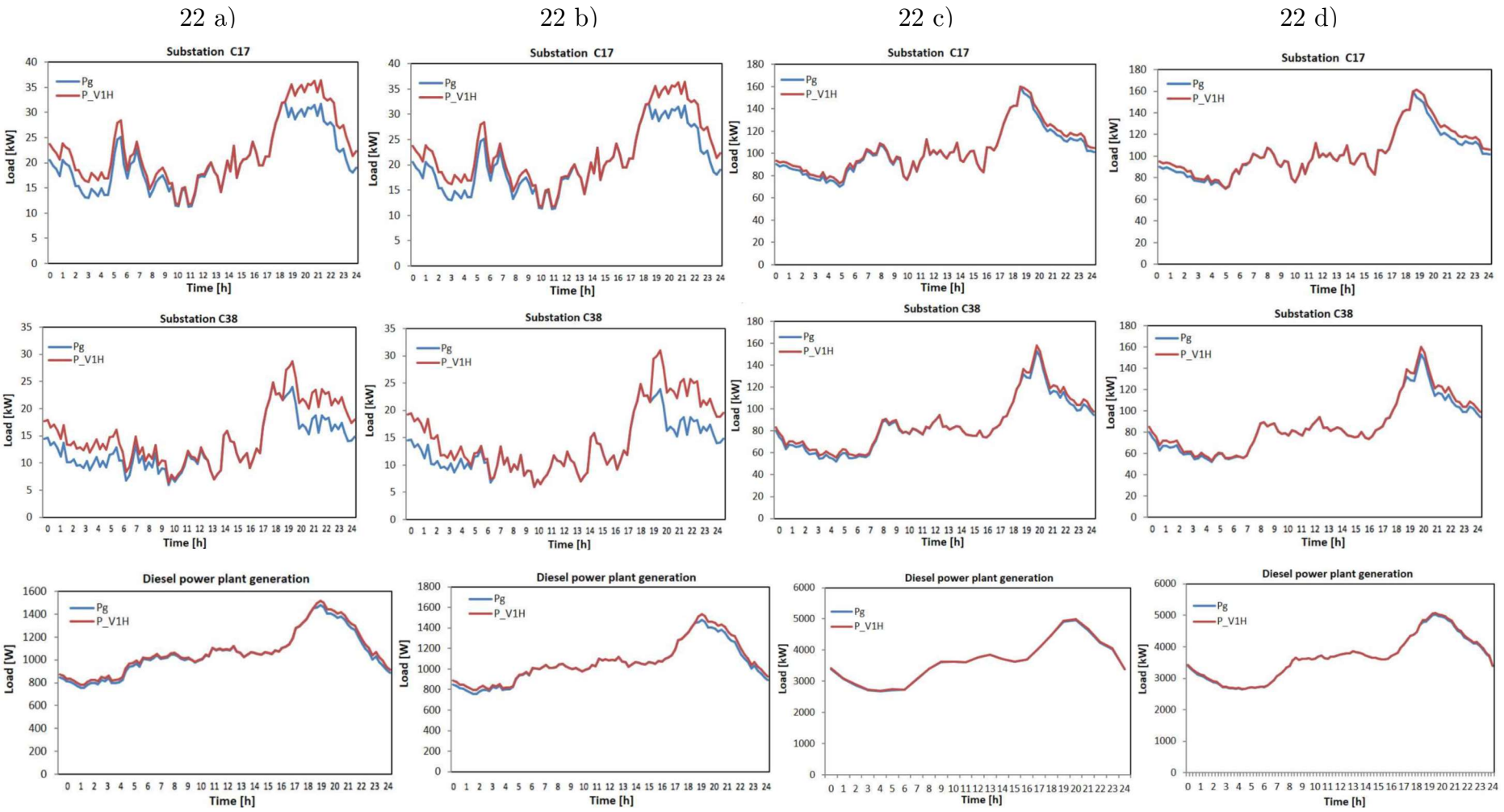

Figure 22 Load diagrams for substations C17, C38 and for the main diesel power plant. In order: a) winter, slow charge scenario; b) winter, fast charge scenario; c) summer, slow charge scenario; d) summer, fast charge scenario.

In the graphs above, "*Pg*" represents the initial load profile without Plug-in Electric Vehicles (PEVs), while "*P_V1H*" illustrates the adjusted load profile in the presence of PEVs. Analyzing the load diagrams presented allows to conclude that:

- During the winter, significant fluctuations are observed above the base load, representing the standard load without the inclusion of charging vehicles. These deviations from the base load can exceed 30%, and during the hours when vehicles are charging, the total load has the potential to double, as illustrated in Figures 22 a) and 22 b).
- During the summer, there are minor fluctuations from the base load attributed to E) recharging. In the most extreme scenario, this deviation is approximately 10%, as depicted in Figures 22 c) and 22 d).

The load profiles, along with those for the substations considered for EV charging, served as input data for NEPLAN simulations on the island. Across all cases and scenarios scrutinized, the maximum load consistently remains below the rated power of the involved substations. Examining Table 13 Substations load conditions under V1H demand., which outlines the available capacity of each substation following the integration of PEVs in the most challenging scenario, it is evident that the power consumed due to Vehicle-to-Home (V1H) operations significantly falls below the rated transformer size, except for substation 12. Furthermore, it is noteworthy that the maximum load consistently remains below the rated power of both the power plant (12MW) and the designated substations. The currents on the existing power lines consistently stay within acceptable flow rate values, and the variations in load permit a secure and stable operation of the system.

Table 13 Substations load conditions under V1H demand.

Substation	**Transformer rated power [kVA]**	**Max. load due to V1H [kW]**	**Available capacity [% P_n]**
12	160	156	2.5
15	2x1250	634	74.6
17	400	161	59.8
18	2x800	384	76.0
19	800	526	34.3
33	2x800	465	70.9
36	630	276	56.2
38	2x630	160	87.3

The conducted simulations indicate that the power system of Favignana is well-prepared to accommodate a significant influx of EVs with domestic charging. Contrary to potential concerns, electric mobility does not appear to be as destabilizing as anticipated, particularly when vehicle charging is scheduled during off-peak hours. It is crucial to note that the positive impact is contingent on the inclusion of renewables in the energy mix. Without the integration of renewable sources, the effects are either negligible or potentially detrimental in the widespread deployment of EVs.

4.1.3 Simulation Study of V2G Recharge Points in Favignana

The concept of Vehicle-Grid Integration explains how electric vehicles can be employed not only as means of mobility but also as tools to provide grid services. The EV, therefore, becomes an exploitable resource for the above-mentioned purposes in two different modes:

- "Smart charging" (V1G) involves providing network services exclusively through unidirectional flows of energy (from the network to the vehicle), appropriately modulated in time.
- "Vehicle-to-grid" (V2G) involves providing grid services through the management of bidirectional flows of energy between the grid and the vehicle.

The final part of the study on the island of Favignana aims to determine the impact of V2G charging points in regulating Favignana's electrical system after the installation of a significant amount of PV systems. The objective is to determine the minimum number of charging points needed to provide primary frequency regulation and ensure the same frequency deviations in the event of a disturbance as in the absence of PV plants. The study employs a simulation approach in the Matlab/Simulink environment to analyse the dynamics of the isolated power system with 1 MW of PV installations and the contribution of V2G-enabled electric vehicles to frequency regulation.

The analysis of the grid in different load and generation conditions on the island of Favignana involves several scenarios simulated through the following steps:

1. Collection of total electric load data in summer and winter days.

2. Evaluation of PV generation using the online software PV-GIS.

3. Calculation of the hourly electrical inertia of the system using the formula provided by ENTSO-E to determine time constants of the dynamic model.

4. Identification of the time when the inertia value is lowest during both summer and winter days (*critical timeframes*) when the most severe conditions for grid stability occur.

5. Consideration of a scenario with only synchronous generation, evaluating the magnitude of the disturbance causing a steady-state frequency deviation according to ENTSO-E requirements for full activation of primary control reserves. This step is performed for both winter and summer days.

6. Performing dynamic simulations with the introduction of PV generation.

7. Assuming a certain installed power of the Vehicle-to-Grid (V2G) charging points, allowing both charging and discharging of vehicle batteries.

8. Modifying the dynamic model in Simulink by adding a closed loop to simulate the contribution of the charging columns to the FFR.

9. Repeating dynamic simulations with the same power disturbances assumed at point 5) but considering the contribution of V2G charging points.

The electrical inertia of the system is estimated hour by hour by applying the equation:

$$H_h = \sum_{i=1}^{n} \frac{H_{sync,i} \cdot S_{n,sync,i,h} + H_{PV,i} \cdot S_{PV,i,h}}{P_{load,h}} \quad (4.\ 8)$$

Where the index h indicates the hour considered, the index I indicates the *i-th* synchronous machine or the *i-th* inverter, and the index n indicates the total number of generators. While:

- H_h is the overall system inertia at the hour h [s];
- $H_{sync,i}$ is the inertia of the *i-th* synchronous generator [s];
- $H_{P\ V,i}$ is the inertia of the *i-th* inverter of a PV generator [s];

- $S_{n,sync,i,h}$ is the complex power supplied by the *i-th* synchronous machine during the the hour h [MVA];
- $S_{PV,i,h}$ is the complex power supplied by the *i-th* PV inverter during the hour h [MVA];
- $P_{load,h}$ is the load demand in the hour h [MW].

Since inverter-based resources have no rotating parts, the value of $H_{PV,i}$ is equal to zero, so equation (4. 8) becomes:

$$H_h = \sum_{i=1}^{n} \frac{H_{sync,i} \cdot S_{n,sync,i,h}}{P_{load,h}}$$

(4. 9)

Equation (4. 9) illustrates that the incorporation of zero-inertia generators, such as PV generators, results in a reduction of the overall inertia of the system, leading to a deterioration of the stability conditions of the power grid.

The primary assumption of the proposed method is to prioritize dispatching solar-generated energy and utilize rotating generators solely for supplying the portion of the load not met by PV. In this context, the method considers the most critical conditions from an inertia perspective, aiming to restore stability levels to those observed before the introduction of PV, facilitated by the use of V2G charging points. The following equation is employed to calculate the power supplied to the load by synchronous generators in the presence of PV generation:

$$P_{n\,synch,h} = P_{load,h} - P_{PV,h}$$

(4. 10)

where:

- $P_{n\,sync\ ,h}$ is the active power supplied by synchronous generators at the hour h [MW];
- $P_{load,h}$ is the load demand at the hour h [MW];
- $P_{PV,h}$ is the active power of the PV generators obtained as output of the PVGIS simulations [MW].

As of now, renewable energy generation does not exert a substantial influence on the system in terms of installed capacity. However, it is anticipated that renewable production will escalate in the near future, aligning with the goals

outlined in the Ministerial Decree published on February 14, 2017 (Minor Islands Decree) [52]. In this investigation, it is posed that 1 MW of PV production will be implemented on the island. The simulations aim to anticipate the performance of the island's electrical system in terms of stability following the installation of the PV plant. The objective is to examine the new frequency parameters post a disturbance and assess the quantity of V2G charging points needed for an optimal integration of these solar plants.

To attain this objective, three scenarios are taken into account:

1. **Scenario 1**: Load supplied exclusively through diesel generation.

2. **Scenario 2**: Load supplied through a combination of diesel and PV, with priority dispatching of energy produced by the solar source.

3. **Scenario 3**: Same supply conditions as in Scenario 2, but with the incorporation of V2G charging points contributing to frequency primary regulation.

The V2G charging points are considered to possess a rated power of 10 kW with an efficiency of 96 %. Additionally, it is assumed that the charging points are equipped to offer regulation services, implying that a car with adequate energy availability is connected to each point to facilitate both absorption and power. The assumed conditions for the island power system reflect an average load, as determined through various measurement campaigns and technical reports [53] then simulations for typical summer and winter days are conducted. In Scenario 1, the system's inertia is assumed to remain constant throughout the day, relying entirely on the dynamic characteristics of the operational synchronous machines. However, the substantial variations in load on an island like Favignana necessitate considering different inertia values for summer and winter periods. During summer, the island experiences its annual peak load, requiring the use of larger generators with greater inertia to meet the demand. Conversely, in winter, generators with smaller size and less inertia are utilized due to lower demand. Taking these considerations into account, to assess the two periods separately, simulations were carried out with two distinct inertia values for the rotating generators:

- Summer inertia, $H_s = 2$ s

- Winter inertia, $H_w = 1.5$ s

In Scenario 2 and 3, the overall inertia of the power system is calculated hour by hour using Equation (4. 9), considering the significant contribution of PV energy production. The trend of overall inertia during the summer and winter reference days is illustrated in Figure 23. The blue lines represent the inertia in Scenario 1 (which is constant), while the orange lines represent the inertia in Scenario 2. The diagrams show that the variations in inertia are more pronounced in winter than in summer. This is not due to higher photovoltaic generation in winter but rather to lower energy demand, which is mostly supplied by renewable sources. The critical timeframes with the smallest inertia values (11:30 AM in summer and 4:30 PM in winter) were used for conducting simulations in the three defined scenarios.

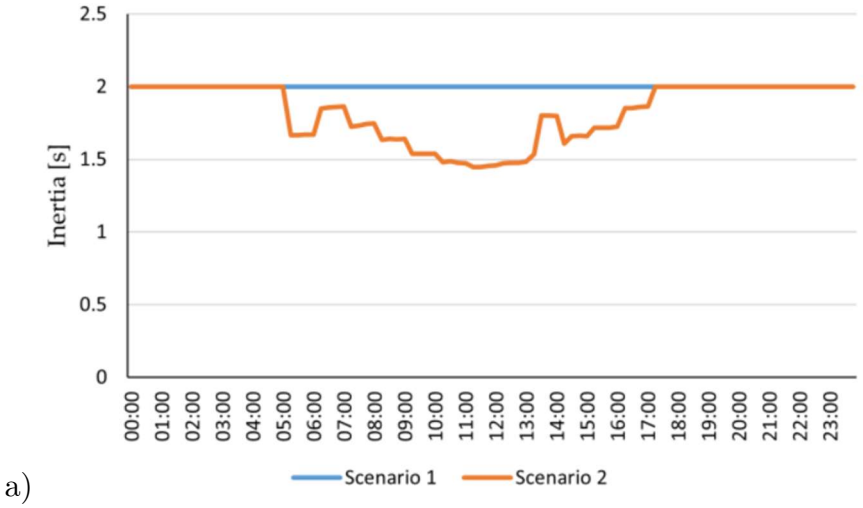

a)

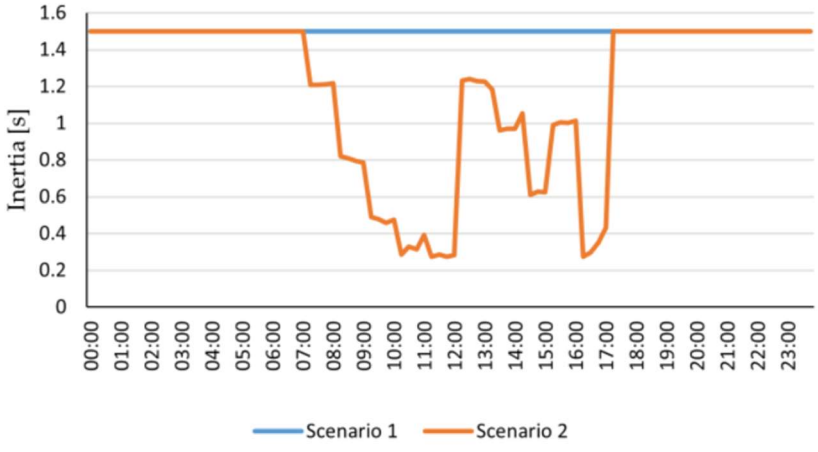

b)

Figure 23 Inertia daily trend for summer (a) and winter (b) reference days.

Once critical timeframes for summer and winter days are identified, dynamic simulations of Favignana's power system are initially performed in Scenario 1; the goal of this first simulations is to evaluate the magnitude of the power disturbance that causes a steady state frequency error equal to $\Delta F_{stat} = 0.2\,Hz$. Additionally, to model a significant load disconnection or a failure in a medium voltage line, the assumed disturbance is considered negative. Moving forward, the following indices will be employed to distinguish various quantities:

- S for Summer;

- W for Winter;

- 1 for Scenario 1;

- 2 for Scenario 2;

- 3 for Scenario 3;

In Table 14 the data for the simulations are reported. Specifically, the disturbances that causes the target steady-state frequency deviation are equal to:

- $\Delta P_{D,S} = -335\,KW$ for summer day;
- $\Delta P_{D,W} = -110\,KW$ for winter day.

Table 14 Simulation data for scenarios 1 and 2

Scenario 1, Summer		**Scenario 2, Summer**	
Initial load $P_{load,0}$	3692 kW	Critical Timeframe	11:30 am
Disturbance ΔP_d	-335 kW	Photovoltaic power P_{PV}	1017 kW
System Inertia H_{sys}	2 s	System Inertia H_{sys}	1.45 s
Scenario 1, Winter		**Scenario 2, Winter**	
Initial load $P_{load,0}$	1113 kW	Critical Timeframe	4:30 pm
Disturbance ΔP_d	-110 kW	Photovoltaic power P_{PV}	910 kW
System Inertia H_{sys}	1.5 s	System Inertia H_{sys}	0.27 s

Figure 24 illustrates the frequency trends in Scenario 1. It is evident that the simulated disturbance results in a steady-state deviation of 0.20 Hz, as indicated by the steady-state frequency value.

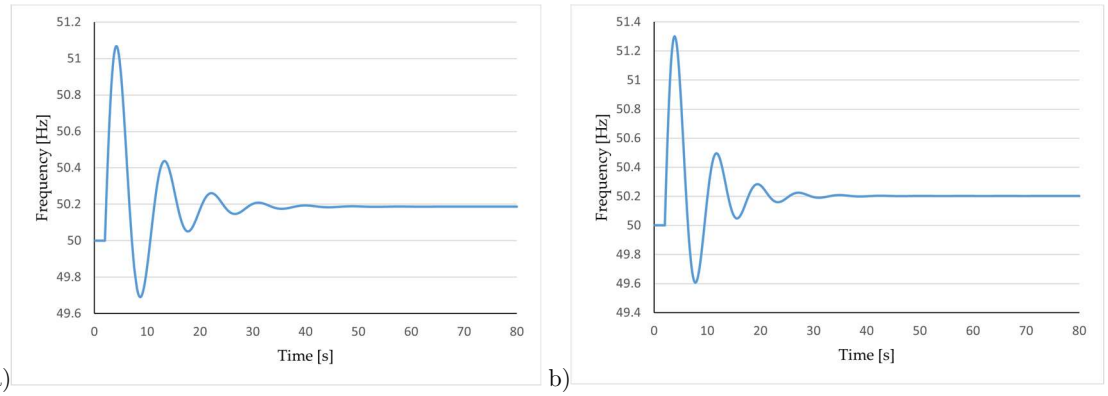

Figure 24 Frequency trend in scenario 1, summer (a) and winter (b) reference days.

After determining the magnitude of the disturbance, simulations for primary control are carried out in Scenario 2. Figure 25displays the frequency trends in Scenario 2 for summer and winter days, respectively. It is evident from the graphical representation that the system's frequency-related parameters are considerably affected by the reduction in inertia.

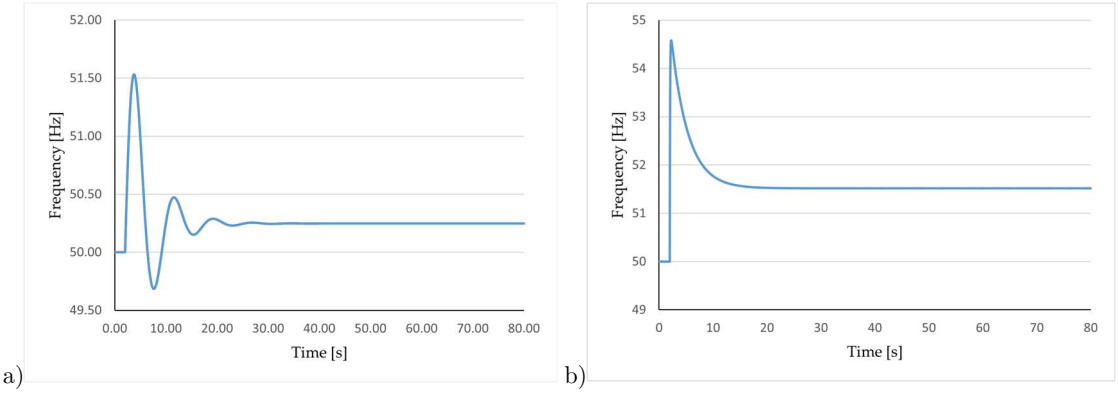

Figure 25 Frequency trend in scenario 2, summer (a) and winter (b) reference days.

The issue is less pronounced in the summer, with the frequency nadir and steady state frequency deviation being:

- $f_{nadir,S,2} = 51.53$ Hz
- $F_{stat,S,2} = 0.26$ Hz

These values are comparable to those of Scenario 1. However, in winter, the minimum stability conditions for network operation would not be met, with the frequency nadir and steady-state frequency deviation being:

- $f_{nadir,W,2} = 54.27$ Hz
- $F_{stat,S,2} = 0.96$ Hz

Given that the upper frequency limit is 51.5 Hz, a disturbance of this magnitude would trigger the maximum frequency protections. This would result in the intervention of the protections, leading to a loss of synchronism and, consequently, the detachment of the generators. Numerous simulations were carried out for Scenario 3, each assuming an increasing number of charging points participating in regulation. Figures 8 and 9 depict the values of the steady-state frequency deviations as a function of the number of V2G columns. The graphs illustrate a decreasing trend in the steady-state frequency deviation value as the number of active charging points increases. The value eventually equals that of Scenario 1 when at least 6 V2G charging points are active in summer and 9 in winter.

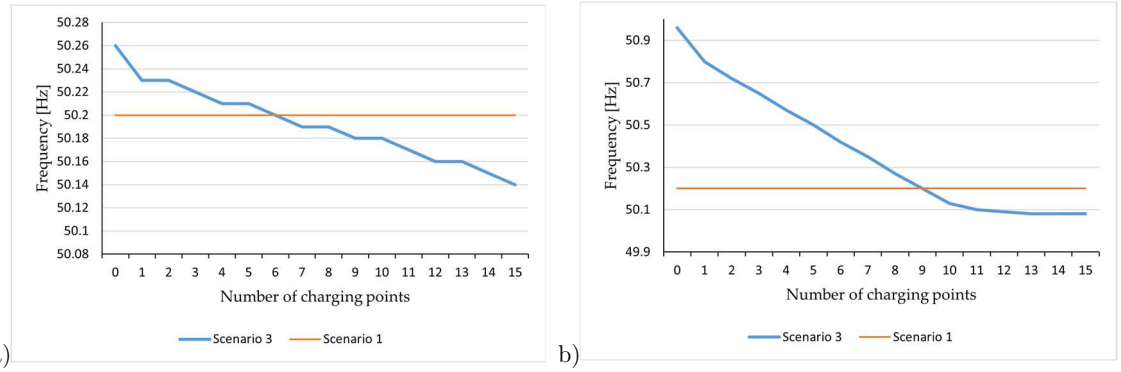

Figure 26 Steady state frequency deviation as a function of the number of V2G columns, summer (a) and winter (b) reference days.

Finally, Figure 27 depicts the frequency trends in Scenario 3, assuming the presence of the minimum number of V2G recharge points just identified, while Table 15 provides the data from the simulations conducted for all the considered scenarios.

a)

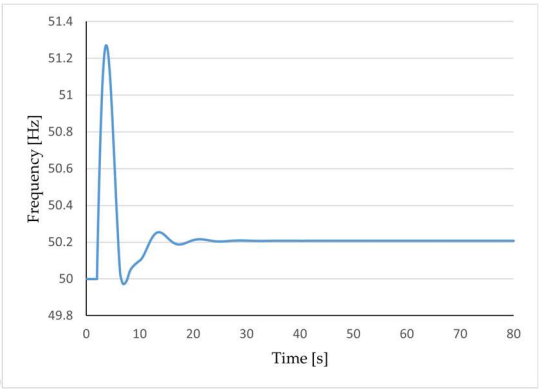

b)

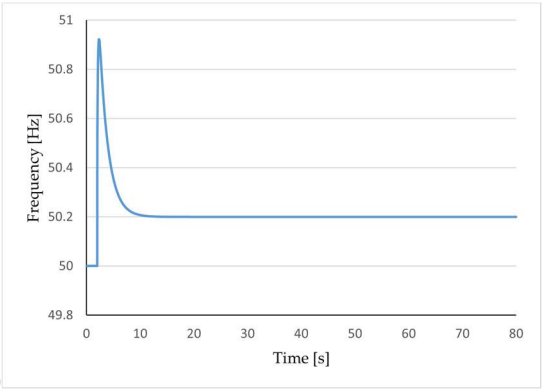

Figure 27 Frequency trend in scenario 3, summer with 6 V2G recharge points (a) and winter with 9 recharge points (b).

Table 15 Summary of simulations results for all scenarios.

Scenario	**PV [kW]**	**V2G points**	**f_{nadir} [Hz]**	**Δf_{stat} [Hz]**
1.S	0	0	51.07	+ 0.20
1.W	0	0	51.30	+ 0.20
2.S	1017	0	51.53	+ 0.26
2.W	910	0	54.27	+ 0.96
3.S	1017	6	51.10	+ 0.20
3.W	910	9	50.57	+ 0.20

The simulations of primary frequency regulation have demonstrated that, during the identified critical timeframes, a small number of V2G charging points enables the seamless integration of the aforementioned photovoltaic power without compromising grid stability. This brings the frequency indicators to levels comparable to those of a system based on diesel generation. However, it's important to note that the study does not address the allocation of charging points on the island or the availability of electric vehicles to provide regulation services. Regarding power flows in the network, phase 2 indicates that, according to different scenarios involving the number of vehicles and charging times, the Favignana network can accommodate this load demand without requiring significant interventions. After identifying the minimum number of V2G charging points, a potential continuation of the study could involve determining the remuneration for owners offering their vehicles for grid services and assessing the economic feasibility of the associated business model.

4.2 The Country of Malta

As mentioned in the introduction of this thesis, studies were conducted at the University of Malta during the three-year doctoral program. Throughout this six-month period, the Maltese electrical system was examined. Despite being interconnected with Italy, it exhibits all the vulnerabilities of a low-resilience or even isolated system. The choice of the location for this international period was not arbitrary but carefully considered based on the thesis and research project to be undertaken. From this experience, a paper was produced and was awarded the "Best Student Paper" at the AEIT International Conference 2023. Specifically, a simulation study was conducted, proposing the use of Grid-Forming converters in the Maltese MV network to provide regulation services by photovoltaic plants on the island.

4.2.1 The Grid Forming Control

The term "Grid-Forming" (GFM) first appeared in 2001 [54], but the initial proposal for using inverters to support the grid during power imbalances and frequency deviations can be traced back to 2008 with the introduction of the Virtual Synchronous Machine (VSM) concept [55]. In essence, a GFM inverter is a converter that enables the direct control of the voltage at its terminals independently of the grid voltage. This sets GFM apart from classical Grid-Following (GFL) converters, where the directly controlled output is the current. Conceptually, a GFM converter can be represented, in its simplest form, as a voltage source with a low series impedance, while a GFL converter is represented, in a dual manner, as a current source with a high parallel impedance.

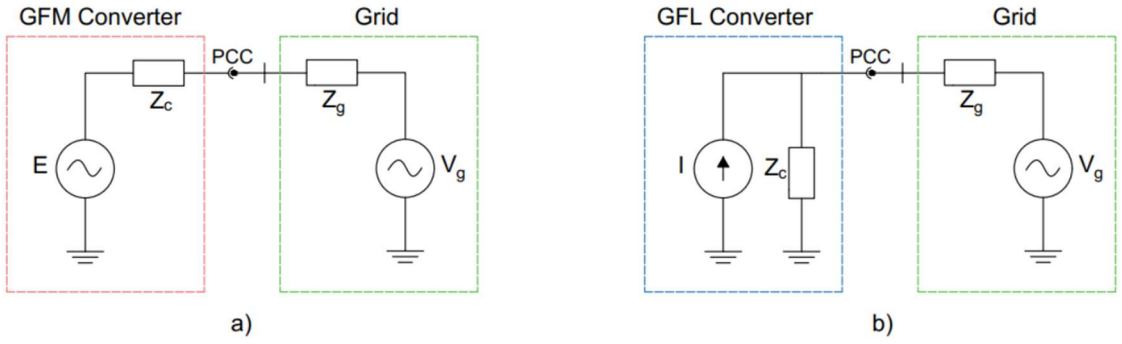

Figure 28 Basic representation of a GFM converter (a) and of a GFL converter (b).

GFM converters have the capability to provide a voltage signal even in the absence of load or grid voltage. This is in contrast to GFL converters, which necessitate the presence of a network signal for synchronization and current injection. The concept of GFM was initially introduced for applications in smart grids and autonomous power systems; however, GFM converters are also being explored as a compelling solution to support the stable operation of large, interconnected power systems with high penetration of non-synchronous generation interfaced through power electronics. Although the behavior of GFM inverters can be beneficial for the network, the imposition of the voltage phasor may result in abrupt increases in current. In extreme cases, this could lead to damage to the components. This contrasts with GFL inverters where the amplitude of the current phasor is directly controlled and cannot exceed predefined thresholds. Over the past few years, numerous GFM control structures have been proposed and analyzed, they can be classified into the following classes:

- Droop methods;
- Power synchronization control;
- Synchronverter;
- Virtual synchronous machines;
- Matching control;
- Direct power control;
- Others;

Among the various methods found in the literature, the one studied and implemented for the current case study belongs to the "power synchronization control" class. The choice was made based on previous studies that demonstrated its effectiveness for similar applications [56][57].

The grid-forming control implemented is shown in Figure 29.

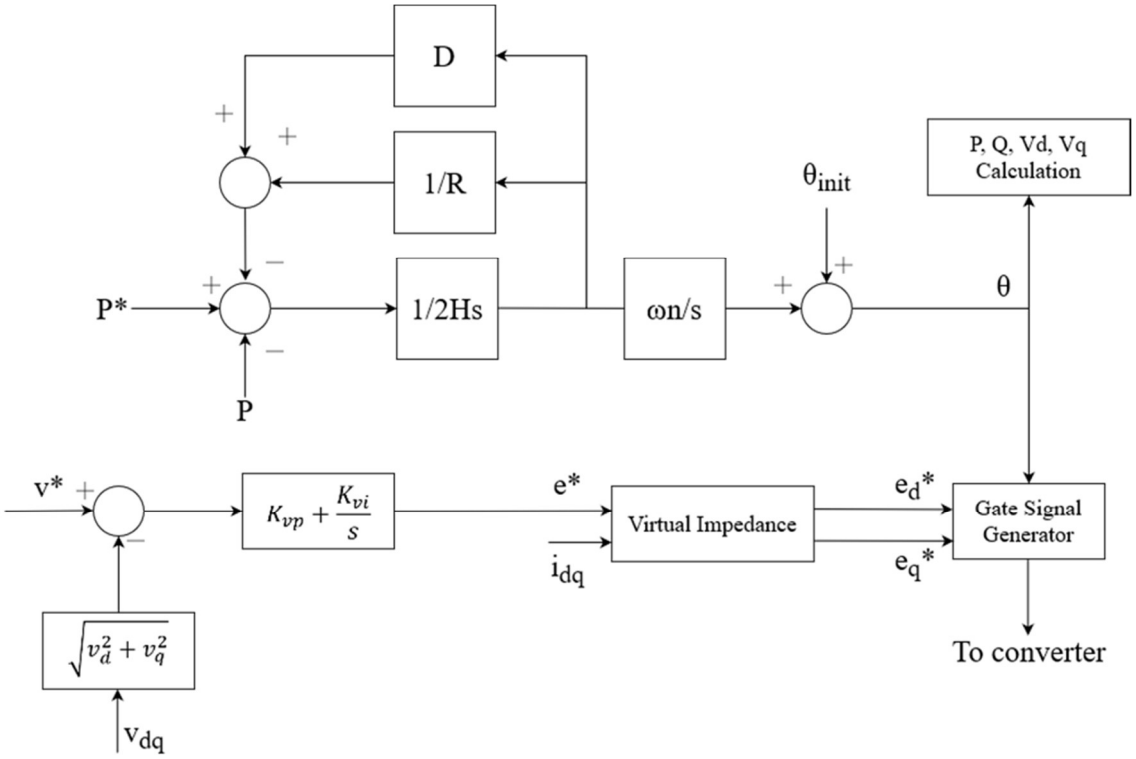

Figure 29 Block diagram of the implemented GFM control.

The principle of this control consists in emulating the behavior of a synchronous machine through the implementation of the swing equation. The power reference is compared with the power at the PCC, the power error is processed by a system of blocks that simulate inertia H, damping D, and droop R. The result of these operations is an angular speed which is multiplied by the nominal angular speed ω_n and integrated. Finally, the output is added to the initial reference angle θ_{init} to obtain the angle θ needed for the transformations in the synchronous rotation frame (SFR). The voltage controller is of the proportional-integral type, the voltage error is calculated as the difference between the reference and the voltage at the PCC. The proportional and integral gains of the controller are respectively K_{vp} and K_{vi}, the resulting voltage e^* is processed by a virtual impedance block, $R_v + jX_v$, in which the current at the PCC in the SFR i_{dq} is used for the calculation of the voltage drop. The resulting output is the reference voltage in SFR e_d^* and e_q^* these signals will be used, together with the theta angle, for converter modulation. The H and D parameters of the synchronization loop assume particular importance in the control. If chosen appropriately, they enable the converter to operate relatively slowly, with response times on the order of seconds.

In this manner, photovoltaic plants can contribute inertia to the grid, supporting traditional primary control without replacing it.

The analysis of the literature revealed a large number of control strategies and proposed schemes but a lack of references to pilot projects and utility-scale implementations. To contribute to filling this research gap, a study was conducted on demonstrators and pilot projects implementing GFM for various applications in different parts of the world [JA.2]. The result of the research identified the main potential of this technology in large-scale power applications to experimentally assess its impact in different systems. The results of the study are reported in Table X. It is evident how the push for new installations started at the end of the last decade; pioneers in this field are Australia, thanks to an open and diversified market that allows for experimentation. Europe and the USA contribute to experiments with the aim of standardizing the services offered by the end of this decade. The majority of the analyzed pilot plants are connected to the MV grid. This choice can be attributed to several factors. One possible explanation is that GFM converters are often associated with BESS, PV systems, or wind generators. Additionally, the targets and services offered by these pilot plant demonstrators are more aligned with the needs of distribution networks rather than transmission networks. Distribution networks are closer to end-users and distributed energy resources, therefore, the deployment of GFM converters at the MV level allows for better integration with existing distribution infrastructure and aligns with its the services and requirements. The rated power of the demonstrators varies depending on the specific application. There are two distinct groups: plants with a rated power close to 1 MW and systems with a rated power of tens of megawatts. From this analysis, it can be inferred that there is greater interest in grid-forming technologies at an industrial scale. The motivations behind this interest can be attributed to both the grid's needs, where GFM technologies are seen as an optimal solution, and legislative advancements that facilitate the immediate integration of these plants into the respective energy markets. The versatility of GFM technology enables its application in various scenarios, ranging from grid support to market operations. The analysis conducted highlights a particular emphasis on the provision of ancillary services in MV and HV networks. Additionally, the capability for black-start from non-conventional

energy sources is of significant interest. The ability to initiate a black-start from non-conventional energy sources is considered a key feature of grid-forming technology. This feature holds strategic importance, as it allows for better system management and resilience, especially in the context of future decarbonization efforts.

Table 16 Summary of the analyzed pilot projects and demonstrators [JA.2].

Project	Owner	Kind of Owner	Location	Year	Rated Power [MW]	Energy Capacity [MWh]	Voltage Level	Applications*
Zurich BESS	EKZ	Energy company	Switzerland	2012	1	0.58	LV-MV	AS, EM, IO
Ausnet GESS	AusNet	Energy Company	Australia	2012	1	1	MV	AS, IO
Mackinac HVDC	ATC	TSO	USA	2012	200	-	HV	HVDC
SMA Projects	Misc.	-	Europe - USA	2017-2019	0.8 - 15	0.4 - 15	LV-MV	RI, IO
Dersalloch Wind Farm	SPR	Energy Company	Europe	2019	69	-	MV	AS, BS, IO
Hornsdale Power Reserve	Neoen	Energy Company	Australia	2017-2020	150	194	HV	AS, EM
ESCRI-SA Project	Electranet	TSO	Australia	2018-2019	30	8	HV	AS, EM
La Plana Hybrid Project	Siemens-Gamesa	Energy Company	Europe	2018	-	-	MV	AS, BS, EM, IO
DEMOCRAT Demostrator	Efacec	Energy Company	Europe	2018	0.25	0.22	LV-MV	BS, EM, IO
NREL Campus	NREL	Research Center	USA	2019	1.25	1.25	MV	AS, RI
GE Projects	Misc.	-	USA	2017-2019	-	-	MV	AS, BS
OSMOSE Project	Misc	-	Europe	2018	0.1 - 0.72	0.025 - 560	LV-MV	RI
ABB PEGS	ABB	Component production Company	-	2020	20	-	MV	Other
Fluence-Siemens Project	Litgrid	TSO	Europe	2021	-	-	HV	Other

Starting from the conclusions drawn in the study on demonstrators, a simulation study was conducted to assess the implementation of GFM control in two

photovoltaic power plants connected to the Maltese medium-voltage grid, in order to evaluate its effect on frequency regulation following a disturbance.

4.2.2 The Maltese electrical system and the simulated case study

Malta, a small archipelago in the Mediterranean Sea, is situated south of Italy and east of Tunisia. Comprising three main islands—Malta, Gozo, and Comino—along with smaller uninhabited islets, the nation relies on a relatively compact and interconnected electrical grid to meet its energy demands. The predominant method of electricity generation involves thermal power plants that run on imported fossil fuels, mainly oil. Enemalta Corporation - the Maltese DSO [58] -, oversees the generation, high-voltage transmission (132 kV), and supply of electricity. Additionally, Enemalta operates the distribution network, which encompasses medium-voltage power lines (33 kV-11 kV), low-voltage power lines (0.4 kV), transformers, and distribution substations. Malta is connected to Sicily, Italy, through an underwater High Voltage Alternate Current (HVAC) submarine cable called the Malta-Italy Interconnector. This interconnection fosters electricity exchange between the two regions, bolstering Malta's energy security and enabling the import and export of power. In recent years, Malta has been actively working to augment the share of renewable energy in its electricity production. Initiatives include the installation of solar PV systems on rooftops, the establishment of solar farms, and the implementation of wind farms. The Maltese grid has faced challenges in terms of reliability, experiencing disconnections in response to various events such as load peaks, heat waves, storms, or grid faults. With an anticipated rise in the percentage of installed renewables in the coming years, the system's inertia and overall dynamic performance are expected to decrease. Consequently, there is a growing need for regulation services from renewable power plants to ensure and enhance the reliability of the grid.

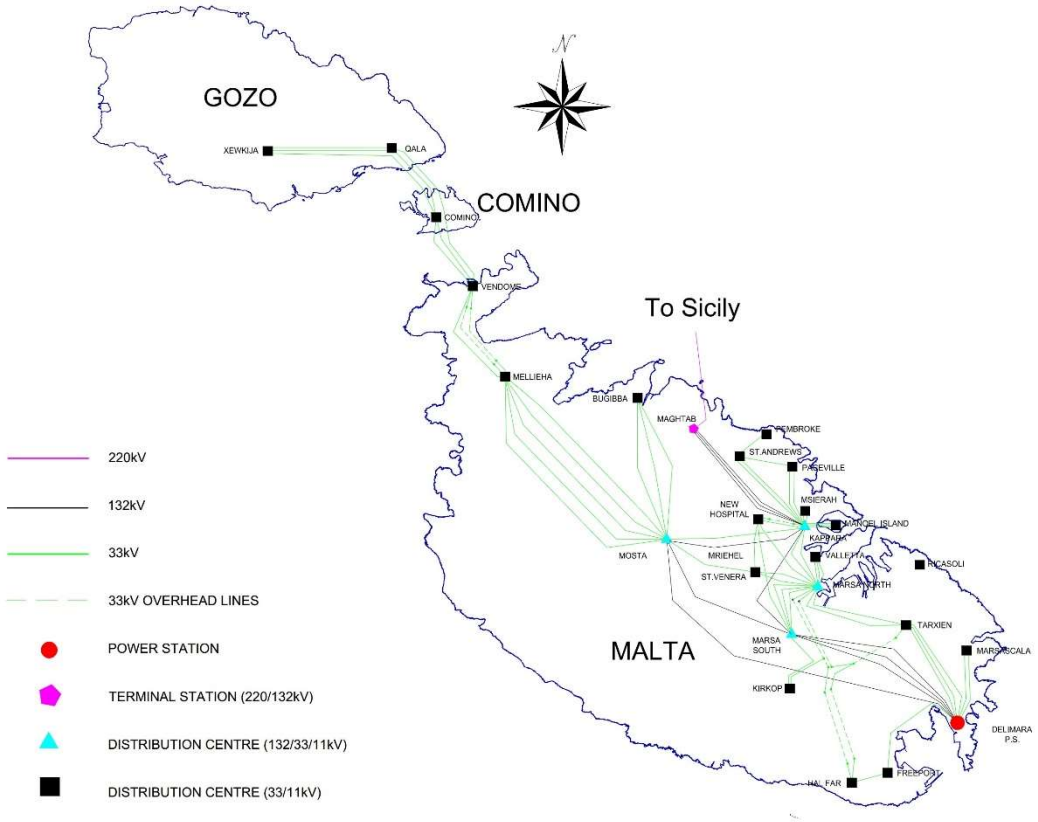

Figure 30 Malta - Maltese electrical system.

The case study considered consists in a portion of the network in the island of Gozo, one of the main islands of the Maltese archipelago located north of Malta. Gozo, the second-largest island of the Maltese archipelago, is more rural compared to Malta but still has some industrial facilities that account for a significant portion of the energy demand. The island has two 33 kV distribution centers, called "Qala" and "Xewkija". For this study, the Xewkija center is considered, serving as the last terminal of the distribution network on the island. In the Xewkija station, there are two transformers with a transformation ratio of 33/11 kV/kV. An 11 kV sub-distribution network extends from these transformers, supplying power to various 11/0.4 kV/kV secondary cabins. These secondary cabins serve both low voltage users and connect to solar farms. A comprehensive model of the network, powered by one of the two transformers in the Xewkija distribution center, has been developed. This model comprises 21 secondary substations. Each node in the model incorporates simulations of the corresponding loads and photovoltaic systems. The data required for implementation were sourced from Enemalta and the University of Malta, Figure 31 presents a diagram

illustrating the structure of the analyzed grid. In all the simulations, the assumption to consider the Maltese electrical system as isolated was made: This is justified by both the limited regulation capacity of the connection with Italy (max 200 MW) and the need to assess the impact of GFM regulation in the Maltese system operating in an isolated frequency mode.

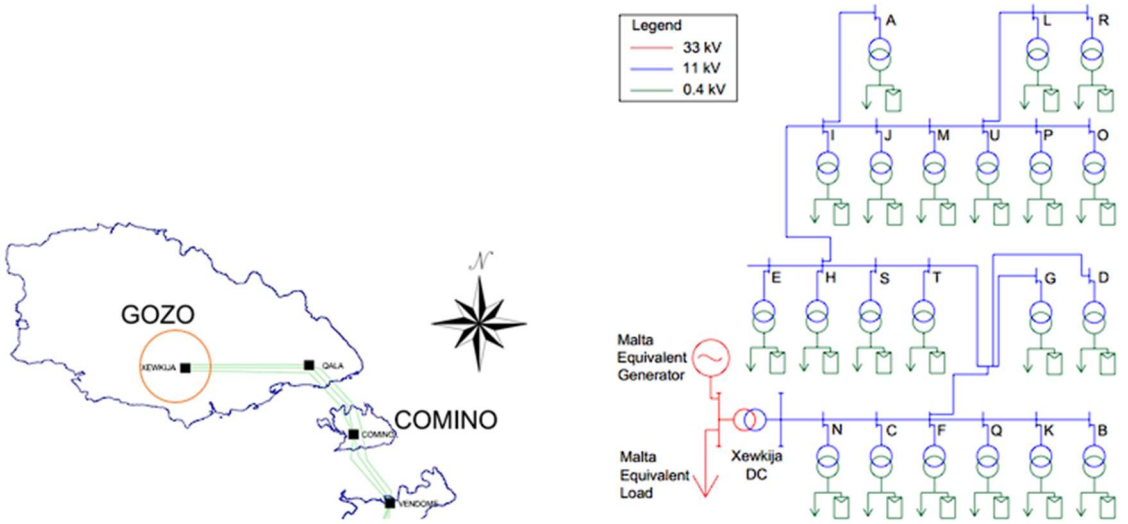

Figure 31 Case study: Xewkija Distribution centre, secondary substations detail.

For the dynamic analysis of the system, a portion of the distribution network is implemented in Neplan environment. The simulations consider the implementation of GFM control into the converters of the two largest PV plants of the island. The simulation scenarios were defined based on measurement data from the year 2020, focusing on the secondary substation "Xewkija." The simulations were conducted during the most demanding instances for the network, specifically:

- **Maximum Load**: August 17, 2020, 21:30
- **Maximum PV Generation**: June 3, 2020, 13:00

During the identified time instances, load flow simulations were conducted initially, followed by dynamic simulations involving the introduction of a disturbance. GFM control was implemented in the two largest solar farms on the island, which are connected to nodes "A" and "M" in the network shown in Figure 31. These two solar farms have peak powers of 636 kWp and 311 kWp, contributing to a hypothetical total control power of 947 kW. It is worth noting that the first of the two conditions occurs in the evening. To ensure frequency

support from the photovoltaic plants under investigation, the presence of storage systems was assumed at the nodes to which the plants are connected. The rated power of these storage systems is assumed to be equal to the power of the respective solar farm, while the energy content is deduced from [59].

4.2.3 Neplan Implementation and simulation results

The simulations were carried out in the Neplan environment, a specialized software particularly suitable for this type of application. The network segment under study was reconstructed using information provided by the research group at the University of Malta in collaboration with Enemalta. This allowed the creation of a realistic model for all the substations considered. Regarding the GFM control, this is not present in the standard Neplan library. To overcome this issue, a GFM control model was created using the specific Neplan function that allows the custom encoding and programming of various elements of the network. This approach made it possible to control generators A and M differently from the other photovoltaic plants, thus simulating the Power-synchronization class GFM control. The library used for the encoding is called SYMDEF [60], in Table 17, the parameters set in the simulation are reported. For the provision of this kind of service, Electrochemical lithium-ion BESS are the ideal solution that allows for the delivery of large quantities of electrical power, even for several hours, depending on the capacity.

Table 17 Grid Forming control parameters.

Parameter	**Value**
Inertia H	10 s
Droop R	0.05 pu
Damping Factor D	500 pu
Voltage controller Proportional gain K_{vp}	1
Voltage controller Integral gain K_{vi}	100
Virtual Resistance R_v	0.1 pu
Virtua Reactance X_v	1 pu

The load flow calculations were performed using the extended Newton-Raphson method, with a minimum number of iterations set to 20 and a convergence condition of 0.001 pu. The load flow converged in all the investigated cases, and the results in the two scenarios analyzed indicate a network adequately sized for the current load. In some sections, it is also well inclined to accommodate future

load and generation increases. In the "Maximum Load Demand" scenario, all node voltages remain above 90% of the rated voltage, with a minimum recorded at the "I" node equal to 93.05%. Individual secondary substations show no overloads, and only the "Q" transformer exceeds 80% of its rated capacity, reaching 86.34%. In the "Maximum PV Generation" scenario, voltage levels are significantly higher than in the previous case, as this period corresponds to low electricity demands. However, the voltage levels remain within +10% of the rated voltage. The highest voltage values occur at nodes “A” and “M” due to the presence of the two solar farms. Similar to the Maximum Load scenario, there is no overloading, and transformers in solar farms “A” and “M” bear the heaviest loads. Transformers and MV lines at nodes with both PV and load connections are relieved due to power supply by DGs. Table 18 presents the most significant data from the load flow simulations.

Table 18 Load Flow results in simulated scenarios.

Maximum Load scenario		**Maximum PV Generation scenario**	
Under-Voltage Nodes	None	Overvoltage Nodes	None
Minimum Voltage Node	I	Maximum Voltage Node	A
Minimum Voltage Value	93.05 %	Minimum Voltage Value	103.2%
Overloaded Nodes	None	Overloaded Nodes	None
Maximum Load Node	Q	Maximum Load Node	A
Maximum Load Value	86.34 %	Maximum Load Value	96.63 %

For dynamic simulations, the focus was on primary frequency control dynamics in the examined grid portion. The applied disturbance involves interrupting the power supply to the loads at node G, the secondary substation with the largest load. The immediate disconnection leads to a noticeable increase in frequency. The power system is modelled using a positive-sequence phasor model, suitable for investigating frequency transients. Key elements in the system dynamics include synchronous generators and their regulators, loads, and converters where GFM is implemented. The Xewkija Distribution Center serves as the slack bus in the system. The upstream network is represented by an equivalent synchronous generator and a load connected to the 33 kV side of the transformer (Figure 31), and their characteristics are derived from various data and measurements provided by Enemalta plc. The synchronous generator is equipped with an automatic voltage regulator (AVR), a power system stabilizer (PSS), and a turbine governor (T-GOV). The parameters of these controllers are extracted

from the ENTSOE dynamic model [35], and further details about the control schemes can be found in [48]. Loads are simulated using a frequency-dependent ZIP model, where voltage depends on both active and reactive power. Traditional solar farms are modelled with a classical GFL control independent of frequency dynamics. The plants connected to nodes “A” and “M” are simulated with an average model of the power electronic converter and the control strategy outlined in the previous section. Two battery energy storage systems are connected to nodes “A” and “M” to provide regulation services during nighttime. Table 19 provides the parameters used for simulations investigating the maximum load and maximum generation scenarios, with a simulation duration of 30 seconds, consistent with normal primary control operations.

Table 19 Scenario parameters for dynamic simulations.

Maximum Load Scenario		**Maximum Generation Scenario**	
Disturbance	661 kW	Disturbance	335 kW
Xewkija Station Load	6162 kW	Xewkija Station Load	-1247 kW
Node A PV plant active power	0 kW	Node A PV plant active power	-510 kW
Node A BESS active power	630 kW	Node A BESS active power	0 kW
Node M PV plant active power	0	Node M PV plant active power	-306 kW
Node M BESS active power	300 kW	Node M BESS active power	0 kW

For both identified scenarios, two different simulations were conducted using the same disturbance:

1) PV power plants in nodes "A" and "M" operated with traditional GFL control without any regulatory contribution.
2) PV power plants in nodes "A" and "M" operated with GFM control and provision of regulatory contribution.

The graphs in Figure 32depict the simulation results of grid frequency deviation for the Max Load scenario. At time instant t = 10 s, the tripping of the protection system of node G is introduced, corresponding to a load loss of 661 kW. In the case of GFM operation of the plants in nodes “A” and “M” (orange waveform in the figures), there is a reduced steady-state frequency error of less than 47.2%, a significant improvement compared to the base case in which all plants are operated in GFL mode (blue waveform in the figures). Figure 33shows the trend of active power at nodes “A” and “M” respectively. As the nature of the disturbance is a sudden load shedding, the GFM control responds in a way that

compensates for this disturbance by activating the charging of the storage systems connected to the solar farms, which restores, at least partially, the electrical balance. Indeed, as observed from the figures, in the GFL control case, both PV farms at Nodes “A” and “M” do not change their consumption profile, while in the GFM case, the two accumulators at nodes “A” and “M” absorb an active power of 0.35 pu. Figure 34 illustrates the simulation results for the Max PV Generation scenario. At time instant t = 10 s, the tripping of the protection system at node “G” is introduced, corresponding to a load loss of 335 kW. Even in this case, the GFM operation of PV plants in “A” and “C” nodes benefits the grid with a steady-state frequency improvement of 45.7% compared to the GFL case. In contrast to the previous case, the photovoltaic power plants are feeding power into the grid. The response of the GFM control is to reduce the power fed into the grid to counterbalance the load shedding. This results in an active power drop of the PV plant at node “A” from -0.8 pu to -0.64 pu , while the PV plant at node “M” drops from -0.985 pu to -0.82 pu (Figure 35).

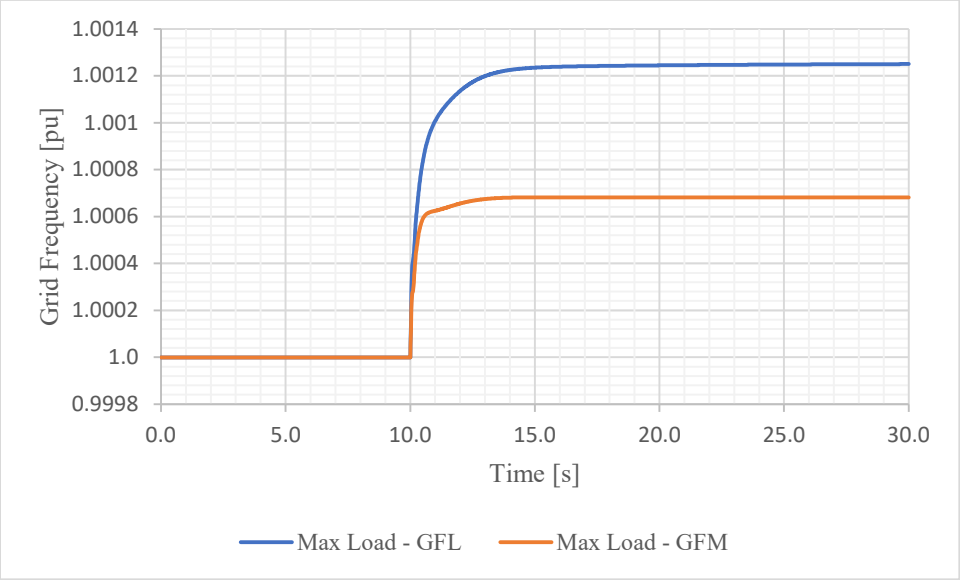

Figure 32 Grid Frequency in Scenario 1.

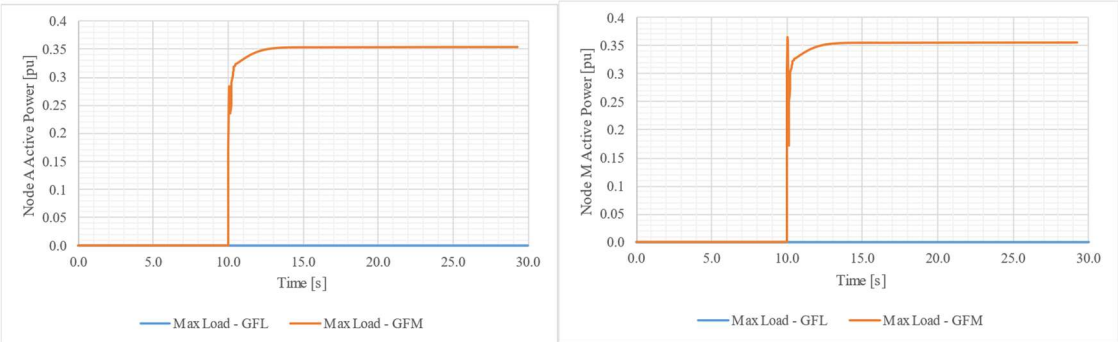

Figure 33 Power delivery in Noda "A" and "M", Scenario 1.

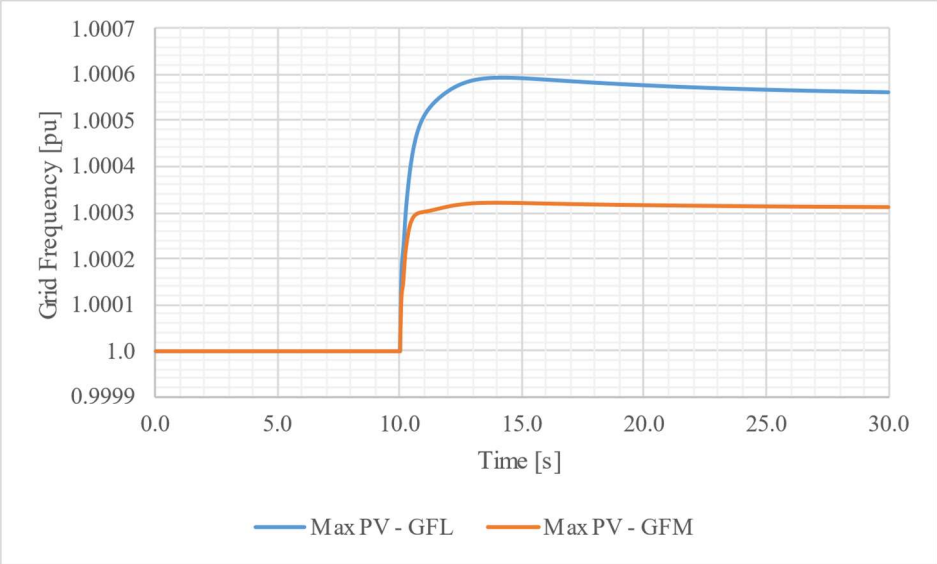

Figure 34 Grid Frequency in Scenario 2.

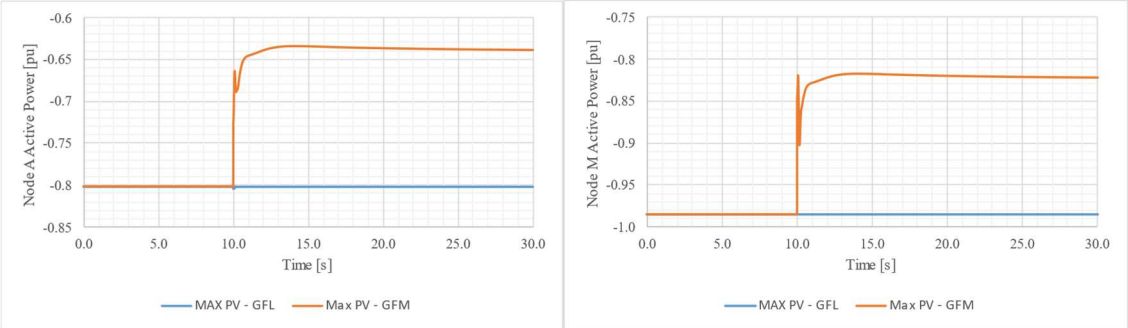

Figure 35 Power delivery in Noda "A" and "M", Scenario 2.

The study demonstrates that GFM control is rightly considered one of the most effective solutions to ensure a reliable and safe integration of RES into the electrical system. This is particularly relevant as distribution networks, not just HV systems, are expected to play a role in providing ancillary services in the

future. The case study focused on a portion of the Maltese network, utilizing parameters derived from the Maltese DSO for accurate system modelling. The regulation service was provided by converters interfacing two solar farms connected to the same secondary substation.

The results of the study indicate a general improvement in grid frequency parameters when employing GFM control. There was a reduction of 47.2% in the frequency nadir during the Maximum Load Demand scenario and a reduction of 45.7% during the Maximum PV Generation scenario. This underscores the effectiveness of the control in enhancing the stability and reliability of the grid, especially in scenarios with high renewable energy generation.

Chapter 5

5. Analysis of the Sicilian Power System

After analyzing the application of innovative regulation services in both large, interconnected networks and weak or isolated systems, the last chapter of the thesis focuses on all the investigations that have been carried out over the three-year period on the Sicilian power grid. Sicily holds a highly strategic position in terms of electricity production and dispatch, making it an ideal candidate to play the role of an energy hub in the Mediterranean area in the coming years. The Sicilian electrical system is normally operated synchronously and interconnected with the European Synchronous Area through a connection with Calabria, the southernmost region of the Italian peninsula. However, its behavior in frequency island is of great scientific and technical interest because the system has the ability to operate independently if the connection with the rest of the country was lost. In the near future, the system will experience a real revolution both in terms of energy generation and interconnections. On one hand, there is a forecast for a massive injection of electric power from RES-based power plants, including offshore wind and PV plants. On the other hand, interconnections with Italy and North-Africa will be strengthened through new HVDC links. In this scenario, the choice to gather all the studies conducted on the Sicilian grid in a single chapter was made, providing an overview of what this revolution could mean at regional and national levels. The chapter also explores how new and innovative grid regulation services will contribute to ensure a more effective and reliable transition, such as the application of GFM control for the provision of frequency support services.

5.1 Study's objectives and applied methodology

The main objective of the study is the analysis and evaluation of the expansion of the Sicilian grid considering new DC infrastructures. The studies were conducted in the Neplan environment, considering a Sicilian grid model developed by the University of Palermo's electrical systems research group through various collaborations with the Italian TSO Terna over the years [61]-[65]. The study, conducted in collaboration with RSE, was divided into multiple phases:

- **Phase 1**: Definition and updating of the Sicilian grid model with the interventions planned in the Terna development plan;
- **Phase 2**: Power-Flow study of the Sicilian grid in different scenarios and comparison with current operating conditions.
- **Phase 3**: Dynamic studies on the Sicilian power grid in different scenarios.
- **Phase 4**: Application of GFM schemes for black-start, frequency regulation and synthetic inertia.

For the purposes of this thesis, only the aspects related to phases 3 and 4 will be discussed in detail, considering the work done during phases 1 and 2 as the foundation for further analyses.

The research activity conducted involves the following steps:

1. Study of the state-of-the-art regarding the applications of HVDC for frequency control, grid-forming, and the provision of other ancillary services;
2. Review of previous dynamic studies on the Sicilian grid;
3. Updating the Sicilian grid model based on the new Terna Development Plan 2023;
4. Definition of models for the control of power electronic converters in the network;
5. Definition of simulation scenarios;
6. Simulations performance and results discussion.

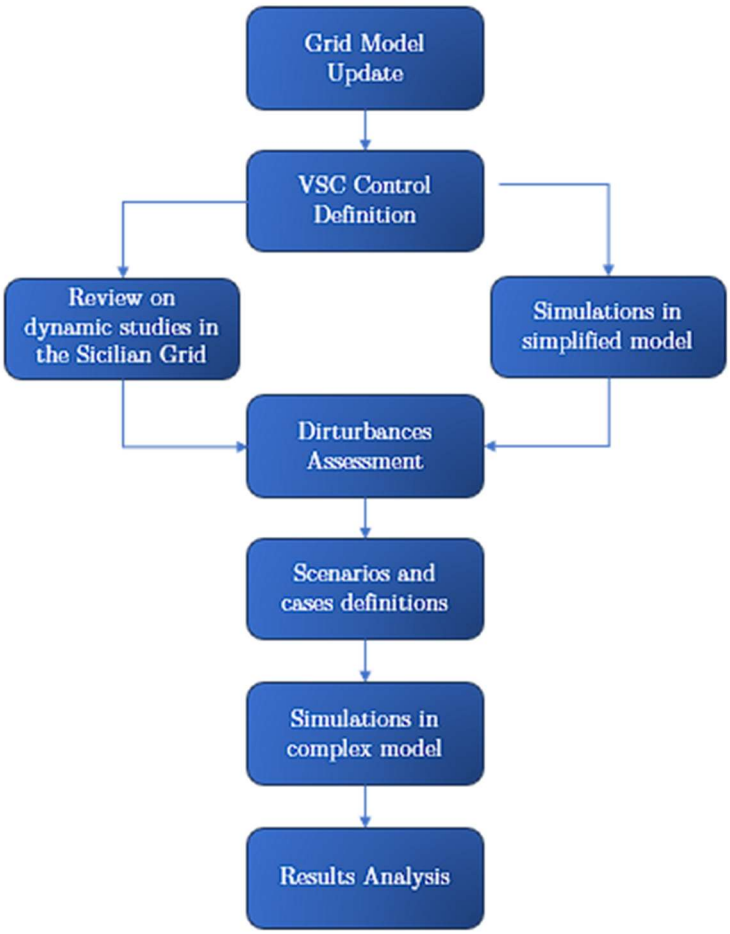

Figure 36 Flowchart of applied methodology.

5.1.1 HVDC and ancillary services

The HVDC technology attracts the interest of all actors in the electrical system, thanks not only to the well-known economic advantage for long distances but also to the applications it lends itself to when appropriately controlled. In addition to transporting large powers over long distances, direct current transmission is also used for the following applications:

- Connection between AC systems operating at different frequencies or systems operating at the same frequency but with different phase angles;
- Connection between two nodes of a synchronous network;
- Connection of offshore facilities with the onshore grid.

HVDC connections and the converters that comprise them can be controlled in such a way as to provide ancillary services to the transmission electrical network,

contributing to the stiffness and stability of the electrical system. However, the ability to provide a specific service is not a universal characteristic of HVDC but depends heavily on the nature of the involved converters and the components that constitute them.

Table 20 Tech comparison HVAC - HVDC

	PARAMETER	HVAC	HVDC
Cables/lines	Number of conductors	High	Low
	Utilization	Limited by skin effect	Only thermal limitations
	Losses	High (resistive and reactive)	Low (resistive and corona)
Substations	Costs	Lower	Higher
	Losses	Around 0.3%	Above 1%
Economic feasibility		Earthed cables < 50–100 km Aerial lines < 300–800 km	Earthed cables > 50–100 km Aerial lines > 300–800 km

Two types of HVDC converter stations exist, differing both in the technology constituting the converters and in the performance the connections can offer. The first type is called Line Commutated Converters (LCC), which, as indicated by the name, relies on the AC network for component commutation. Conventional LCC stations use 6 or 12-pulse rectifiers consisting of thyristors, power electronic components controllable during turn-on but not during turn-off. They utilize the zero-current passage for turn-off and, for this reason, require a sufficiently strong and resilient AC network to connect to. Classified as current-controlled converters, they demonstrate a solid technological maturity and are well-suited for the transfer of high power over long distances. One of the main issues with this type of converter is the high consumption of reactive power for current rectification. A significant portion of the costs involves expenses for current filtering equipment to reduce harmonic pollution in AC networks. The second type is called Voltage Source Converter (VSC) and is, between the two, the more recent. VSC converters are controlled as voltage sources and are typically equipped with the most modern IGBTs (Insulated Gate Bipolar Transistors). This type of transistors allows independent turn-off from the upstream network according to a well-defined control logic. This feature makes them suitable for connections with less resilient networks and adds to the converter's capabilities

the ability to power de-energized networks (Black Start capability). Additionally, the switching frequency of the components is typically in the kilohertz (kHz) range, resulting in lower reactive power demand and consequent savings in filtering equipment. This characteristic makes VSCs particularly suitable for connecting offshore facilities, given the smaller installation space required (estimated to be around 50% less than LCCs). The main disadvantage of this type of converter is the lower transport capacity compared to an equivalent LCC, essentially due to the higher currents that thyristors can handle compared to IGBTs. However, despite this drawback, VSCs allow for offering a whole range of network services that are completely inaccessible to LCCs.

The injection of electrical power into the grid is decided based on technical-economic optimization logic and follows the results of the electricity market. However, the electricity market relies on forecast estimates that follow consumption models, which is why it is not possible to know in advance and with precision the power required by loads. The electrical system must, by its nature, maintain a highly precarious balance. The balance between power produced and power absorbed by users (plus losses) must be constantly monitored, under the penalty of a variation in the frequency of the grid. The transmission network operator must address this and other similar problems to ensure effective, efficient, and reliable system operation. To cope with imbalances or unforeseen contingencies, the operator can rely on **ancillary services**. By definition, ancillary services are "*services that ensure reliability and support the transmission of electricity from generation sites to customer loads*" [66]. These services can be provided on a national scale (global services) or on a regional scale (local services) and essentially involve modifying previously fixed injection or withdrawal plans to support the electrical grid. The importance of these services is such that they can be mandated by the TSO (impositions, even if not remunerated), although in most cases, the operator procures these services in a dedicated market window. Depending on the type of converters constituting the system, HVDC connections can be used to provide flexibility services. Table 4.2 provides a summary of the possibilities related to LCC and VSC types and the corresponding comparison with the equivalent service offered by AC systems [67].

Table 21 Summary of ancillary services based on the type of converter station.

System	Asynchronous grids		Synchronous grids nodes		Offshore		Comments
Services	**LCC**	**VSC**	**LCC**	**VSC**	**LCC**	**VSC**	
Inertia	++	++	NA	NA	++*	+++*	VSC converters offer better controllability for offshore facilities.
Primary Reserve	++	++	NA	NA	++*	++*	It is not possible for HVDC to provide inertia and reserve for internal nodes of synchronous networks.
Secondary Reserve	+++	+++	NA	NA	++*	++*	HVDC converters offer better controllability compared to AC systems.
Tertiary Reserve	+++	+++	NA	NA	++*	++*	
Voltage Control	-	+++	-	+++	-	+++	HVDC LCC converters do not have Black Start capability and voltage control.
Black Start	-	++	-	++	-	++	
Congestion Management	+++	+++	+++	+++	-	-	HVDC systems outperform AC systems in congestion management.

The symbolism used in Table 21 allows for an immediate visualization of the system characteristics for a given service in relation to AC systems, in particular:

- The symbol "-" indicates the impossibility of providing the service;
- The symbol "+" indicates the possibility of providing the service;
- The symbol "++" indicates performance similar to AC equivalents;
- The symbol "+++" indicates better performance than AC equivalents;
- The symbol "*" indicates the need for specific control for operation;
- The symbol "NA" indicates that the service cannot be provided by any HVDC system.

From the analysis, it is evident that in most cases, HVDC systems can provide flexibility services with performance equal to or better than AC equivalents. Between the two types of stations, it is also clear that VSC types have greater possibilities than LCC converters, which, due to the absence of completely

controllable components, are unable to control voltage and perform Black Start operations.

5.1.2 Review of previous dynamic studies on the Sicilian power system

In order to define meaningful scenarios for studying the island's dynamics in the presence of HVDC converters and distributed generation capable of providing frequency regulation services, a preliminary study of the state of the art on the subject was conducted, analyzing the works available in the literature. The results of the state-of-the-art study are reported in the following table. From the study of the state of the art, it emerges that one of the most studied situations concerns the creation of the electrical island with the interruption of the connection between Sicily and Calabria. In most studies, several scenarios of import and export are analyzed, and it is highlighted that the most critical cases for stability are found under conditions of high import from Italy and loss of synchronous generation during island operation. Given the novelty introduced by the Tyrrhenian Link, in none of the examined studies is the contribution to the stability of the Sicilian network given by the new HVDC links is considered, only in [70] is supposed the possible contribution to the system dynamics given by the TL analyzed during a short circuit on a 400 kV line.

Table 22 Summary of the dynamic studies on Sicilian electrical system.

Paper	Simulated Event	Scenario/Loads	Year	RES	Tyrrhenian Link
Renewable power integration in Sicily: frequency stability issues and possible countermeasures (conference paper) [68]	Loss of diesel generation while Sicily was in electrical island for scheduled maintenance, 18/05/2011	Equal to that recorded at the time of the incident (unspecified).	2011	PV participating in regulation, storage, and pumping stations for FFR, wind with SI control.	None
The Malta-Sicily EHV-AC interconnector [69]	Analysis of the connection between Italy and Malta: maximum transferable	Various, P_n link = 225 MW	2016	Not participating.	None

	power, load flow analysis, short circuit, small signal stability, electromechanical transients.				
Tyrrhenian Link: path towards a decarbonized electrical system [70]	Power flow under maximum load conditions, short circuit analysis with a focus on damping and oscillations.	Various, P_nTL=1000 MW	2030 2040	Not participating.	Present and participating.
Coordinated Inertial Response Provision by Wind Turbine Generators: Effect on Power System Small Signal Stability of the Sicilian Network [71]	Line loss, network in 2030 extrapolated from the OSMOSE project, modal analysis, dynamic simulation with and without synthetic inertia.	High export and high import, loss of two lines corresponding to 500 MW of generation.	2030	Inertial support provided by permanent magnet wind generators.	None
Stability analysis of the OSMOSE scenarios: main findings, problems, and solutions adopted [72]	Several scenarios simulated, primary regulation with different support services, modal analysis, voltage stability.	Maximum/minimum load, maximum/minimum export, islanded network.	2030	Participating in regulation, load participating through Demand Side Response.	None
Opportunities and Challenges in the Mediterranean Region with Grid Forming Control for HVDC Systems [73]	Supplying regulation from HVDC, power step response, angle step response, DC-Link voltage stability.	Unspecified	N.D.	Unspecified	Not directly involved, the VSC-HVDC technology evaluated in general.
Power System Stability Analysis of the Sicilian Network in the 2050 OSMOSE Project Scenario [74]	Primary control with different support services, modal analysis, voltage stability.	High export, high import, high load, islanded network, low load, and failure of some lines.	2050	Participating in regulation, load participating through Demand Side Response.	Unspecified.

5.1.3 Sicilian Grid model and implementation of planned improvements

As already stated, there was a significant collaboration between the University of Palermo and Terna SpA to develop the model of the Sicilian power grid in the Neplan 360 environment. The model has undergone continuous updates, taking into account Terna's development plans and insights gathered through collaborations with diverse stakeholders. This includes companies operating in petrochemical hubs and private entities investing in substantial renewable power projects in Sicily. Additionally, the model incorporates information from publicly accessible documents, which can be freely consulted on the Ministry of Environment and Energy Security's website (MASE, [80]). The grid model updated to 2022 includes:

- overhead and underground transmission lines of the Sicilian network at 380 kV, 220 kV, 150 kV, and 60 kV;
- transformation substations at 380/220 kV, 220/150 kV, 150/60 kV, and 150/20 kV;
- thermal power plants and pumped storage power plants in the Sicilian network, including models of speed regulators;
- the electrical storage system in the busbar of Ciminna;
- synchronous compensators in the busbars of Partinico and Favara;
- electric loads at the respective voltage level;
- photovoltaic and wind generators.

An equivalent generator representing the European network completes the model, whose dynamic characteristics are established using the Initial Dynamic Model provided by ENTSO-E. The network model was updated to incorporate the interventions outlined in Table 23, encompassing all the 2030 network reinforcement projects outlined in Terna's development plan [81]. Additional insights are depicted in Figure 37, illustrating the proposed, planned, and ongoing interventions in the Sicilian power grid. In the implementation of the new network configuration, the connection of the HVDC link of Tyrrhenian Link East (TL-E) to the Montecorvino power station in the Italian Mainland (Campania region) is considered part of the equivalent station representing the entire continent. The

upstream network is modelled through a synchronous generator and a load. Similarly, for the TL-E, the upstream network of the Selargius station in Sardinia is modelled as a synchronous generator with three loads. The downstream system of Tunisia is represented as a node that doesn't participate in the dynamic simulations of the network. The offshore wind farms currently in the authorization or construction phase are depicted as connected to network nodes through cables, with technical characteristics (length, capacity, resistance, and reactance) determined from freely downloadable project documents on the MASE website. In cases where this information is unavailable, the wind farms are represented as generators directly connected to the nearest 220 kV node of the Sicilian network along the coast in the province where the wind farm is located.

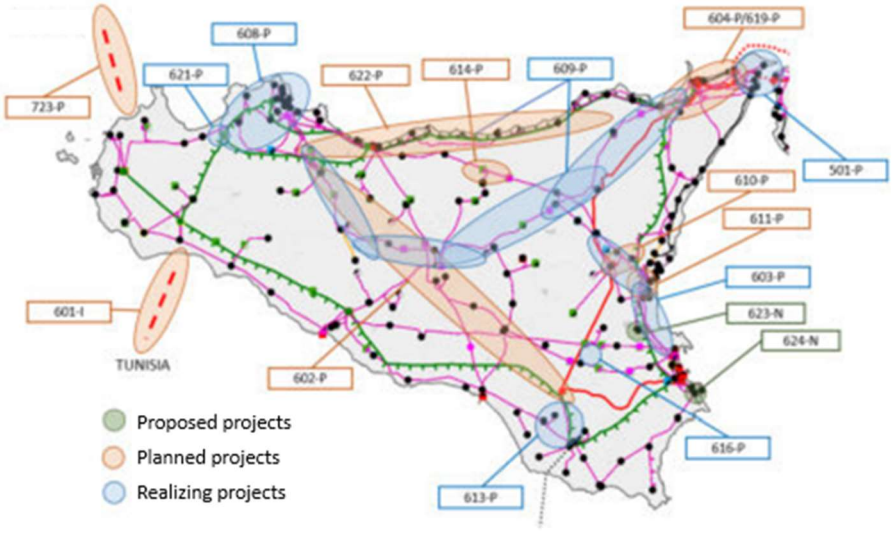

Figure 37 Interventions listed in Terna's development plan [81].

Table 23 List of scheduled interventions in Sicily to 2030.

Code	Name	Code	Name
555-N	New 380 kV "Bolano – Paradiso" connection	**621-P**	Partinico 220 kV station
601-I	New "Italy – Tunisia" interconnection	**622-P**	150 kV line "SE Caracoli – SSE Furnari RT"
602-P	380 kV "Chiaramonte Gulfi – Ciminna" power line	**623-P**	New 150 kV power line "Lentini – Lentini RT (ex FS)"
603-P	380 kV "Paternò – Pantano – Priolo" power line	**624-P**	New 150 kV junction "CP Siracusa est – CP Siracusa RT (ex FS)"
604-P/619-P	380 kV "Assoro – Sorgente 2 – Villafranca" power line	**625-P**	Rationalization of the HV network in the Caltanissetta area

607-P	220 kV “Partinico – Fulgatore” Power Line	**626-P**	New 150 kV power line “Vallelunga RT – SE Cammarata”
608-P	Palermo's Metropolitan Area Restoration	**627-P**	380 kV “Caracoli – Ciminna” power line
609-P	HV Lines general interventions for renewable integration	**628-N**	Meshing interventions in the industrial area of Catania
610-P	Line 150 kV “Paternò – Belpasso”	**629-N**	Rationalization of the Cefalù area
611-P	Interventions on the HV network in the Catania area	**630-N**	Island of Favignana interconnection
612-P	Interventions on the HV network in the northern area of Catania	**632-N**	Mesh increase 150 kV Trapani area
613-P	Interventions on the HV network in the Ragusa area	**723/E-P**	HVDC connection "Sicily - Mainland (Tyrrhenian Link East)"
614-P	Removal of the 150 kV Castel di Lucio rigid branch line	**723/W-P**	HVDC connection "Sicily - Sardinia (Tyrrhenian Link West)"
616-P	380 kV Vizzini substation (ex SE 380 kV Mineo)		

5.1.4 Converters Control Schemes

The power converters in the AC/DC conversion stations are simulated as VSC with an average model, considering a complex modulation index with real and imaginary parts. In the case of GFL control, the proposed model also implements the Phase-Locked Loop (PLL). The PLL-tracked grid angle is used to transform the input and output variables of the control system into the local synchronous reference frame. The variables expressed in the reference frame are indicated with the subscript "*frm.*" The power converters of the HVDC link are then controlled with a simple cascaded PI scheme, considering the control signals of the selected control channel (P/V_{DC} and Q/V_{AC}). The output provides the control variables m_D and m_Q of the complex modulation index. The HVDC control system diagram is shown in Figure 38. The described control approach can be used to represent the dynamics of HVDC interconnections in the power system of continental Europe and can be easily extended to consider frequency-sensitive modes and specific services such as synthetic inertia. In this study, the control scheme is implemented with the values in Table 24. As for the implementation in NEPLAN 360, the HVDC VSC CONTROLLER regulator from the software libraries was used, the dialogue window of model in NEPLAN is shown in Figure 39.

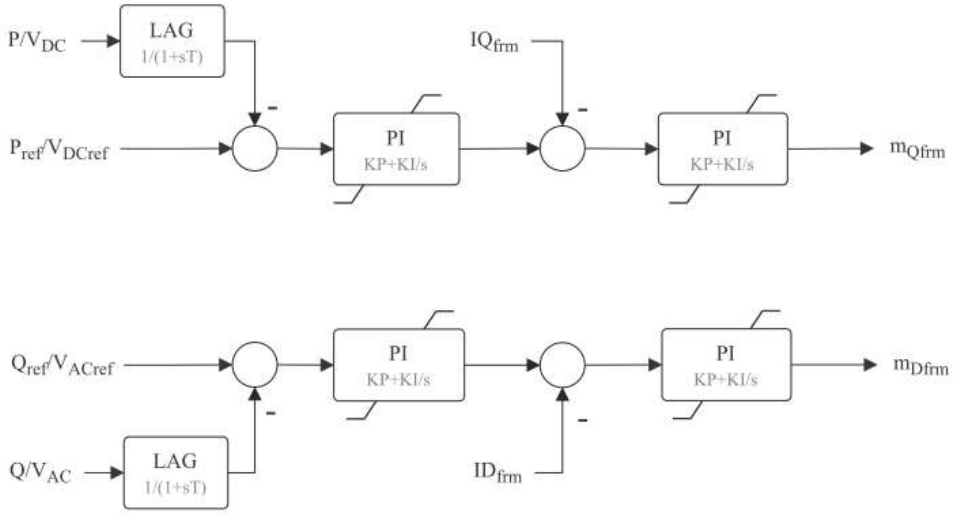

Figure 38 Implemented GFL control.

Table 24 GFL control parameters.

Parameter	Value	Parameter	Value
K_{VDC}	0.05	MIN IDref	-1.5
K_{VAC}	1	MIN IQref	-1.5
T_{VDC}	0.1 s	MAX IDref	1.5
T_{VAC}	0.1 s	MAX IQref	1.5
K_{IQ}	0.3	MIN m_{Dfrm}	-1.5
K_{ID}	0.3	MIN m_{Qfrm}	-1.5
T_{IQ}	0.015 s	MAX m_{Dfrm}	1.5
T_{ID}	0.015 s	MAX m_{Qfrm}	1.5

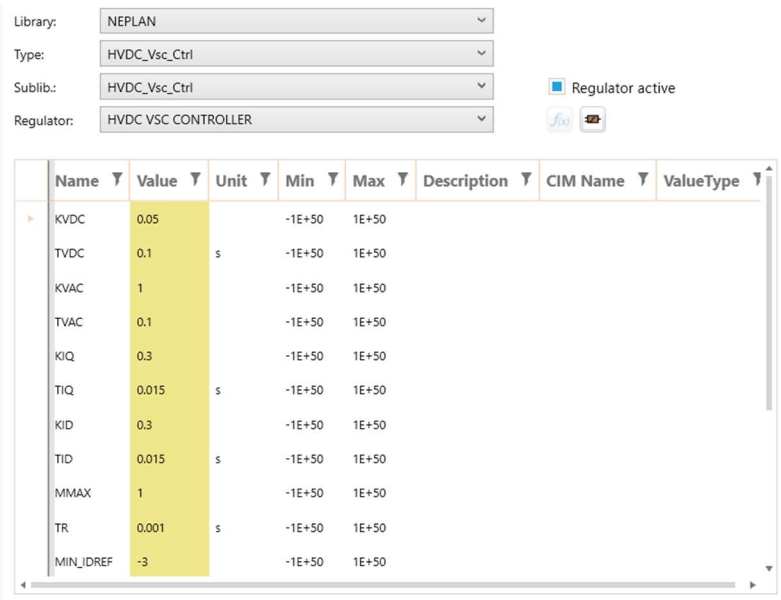

Figure 39 External Mask for the parameter initialization on Neplan, GFL Inverter.

Regarding GFM control, the implemented block scheme is shown in Figure 40. The scheme consists of three main parts: a synchronization loop, a voltage controller, and a virtual impedance. The synchronization loop is of the swing-based type, emulating the fundamental dynamics of a synchronous machine. The gain H defines the time response for determining the internal frequency deviation of the converter and defines its capabilities. The gain R implements a static control and defines the frequency containment reserve that can be provided by the HVDC station. The synchronization loop also includes a damping term with gain K_w and time constant T_w. The time constant is chosen on the order of seconds to preserve the inertial capabilities of the converter. The output θ represents the angle required for the transformation into the Synchronous Rotation Frame (SFR) coordinates, implemented as complex rotations in the phasor model. The voltage control is proportional-integral with constants K_{vp} and K_{vi}; the output e^* is sent to a virtual impedance block. This impedance block finally returns the variables e_d and e_q for the complex modulation of the converter. The control parameters used in the initial test phase are listed in Table 25. As for the implementation in NEPLAN 360, a regulator specially developed in the SYMDEF language was used (see Appendix 2 for details).

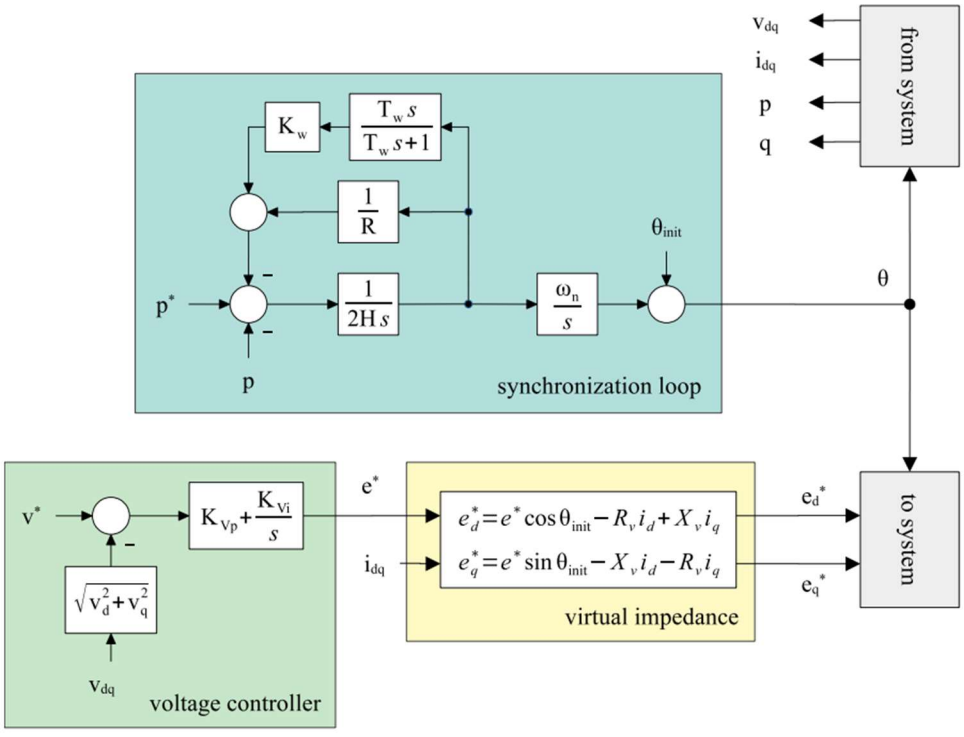

Figure 40 Implemented GFM control.

Table 25 GFM control parameters.

Parameter	Value
H	10 s
R	0.05 pu
K_w	100 pu
T_w	3 s
K_{vp}	1 pu
K_{vi}	100 pu
R_v	0 pu
X_v	0.1 pu

5.2 Dynamic Simulations of the Sicilian power Grid in future scenarios

Starting from the Sicilian network model, dynamic studies with a variable future time horizon were conducted to assess the system's response to contingencies in energy scenarios with high renewable penetration. The complete study was preceded by other preliminary investigations, both static and dynamic, which were already published and discussed in international conferences [78]-[79]. However, this thesis focuses on the results of the comprehensive research and the considerations drawn from the frequency trend analyses in different simulated scenario cases.

Starting from the results of these analyses, two events considered particularly significant for the study of island dynamics have been defined, specifically:

- Disconnection of Sicily from Calabria;
- Loss of the connection between Sicily and Tunisia during the asynchronous operation of Sicily from the rest of Italy.

5.2.1 2030 Scenario and operative conditions definition

Developed by RSE, the 2030 scenario was built following a methodological approach and energy/power models and tools, including TIMES_RSE and sMTSIM, as detailed in [82]. The zonal electricity market simulator sMTSIM, specifically, provides hourly outputs for the Sicilian zone system. For each scenario case, RSE provided information such as installed generation capacity, total demand, hourly load, external interconnection flow, production profiles, and

utilization profiles of electrochemical storage systems and pumping stations for a full year of operation of the Sicilian grid. The regional data were subsequently distributed over the nodal grid model, accounting for the current and planned situation, RES connection requests and locations, and load types and placements. Table 26 reports a summary of the main data for the considered 2030 scenario.

Table 26 2030 Energy Scenario for Sicily.

Rated power capacity of generation units aggregated per source [GW]		**Electric Load per type**	
Gas	3.516	**Total annual demand [TWh]**	21.1
Other Non-RES	0.452	**Total annual demand for H2 production [TWh]**	1.57
Solar (of which CSP)	6.011 (0.550)	**Max Load without electrolyzers [GW]**	3.59
Onshore Wind	4.317	**Min Load without electrolyzers [GW]**	1.41
Offshore Wind	1.218	**Max Load with electrolyzers [GW]**	4.34
Hydro	0.765	**Min Load with electrolyzers [GW]**	1.44
Biomass	0.084	**Max electrolyzers load [GW]**	1.15
Storage	0.612		
Power-to-X	1.200		

The study considered various operating conditions of the Sicilian network in the 2030 scenario to assess its performance under different scenarios:

1. **S.0 MAX GEN-LOAD OG**: This scenario represents the maximum difference between generation (both conventional and renewable) and the load of the island with overgeneration (OG). It simulates a situation where power flows through transmission lines exceed the total capacity of the interconnections, potentially requiring curtailment of renewable generation.
2. **S.0 MAX GEN-LOAD**: This scenario represents the maximum difference between generation (both conventional and renewable) and the load of the island without overgeneration (OG). It reflects a more realistic operating condition where there is a significant difference between generation and load, but curtailment of renewable generation is not

required. This scenario represents the most critical situation in which the system can feasibly operate.

3. **S.1 MAX THERMO**: This scenario represents the maximum power production from conventional and cogeneration (CHP, Combined Heat and Power) thermal power plants.
4. **S.2 MAX RES**: This scenario represents the maximum power production from renewable sources without overgeneration (OG). Simulating this operating condition allows testing the limits of the network in the presence of maximum renewable generation in the Extra High Voltage (EHV)/High Voltage (HV) grid.
5. **S.3 MAX LOAD**: This scenario represents the peak hour of the Sicilian load.
6. **S.4 MAX IMPORT**: This scenario represents the hour with the maximum value of energy import into Sicily from other interconnected areas.

These scenarios aim to evaluate the network's resilience and performance under different critical situations, considering factors such as overgeneration, thermal power production, renewable energy production, peak load, and energy imports.

Once the 2030 scenario cases are defined, the date and time at which the most severe condition occurs are determined. The dynamic simulations were performed only in the two scenarios considered as the most demanding for the frequency control system, respectively **S.0 MAX GEN-LOAD** and **S.3 MAX LOAD.** The first operational condition analyzed, related to the **S.0 MAX GEN-LOAD** scenario, occurs on 28/05/2030 at 13:00. In Table 27 the data related to this condition are reported, divided for each of the nine provinces that make up Sicily, while Table 28 reports the thermal generation from the traditional power plant and pumping station, and the active power flow from and to Sicily through the various interconnections.

Table 27 Load and renewable generation per province, 2030 MAX GEN-LOAD

	LOAD AND RENEWABLE GENERATION – PROVINCIAL DATA (MW)									
	AG	**CL**	**CT**	**EN**	**ME**	**PA**	**RA**	**SR**	**TP**	**Total**
Load	182.29	105.51	630.06	66.86	325.64	545.87	202.07	374.69	219.90	2652.89
	6.87%	3.98%	23.75%	2.52%	12.27%	20.58%	7.62%	14.12%	8.29%	100%
FV	162.91	281.13	728.79	455.04	11.50	508.33	116.01	263.10	471.69	2998.50
	5.43%	9.38%	24.31%	15.18%	0.38%	16.95%	3.87%	8.77%	15.73%	100%
Wind	482.38	94.91	388.69	200.86	262.61	718.08	75.13	223.80	722.39	3168.84
	15.22%	2.99%	12.27%	6.34%	8.29%	22.66%	2.37%	7.06%	22.80%	100%
Wind OS	0.00	136.40	31.43	0.00	0.00	0.00	199.89	0.00	427.44	795.15
	0.00%	17.15%	3.95%	0.00%	0.00%	0.00%	25.14%	0.00%	53.75%	100%
Bio	8.74	0.42	5.10	7.29	1.38	2.91	0.69	1.00	0.31	27.84
	31.40%	1.52%	18.32%	26.17%	4.96%	10.47%	2.48%	3.58%	1.10%	100%
Hydro	0.27	0.02	1.94	0.86	0.04	0.30	0.00	0.15	0.00	3.59
	7.59%	0.53%	54.09%	24.01%	1.19%	8.25%	0.00%	4.29%	0.07%	100%
Load-Gen	-472.02	-407.37	-525.89	-597.19	50.11	-683.76	-189.65	-113.36	-1401.92	

Table 28 Traditional power plant production and interconnections power flows, 2030 S.0.

Active power production [MW]	
Anapo	-482.64
Guadalami	-22.4
Termini Imerese	0
Priolo	0
Porto Empedocle	0
New Plants CCGT-OCGT	0
Nuce	245.98
Milazzo	0
CHP (3 power plants)	268.2
Interconnections power flows [MW]	
Tunisia->Sicilia (TUNITA)	-574.98
Malta->Sicilia	-193.2
Sicilia->Campania (TL-E)	916
Sardegna->Sicilia (TL-W)	-916
Calabria->Sicilia	-1750

In order to simulate the system split with Calabria and subsequently the loss of connection with Tunisia, modifications must be made to this initial operational condition (**S.0 MAX GEN-LOAD *modified***). The first modification involves reducing the production from photovoltaic and wind sources to ensure a regulation margin of 10% of instantaneous power. Therefore, the total production from these sources in the considered operational condition is reduced by 696.2

MW. The second modification involves shutting down other renewable energy plants whose contribution to frequency regulation has not been considered, particularly biomass and hydraulic plants, resulting in an additional production reduction of 31.43 MW. Finally, an additional cut of 432 MW in renewable production is considered, so that only 600 MW are exported to Calabria through the connection between Sicily and Calabria. To simulate the loss of island connection between Sicily and Sardinia, it is considered to start from the same working condition but with an increase in load, bringing the energy import from Tunisia to 575 MW.

The second operational condition analyzed, related to the **S.3 MAX LOAD** scenario, occurs on 10/08/2030 at 13:00. As for the previous case, in Table 29Table 28 the data related to this condition are reported, divided for each of the nine provinces that make up Sicily, while Table 30Table 29 reports the thermal generation from the traditional power plant and pumping station, and the active power flow from and to Sicily through the various interconnections.

Table 29 Load and renewable generation per province, 2030 MAX LOAD.

	LOAD AND RENEWABLE GENERATION – PROVINCIAL DATA (MW)									
	AG	**CL**	**CT**	**EN**	**ME**	**PA**	**RA**	**SR**	**TP**	**Total**
Load	298.11	172.54	1030.41	109.34	532.56	892.73	330.47	612.77	359.63	4338.57
	6.87%	3.98%	23.75%	2.52%	12.27%	20.58%	7.62%	14.12%	8.29%	100%
FV	159.84	275.82	715.03	446.45	11.28	498.74	113.82	258.13	462.79	2941.91
	5.43%	9.38%	24.31%	15.18%	0.38%	16.95%	3.87%	8.77%	15.73%	100%
Wind	113.57	22.34	91.51	47.29	61.83	169.06	17.69	52.69	170.07	746.05
	15.22%	2.99%	12.27%	6.34%	8.29%	22.66%	2.37%	7.06%	22.80%	100%
Wind OS	0.00	89.32	20.58	0.00	0.00	0.00	130.90	0.00	279.91	520.72
	0.00%	17.15%	3.95%	0.00%	0.00%	0.00%	25.14%	0.00%	53.75%	100%
Bio	11.66	0.56	6.80	9.71	1.84	3.89	0.92	1.33	0.41	37.12
	31.40%	1.52%	18.32%	26.17%	4.96%	10.47%	2.48%	3.58%	1.10%	100%
Hydro	0.61	0.04	4.35	1.93	0.10	0.66	0.00	0.34	0.01	8.04
	7.59%	0.53%	54.09%	24.01%	1.19%	8.25%	0.00%	4.29%	0.07%	100%
Load-Gen	12.44	-215.55	192.14	-396.04	457.52	220.38	67.14	300.27	-553.56	

Table 30 Traditional power plant production and interconnections power flows, 2030 S.3.

Active power production [MW]	
Anapo	-441.46
Guadalami	-44.8
Termini Imerese	0
Priolo	0
Porto Empedocle	0
New Plants CCGT-OCGT	0
Nuce	273.09
Milazzo	0
CHP (3 power plants)	268.2
Interconnections power flows [MW]	
Tunisia->Sicilia (TUNITA)	-574.98
Malta->Sicilia	-183.60
Sicilia->Campania (TL-E)	916
Sardegna->Sicilia (TL-W)	916
Calabria->Sicilia	788.25

It has been assumed that all photovoltaic and wind plants by 2030 are capable of contributing to frequency regulation with a static response of 5% and a dead band of 200 mHz. Additionally, it is assumed that the plants can provide SI corresponding to 3 seconds. Finally, to allow upward regulation, it is assumed that the plants operate at 90% of their Maximum Power Point (MPP). To model in NEPLAN the contribution to the dynamics provided by photovoltaic and wind power plants, the AC dispersed generator component controlled by the block diagram in Figure 41 was used, while Figure 42 shows the control scheme for the provision of the FFR and SI services.

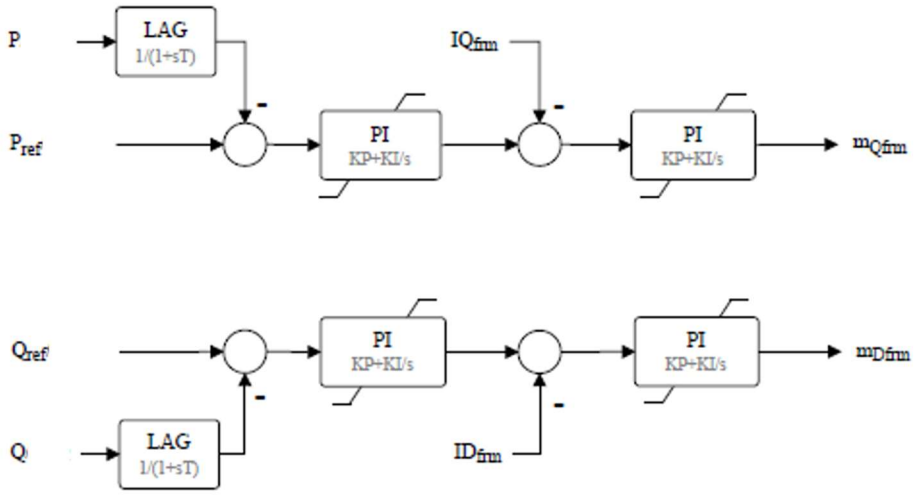

Figure 41 AC disperse generator control scheme, Neplan.

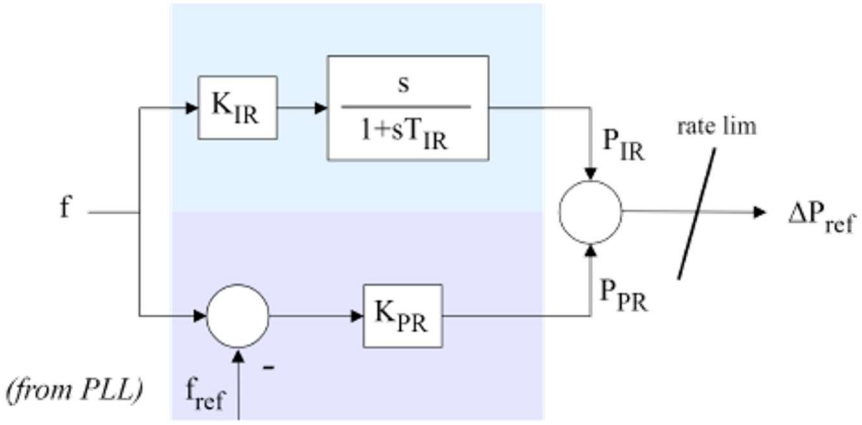

Figure 42 FFR and SI control scheme, Neplan.

5.2.2 Critical events and simulations assessment

In the assessed operational conditions, the following events are simulated:

- Overfrequency event in operational condition **S.0.1** (2030 S.0 MAX GEN-LOAD modified): Disconnection of Sicily from Calabria – loss of load equivalent to 605.46 MW.
- Underfrequency event in operational condition **S.0.2** (2030 S.0 MAX GEN-LOAD modified): Loss of connection between Sicily and Tunisia during the asynchronous operation of Sicily from the rest of Italy – loss of generation equivalent to about 575 MW.
- Underfrequency event in operational condition **S.0.3** (2030 S.3 MAX LOAD): Disconnection of Sicily from Calabria – loss of generation equivalent to about 790 MW.

For each event, multiple simulations are carried out, considering combinations of various contributions to regulation provided by the VSC converters of the Tyrrhenian Link - East (TL-E) and Tyrrhenian Link - West (TL-W), generation from wind and photovoltaic sources (RES), and traditional thermoelectric generation. In Table 31, a summary of the conducted simulations is presented, in which, for each simulation, the identifying code and the regulating contributions of various plants are specified. In all cases where RES plants or TL converters controlled in GFM participate in frequency regulation, they also provide a synthetic inertia service with an inertia time constant of 3 seconds. Is also worth noticing that in scenario S.3, the contribution to GFM regulation from TL-W, which is exporting from Sardinia near its maximum power, is not considered. Therefore, during the event, its contribution would be minimal compared to that

provided by TL-E and TUNITA, which are exporting from Sicily almost at full power.

Table 31 Performed simulations in the 2030 scenario for the operational conditions S.0.1, S.0.2, and S.0.3.

Sim. Code	THERMO	RES	TL-E GFL	TL-W GFL	TL-E GFM	TL-W GFM	TUNITA GFL	TUNITA GFM
S.0.1.1	X		X	X				
S.0.1.2	X	X	X	X				
S.0.1.3	X			X	X			
S.0.1.4	X	X		X	X			
S.0.1.5	X				X	X		
S.0.1.6	X	X			X	X		
S.0.2.1	X		X	X				
S.0.2.2	X	X	X	X				
S.0.2.3	X			X	X			
S.0.2.4	X	X		X	X			
S.0.2.5	X				X	X		
S.0.2.6	X	X			X	X		
S.0.3.1	X		X	X			X	
S.0.3.2	X	X	X	X			X	
S.0.3.3	X			X	X		X	
S.0.3.4	X	X		X	X		X	
S.0.3.5	X	X		X	X			X

5.3 2030 Simulation Results

In this paragraph, the results of primary regulation simulations under the previously presented operational conditions are reported.

5.3.1 Operational condition S.0.1

Table 32 Summary of the results for the S.0.1 operational condition.

	S.0.1.1	S.0.1.2	S.0.1.3	S.0.1.4	S.0.1.5	S.0.1.6
RES		X		X		X
TL-E			X	X	X	X
TL-W					X	X
Nadir [Hz]	N.D.	50.54	51.10	50.30	50. 72	50. 29
Time to nadir [s]	N.D.	2.61	55.78	17.90	56.77	27.27
***f* steady-state [Hz]**	N.D.	50.31	51.09	50.30	50.72	50.28
Time to steady-state [s]	N.D.	30.33	121.29	49.30	56.77	30.22
P_{min} TL-W [MW]	N.D.	916	916	916	1226	1206
Time to P_{min} TL-W [s]	N.D.	N.D.	N.D.	N.D.	3.48	4.23
$P_{steady\text{-}state}$ TL-W [MW]	N.D.	916	916	916	1062	973
P_{min} TL-E [MW]	N.D.	916	1540	1437	1226	1206
Time to P_{min} TL-E [s]	N.D.	N.D.	2.70	2.59	3.48	4.23
$P_{steady\text{-}state}$ TL-E [MW]	N.D.	916	1134	975	1062	973

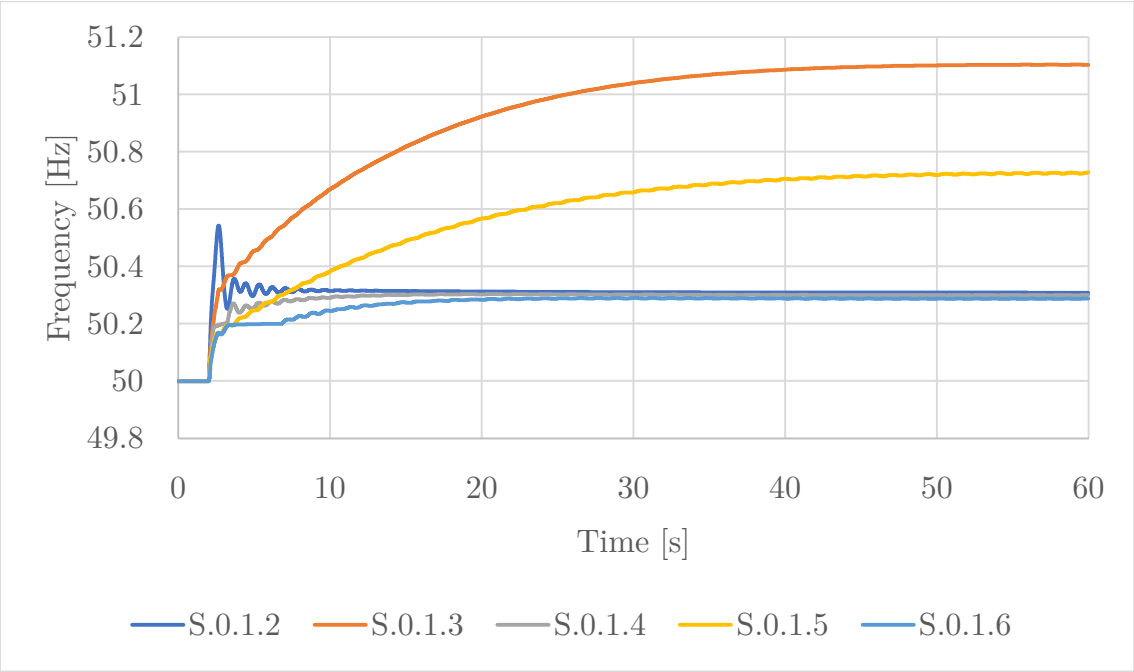

Figure 43 Frequency trends for each of the cases simulated in the operational condition S.0.1

S.0.1.1: Given that the only generators participating in frequency control are thermoelectric ones, and the total production of the generators is just over 520 MW, a loss of load exceeding 600 MW cannot be countered with a corresponding reduction in electrical production. The thermoelectric generators would shut down completely, and yet the disturbance would continue to go uncompensated. Therefore, in this scenario, the disconnection between Sicily and Calabria leads the Sicilian electrical system into a condition of instability.

S.0.1.2: Renewable generation participates in frequency regulation, preventing the frequency from increasing beyond 50.31 Hz, significantly below the limit of 51.5 Hz. The power produced by thermoelectric plants decreases but not completely, while the power generated by photovoltaic and wind plants decreases from the instant in which frequency exceeds 50.2 Hz. Renewables reduce their production by about 8.5% and contribute significantly to frequency regulation compared to thermoelectric, despite the delay in intervention due to the dead band. This condition, although leading to a loss of renewable energy production in favour of a lesser reduction in conventional production, allows the Sicilian grid to maintain the operation of rotating generation with its natural inertia.

S.0.1.3: The converter of TL-E participates in frequency regulation, halting the frequency increase at 51.09 Hz, a value very close to the island overfrequency limit of 51.5 Hz. Thermoelectric generators significantly reduce their production, and the TL-E converter overloads, reaching a peak of 1540 MW for a few moments. This condition is to be avoided as the production of thermoelectric power plants would fall below the technical minimum, while the TL-E converter, operated in Grid-Forming mode, would overload even under normal conditions.

S.0.1.4: The combined intervention of the thermoelectric, regulating renewable sources, and TL-E further mitigates the frequency error at steady-state compared to case S.0.1.2. The TL-E overloads less than in case S.0.1.3 and for a shorter duration. At the end of primary control operations, TL-E delivers a power 975 MW, just below its nominal capacity. However, the advantages of TL-E intervention in primary frequency control are not significant compared to the renewable contribution.

S.0.1.5: The thermoelectric generators must significantly reduce their production, risking falling below the technical minimum. Even though both converters of the Sicilian TL participate in regulation, their intervention leads to an overload condition that needs to be resolved as soon as possible.

S.0.1.6: This case is a variant of case S.0.1.4 with a general improvement in operational conditions following the regulatory intervention of the two TL converters with GFM control.

5.3.2 Operational condition S.0.2

Table 33 Table 31 Summary of the results for the S.0.2 operational condition.

	S.0.2.1	**S.0.2.2**	**S.0.2.3**	**S.0.2.4**	**S.0.2.5**	**S.0.2.6**
RES		X		X		X
TL-E			X	X	X	X
TL-W					X	X
Nadir [Hz]	46.00	49. 58	49.14	49.71	49.36	49.72
Time to nadir [s]	17.12	2.79	36.15	18.33	66.83	22.72
***f* steady-state [Hz]**	48.71	49.71	49.16	49.72	49.36	49.73
Time to steady-state [s]	> 70	40.97	55.42	40.17	66.83	36.82
P_{min} TL-W [MW]	916	916	916	916	687	688
Time to P_{min} TL-W [s]	N.D.	N.D.	N.D.	N.D.	2.70	2.72
$P_{steady\text{-}state}$ TL-W [MW]	916	916	916	916	838	912
P_{min} TL-E [MW]	916	916	417	462	687	688

Time to P_{min} TL-E [s]	N.D.	N.D.	3.54	2.61	2.70	2.72
$P_{steady-state}$ TL-E [MW]	916	916	753	860	838	912

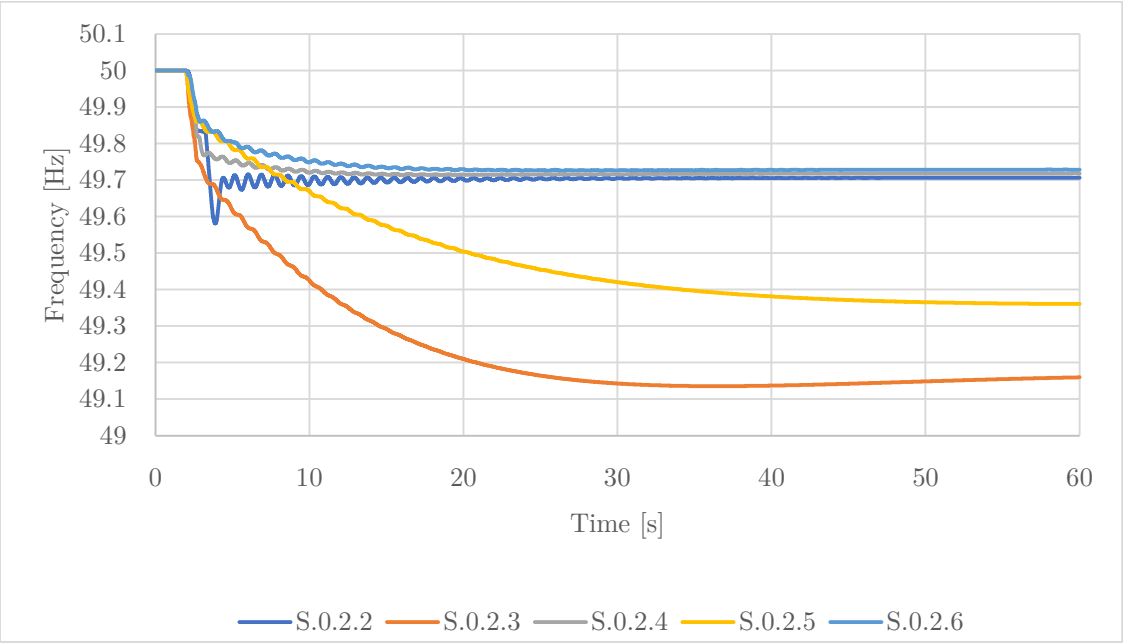

Figure 44 Frequency trends for each of the cases simulated in the operational condition S.0.2

S.0.2.1: In this case, the system is clearly unstable as it reaches a nadir frequency of 46 Hz. The only generators participating in regulation are thermoelectric, which are called upon to rapidly increase their production. However, in doing so, without the intervention of underfrequency protections, the CHP generators would operate at their nominal power at the end of primary regulation with no further regulation margin. This operational condition can be improved by implementing load shedding logic.

S.0.2.2: Renewable generation participates in frequency regulation, preventing the frequency from decreasing to 49.71 Hz, significantly above the limit of 47.5 Hz. The power produced by thermoelectric plants increases, the same happens with the power produced by photovoltaic and wind plants. The renewable power increase occurs within the primary reserve margin of 10% as anticipated in the simulations. In this case as well, renewables contribute significantly to frequency regulation compared to thermoelectric, despite the delay in intervention due to the 200 mHz dead-band.

S.0.2.3: In this case, only the converter of TL-E participates in frequency regulation, preventing the frequency from decreasing to 49.16 Hz. Thermoelectric

generators significantly increase their production, and the TL-E converter reduces the power transfer to Campania. This operational condition is to be avoided as it would require thermoelectric power plants to exert excessive effort to increase their production.

S.0.2.4: In this case, the combined intervention of the thermoelectric, regulating renewable sources, and TL-E further contains the frequency error at steady-state compared to case S.0.2.2. However, the advantages of TL-E's intervention in regulation are not significant compared to the regulating contribution of renewables since the frequency at the end of primary regulation changes only slightly, from 49.71 Hz in case S.0.2.2 to 49.72 Hz.

S.0.2.5: This case is a variant of case S.0.2.3 but with both converters of the Sicilian TL participating in regulation with GFM control. The benefit for the system consists in a fewer power demand from the thermoelectric power plants compared to case S.0.2.3.

S.0.2.6: This case is a variant of case S.0.2.4 with a general improvement in operational conditions following the regulatory intervention of the two TL converters with GFM control.

5.3.3 Operational condition S.0.3

Table 34 Summary of the results for the S.0.3 operational condition.

	S.0.3.1	**S.0.3.2**	**S.0.3.3**	**S.0.3.4**	**S.0.3.5**
RES		X		X	X
TL-E			X	X	X
TL-W					X
TUNITA					X
Nadir [Hz]	42.55	48.96	49.14	49.42	49.83
Time to nadir [s]	14.11	2.62	35.08	27.14	23.41
***f* steady-state [Hz]**	48.00	49.24	49.15	49.43	49.83
Time to steady-state [s]	59.86	59.82	59.99	59.94	59.69
P_{min} TL-W [MW]	916	916	916	916	916
Time to P_{min} TL-W [s]	N.D.	N.D.	N.D.	N.D.	N.D.
$P_{steady\text{-}state}$ TL-W [MW]	916	916	916	916	916
P_{min} TL-E [MW]	916	916	113.44	117.40	496
Time to P_{min} TL-E [s]	N.D.	N.D.	2.36	2.36	2.10
$P_{steady\text{-}state}$ TL-E [MW]	916	916	580.14	687.46	882.60
P_{min} TUNITA [MW]	575	575	575	575	197.00
Time P_{min} TUNITA [s]	N.D.	N.D.	N.D.	N.D.	2.30
$P_{steady\text{-}state}$ TUNITA [MW]	575	575	575	575	555.00

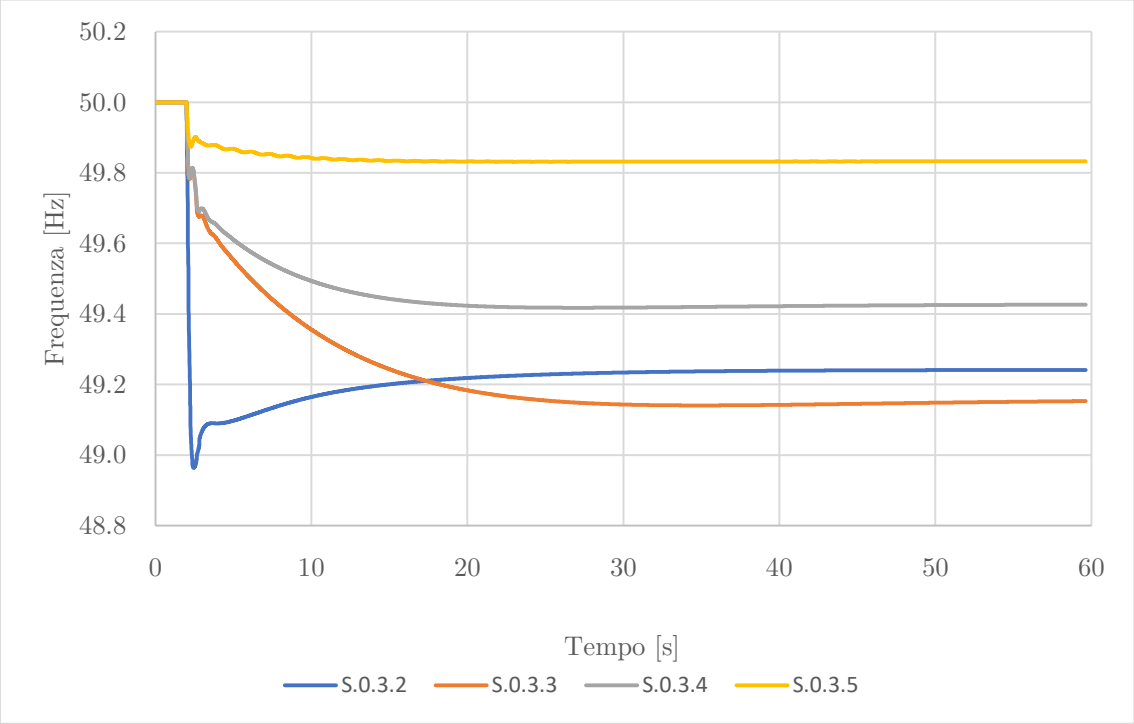

Figure 45 Frequency trends for each of the cases simulated in the operational condition S.0.3

S.0.3.1: The system is clearly unstable as it reaches a nadir frequency of 42.55 Hz. The only generators participating in regulation are thermoelectric, called upon to rapidly increase their production. However, in doing so, without the intervention of underfrequency protections, the CHP generators would operate at their nominal power at the end of primary regulation with no additional regulation margin. This operational condition is worse than the previously presented S.0.2.1, but it can be improved by implementing load shedding logic, for example, by disconnecting the two pumping stations of Guadalami and Anapo.

S.0.3.2: Renewable generation participates in frequency regulation, preventing the frequency from decreasing to 49.24 Hz, significantly above the limit of 47.5 Hz. Once again, renewables contribute significantly to frequency control compared to thermoelectric, despite the delay in intervention due to the 200 mHz dead-band.

S.0.3.3: The converter of TL-E participates in frequency regulation, preventing the frequency from decreasing to 49.14 Hz. Thermoelectric generators significantly increase their production, and the TL-E converter reduces the power transfer to

Campania. In conclusion, this operational condition is to be avoided as it would require thermoelectric power plants to exert excessive effort to increase their production in a timely manner to prevent an excessive decrease in network frequency.

S.0.3.4: The combined intervention of the thermoelectric, regulating renewable sources, and TL-E further contributes to the steady-state frequency error.

S.0.3.5: In this case, the situation improves compared to the previous scenario thanks to the intervention of TUNITA. TUNITA contributes especially in the initial phase of the loss of connection, rapidly reducing Sicily's export power and relieving TL-E while waiting for the intervention of renewable regulation.

5.3.4 2040 Scenario and operative conditions definition

To extend the temporal scope of investigation, the decision was made to analyse the year 2040, which is sufficiently distant from 2030 to denote significant differences between the scenarios. Developed by RSE, the 2040 scenario was built following the very same methodological approach of the previous one but with the generation and consumption projections 10 years further. In addition to an increase in installed renewable capacity, it is expected that numerous hydrogen production facilities (Power To X, P2X) will be present and operational. These facilities will use energy from renewable sources to increase energy consumption and reduce curtailment. Based on this assumption, an operational scenario entirely related to 2040 has been defined, called **S.4 MAX COMP**. This scenario corresponds to the operational condition characterized by the maximum compensation between load (including that of P2X plants) and generation, while simultaneously having the highest production from RES. In this scenario, for the purpose of dynamic studies, it is assumed that Sicily is connected to Calabria through a single line, and in the event of its interruption, a disturbance is generated that will be compensated by resources dedicated to primary control. This operational condition falls on 04/03/2040 at 10:00 and is characterized by the data reported in the following tables. Negative values in Table 35 account for the effect of P2X installations coupled to RES plants.

Table 35 Load and renewable generation per province, 2040 MAX COMP.

	LOAD AND RENEWABLE GENERATION – PROVINCIAL DATA (MW)									
	AG	**CL**	**CT**	**EN**	**ME**	**PA**	**RA**	**SR**	**TP**	**Total**
Load	170.83	98.87	590.46	62.65	305.17	511.56	189.37	351.14	206.08	2486.13
	6.87%	3.98%	23.75%	2.52%	12.27 %	20.58 %	7.62%	14.12 %	8.29%	100%
FV	252.40	435.54	1129.10	704.98	17.81	787.55	179.73	407.62	730.78	4645.53
	5.43%	9.38%	24.31%	15.18 %	0.38%	16.95 %	3.87%	8.77%	15.73 %	100%
Wind	-303.54	-59.72	-244.59	-126.39	-165.25	-451.86	-47.28	-140.83	-454.57	-1994.03
	15.22 %	2.99%	12.27%	6.34%	8.29%	22.66 %	2.37%	7.06%	22.80 %	100%
Wind OS	0.00	39.65	9.14	0.00	0.00	0.00	58.10	0.00	124.24	231.1185
	0.00%	17.15 %	3.95%	0.00%	0.00%	0.00%	25.14 %	0.00%	53.75 %	100%
Bio	14.47	0.70	8.44	12.06	2.28	4.82	1.14	1.65	0.51	46.07
	31.40 %	1.52%	18.32%	26.17 %	4.96%	10.47 %	2.48%	3.58%	1.10%	100%
Hydro	0.68	0.05	4.85	2.15	0.11	0.74	0.00	0.38	0.01	8.97
	7.59%	0.53%	54.09%	24.01 %	1.19%	8.25%	0.00%	4.29%	0.07%	100%
Load-Gen	206.82	-317.34	-316.48	-530.15	450.22	170.30	-2.33	82.31	-194.88	

Table 36 Traditional power plant production and interconnections power flows, 2040 S.4.

Active power production [MW]	
Anapo	-441.46
Guadalami	-44.8
Termini Imerese	0
Priolo	0
Porto Empedocle	0
New Plants CCGT-OCGT	0
Nuce	273.09
Milazzo	0
CHP (3 power plants)	268.2
Interconnections power flows [MW]	
Tunisia->Sicilia (TUNITA)	-574.98
Malta->Sicilia	-183.60
Sicilia->Campania (TL-E)	916
Sardegna->Sicilia (TL-W)	916
Calabria->Sicilia	788.25

In this operational condition, referred to as S.0.4, the following event is simulated:

- Overfrequency event in operational condition S.0.4: Disconnection of Sicily from Calabria - loss of load equivalent to approximately 380 MW.

In addition, two variant version of the previous case are simulated. In the first one, it is assumed that the Anapo and Guadalami power plants are not in service, resulting in a consequent reduction in the island's electrical load. The disconnection of Sicily from Calabria in this scenario leads to a loss of approximately 890 MW. This additional study is introduced as an extreme case in the 2040 scenario, where a considerable and rapid reduction in production is required to address the disturbance. In the second one, it is assumed the conversion from AC to DC of a line connecting two important nodes, known as "Partanna-Partinico". The current line operates at 220 kV and has a length of about 39 km. In accordance with previous studies carried out by RSE [83]-[84], it is converted into an HVDC line with a nominal voltage of 1000 kV and powered by two VSC converters, each with a power of 1000 MW. The two converters are named VSC-Partinico and VSC-Partanna. In this hypothesis, new simulations are carried out assuming two different control modes for the converters.

The study of the 2040 scenario in the presence of the event S.0.4 and its variants is interesting compared to the study of previous operational conditions because, as shown in Table 36, there are no thermoelectric power plants in operation during the considered event. In Table 31, a summary of the conducted simulations is presented, in which, for each simulation, the identifying code and the regulating contributions of various plants are specified. In all cases where RES plants or TL converters controlled in GFM participate in frequency regulation, they also provide a synthetic inertia service with an inertia time constant of 3 seconds.

Table 37 Performed simulations in the 2040 scenario for the operational condition S.0.4.

Sim. Code	Variant	RES	TL-E GFL	TL-W GFL	TL-E GFM	TL-W GFM	TUNITA GFL	TUNITA GFM	P-P GFL	P-P GFM
S.0.4.1		X	X	X			X			
S.0.4.2		X		X	X		X			
S.0.4.3		X			X	X	X			
S.0.4.4		X			X	X		X		
S.0.4.5	1	X	X	X			X			
S.0.4.6	1	X		X	X		X			
S.0.4.7	1	X			X	X	X			

S.0.4.8	1	X			X	X		X		
S.0.4.9	2	X	X	X			X		X	
S.0.4.10	2	X	X	X			X			X

5.4 2040 Simulation Results

In this paragraph, the results of primary regulation simulations under the previously presented operational conditions are reported.

5.4.1 Operational condition S.0.4

Table 38 Summary of the results for the S.0.4 operational condition.

	S.0.4.1	**S.0.4.2**	**S.0.4.3**	**S.0.4.4**
RES	X	X	X	X
TL-E		X	X	X
TL-W			X	X
TUNITA				X
Nadir [Hz]	50.48	50.27	50.09	50.087
Tempo al nadir [s]	52.63	40.0	52.40	59.26
***f* steady-state [Hz]**	50.48	50.27	50.09	50.087
Tempo allo steady-state [s]	52.63	40.0	52.40	58.77
P_{max} TL-W-S [MW]	0	0	191.22	128.14
Tempo a P_{max} TL-W-S [s]	N.D.	N.D.	2.59	2.10
$P_{steady\text{-}state}$ TL-W-S [MW]	0	0	50.36	17.50
P_{max} TL-E-S [MW]	0	376.41	191.22	128.14
Tempo a P_{max} TL-E-S [s]	N.D.	2.76	2.59	2.10
$P_{steady\text{-}state}$ TL-E-S [MW]	0	52.18	50.36	17.50
P_{max} TUNITA [MW]	0	0	0	68.11
Tempo a P_{max} TUNITA [s]	N.D.	N.D.	N.D.	2.30
$P_{steady\text{-}state}$ TUNITA[MW]	0	0	0	10.46

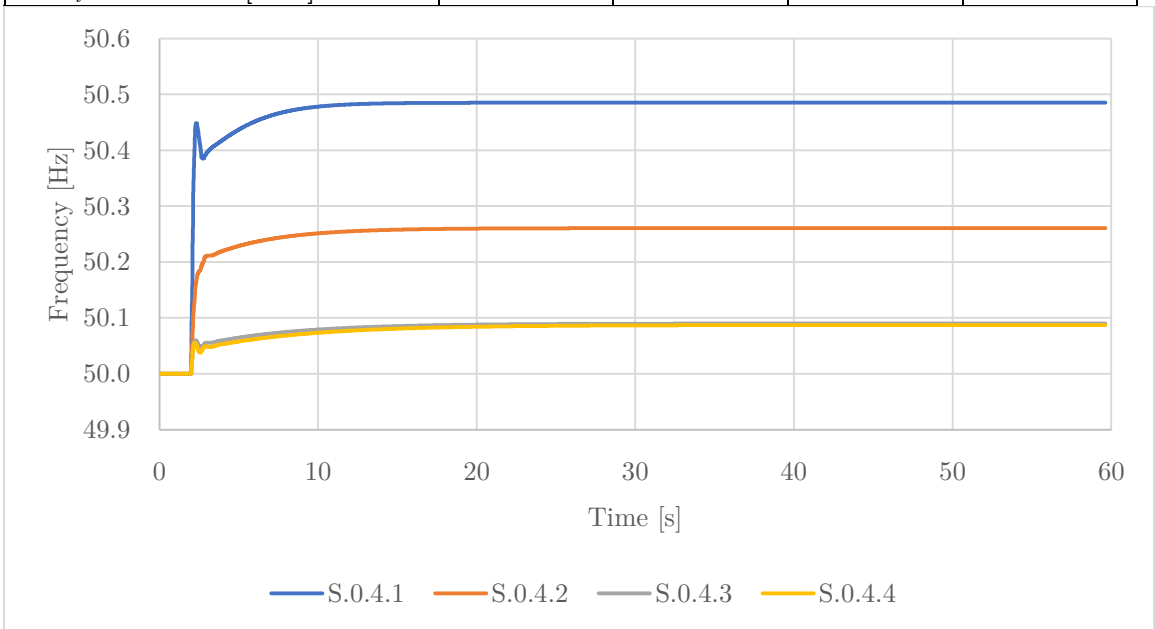

Figure 46 Frequency trends for each of the cases simulated in the operational condition S.0.4.

S.0.4.1: Frequency does not experience significant variations thanks to the regulating action of renewable sources. At the end of primary regulation, these sources have reduced their contribution by about 390 MW, corresponding to the power transmitted to Calabria before the interruption of Sicily's connection plus a small contribution to losses. Both the TL and TUNITA do not change their power output, which is equal to 0 at the time of the disturbance.

S.0.4.2: The intervention of the TL-E converter allows for a reduction in the frequency error at steady state due to the immediate action of the VSC converter regulation, which, in the simulations, is assumed to have no dead band (the effect of the 10 mHz dead band is neglected).

S.0.4.3: Compared to the previous case, the intervention of the second GFM converter of the TL slightly improves the steady-state frequency value. The main frequency regulation action is carried out by renewable sources, as in cases S.0.4.1 and S.0.4.2.

S.0.4.4: Compared to the previous case, the intervention of the TUNITA in GFM almost does not alter the steady-state frequency value. The main frequency regulation action is once again carried out by renewable sources.

5.4.2 Operational condition S.0.4 Variant 1

Table 39 Summary of the results for the S.0.4 operational condition, Variant 1.

	S.0.4.5	**S.0.4.6**	**S.0.4.7**	**S.0.4.8**
RES	X	X	X	X
TL-E		X	X	X
TL-W			X	X
TUNITA				X
Nadir [Hz]	50.938	50.415	50.395	50.384
Tempo al nadir [s]	31.12	48.54	56.53	59.00
***f* steady-state [Hz]**	50.938	50.415	50.395	50.384
Tempo allo steady-state [s]	31.12	48.54	56.53	59.00
P_{max} TL-W-S [MW]	0	0	441.93	357.37
Tempo a P_{max} TL-W-S [s]	N.D.	N.D.	2.57	2.47
$P_{steady\text{-}state}$ TL-W-S [MW]	0	0	79.09	76.88
P_{max} TL-E-S [MW]	0	799	441.93	357.37
Tempo a P_{max} TL-E-S [s]	N.D.	2.26	2.57	2.47
$P_{steady\text{-}state}$ TL-E-S [MW]	0	83	79.09	76.88
P_{max} TUNITA [MW]	0	0	0	230.07
Tempo a P_{max} TUNITA [s]	N.D.	N.D.	N.D.	2.47
$P_{steady\text{-}state}$ TUNITA[MW]	0	0	0	46.07

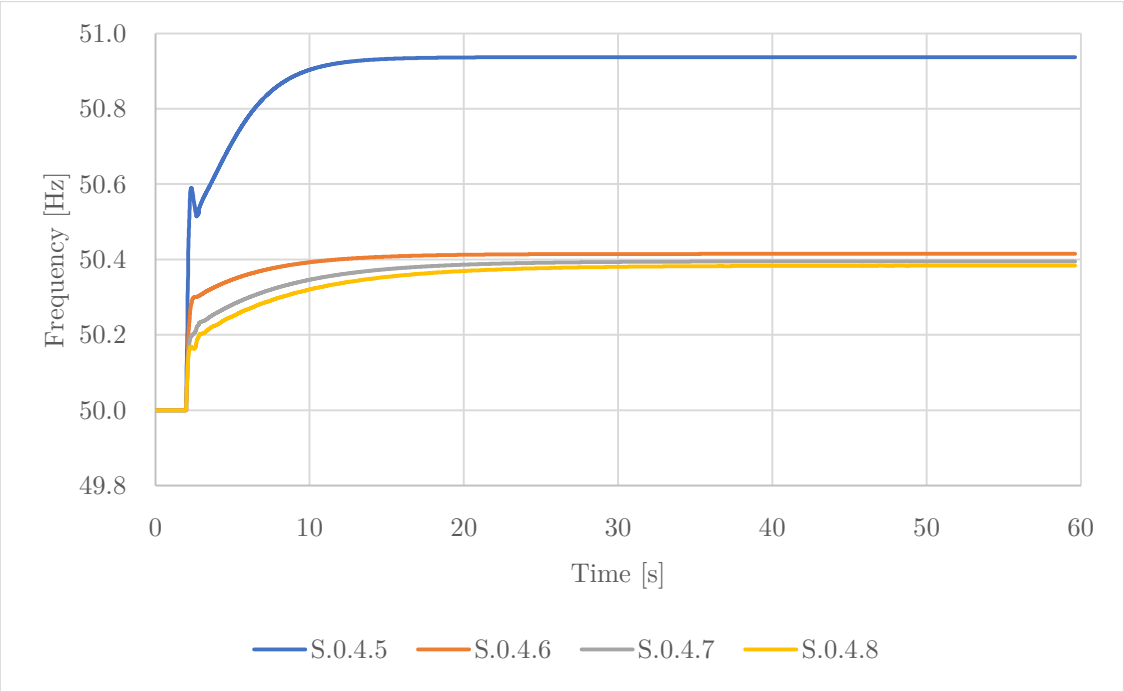

Figure 47 Frequency trends for each of the cases simulated in the operational condition S.0.4 Variant 1.

S.0.4.5: Frequency experiences a significant variation but within the allowed overfrequency range. Renewable sources reduce their production but with a delay compared to the frequency variation due to the 200 mHz dead band set in the control of RES generators. Both the TL and TUNITA do not change their power output, which is equal to 0 at the time of the disturbance.

S.0.4.6: The absence of the regulating contribution from the thermoelectric and the dead band of the renewable sources means that, as soon as the regulating action of the TL-E is introduced, there is a significant improvement in the steady-state frequency. This behavior is due to the absence of a dead band in the TL converter, allowing the immediate activation of primary frequency regulation. The effect would be almost identical even in the presence of a 10 mHz dead band in the TL, equal to the current one in thermoelectric power plants.

S.0.4.7: Compared to the previous case, the intervention of the second GFM converter of the TL slightly improves the steady-state frequency value.

S.0.4.8: Compared to the previous case, the intervention of the TUNITA in GFM almost does not alter the steady-state frequency value. The TL is slightly relieved in the frequency regulation action, while the contribution of renewables is reduced compared to case S.0.4.7.

5.4.3 Operational condition S.0.4 Variant 2

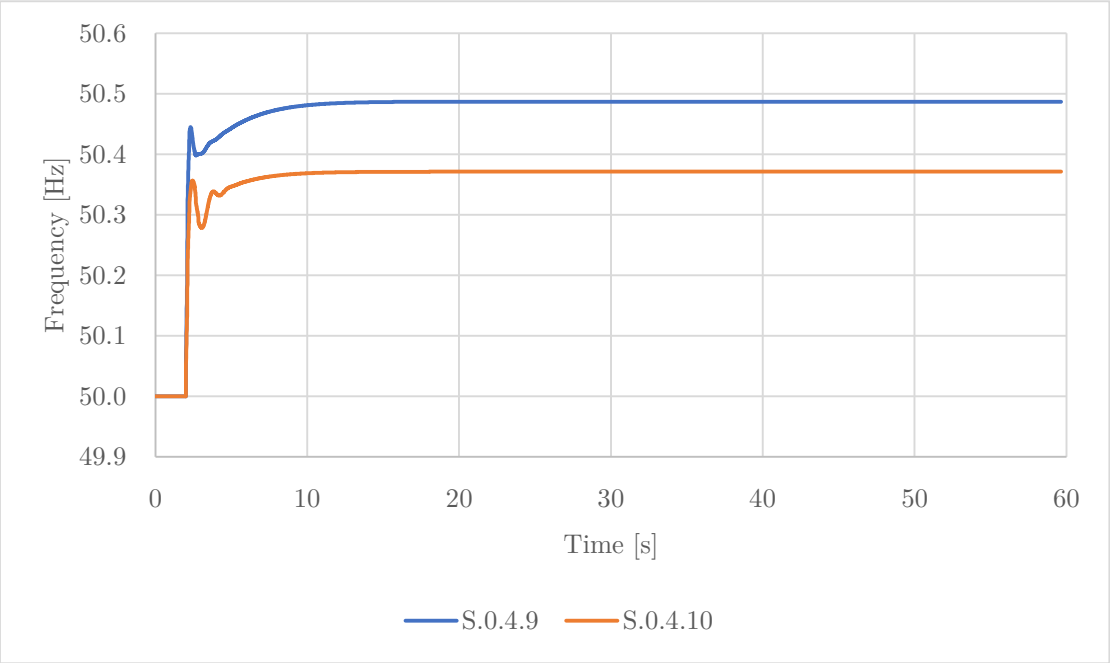

Figure 48 Frequency trends for each of the cases simulated in the operational condition S.0.4 Variant 2.

S.0.4.9: The presence of the two VSC converters on the Partanna-Partinico line does not alter the frequency response during the event, nor does it affect the power output from renewable generation and from the TL and TUNITA. The GFL control of the two VSC converters within the island allows for the maintenance of an unchanged power flow between the Partanna and Partinico stations without influencing frequency regulation. It can be stated that the results of case S.0.4.9 are identical to those of case S.0.4.1.

S.0.4.10: the GFM operation of the VSC-Partanna converter reduces the steady-state frequency error. Therefore, the combined effect of the two converters results in a power response that supports frequency regulation with a slight reduction in the steady-state error. This is presumably due to the instantaneous intervention of the combined action of the two HVDC line converters, which reduces the frequency drift while waiting for the regulation of renewable generators to take effect.

5.4.4 Final considerations on the Sicilian Power Grid

In this chapter, the results of a complex and detailed research study conducted on the Sicilian power grid in the framework of the PTR 2022-2024 have been presented. The main objective of the study was to assess the state of the Sicilian grid in future energy scenarios built upon the development plans of the Italian TSO Terna and the forecasts for renewable installations that will impact the island. Already in the scenario definition phase, several critical issues emerged related to the weakening of the electrical system, primarily due to a degradation of system inertia. In a large number of simulated hours, the share of renewables exceeds 80%, and in some purely theoretical cases, the entire demand is covered by RES. In this scenario, the contribution of renewables to the grid regulation is crucial. Without them, the system would be exposed to the risk of instability for many hours of the year. Aware of these challenges, Terna's development plan includes numerous interventions to strengthen the Sicilian grid in its main backbones. Among these interventions, the contribution of HVDC will be crucial in increasing the reliability of the system: the Tyrrhenian Link project, indeed, aims to facilitate the exchange of renewable energy between Sicily and other regions of Italy, reducing curtailment through new export channels.

From a dynamic perspective, various contingencies that could compromise the stability of the Sicilian power system have been analyzed, such as the opening of the connection with Calabria or the disconnection of large generation parks due to faults. The main result that emerges from all simulations is that the system, in the presence of only traditional regulating sources, would not be able to withstand disturbances of such magnitude. The contribution of RESs, controlled to provide FFR and SI, becomes crucial in containing the frequency drift and keeping the system operational even under critical conditions. In addition to these considerations, the possibility of operating the converters of the main VSC-HVDC infrastructures to be implemented on the island - Tyrrhenian Link and TUNITA - in GFM mode to provide support services for primary regulation has been explored. The results clearly demonstrate a positive effect of these implementations even in extreme energy scenarios, such as the one presented in 2040, in which conventional power plants are completely excluded from the energy mix.

6. Conclusions

In this thesis, various innovative frequency control techniques for power systems have been explored and analyzed, aiming to address the challenges posed by the increasing integration of renewable energy sources and the evolving nature of modern power grids. The research theme is part of the broader context of the energy transition, promoted by national and European institutions since the end of the last century when the issue of climate change was brought to the attention of governments and the public. The thesis has proposed and evaluated innovative control strategies for frequency support, including Fast Frequency Reserve, Synthetic Inertia, Vehicle-to-Grid, and Grid Forming Control. Through extensive simulation studies, these strategies have demonstrated their effectiveness in enhancing the stability and resilience of power systems.

After a brief examination of the legislative context that led to an unprecedented increase in renewable sources in the electricity production mix, the thesis presented the characteristics of the frequency control system as it is currently operated. The analysis included various documents and reports from ENTSO-E to provide a European overview of regulations regarding frequency regulation and control. The research has shown the implications of high renewable penetration, highlighting the need for adaptive and flexible control strategies that can accommodate the variability and intermittency inherent in renewable sources. With these necessary premises, starting from Chapter 3 the original work conducted during the three-year doctoral period was presented, part of which has already been made public through individual articles or conference proceedings. The structure of the thesis fully reflects the main objective of the research, which is to assess different frequency control strategies in relation to the state of interconnection and robustness of the electrical systems.

The first studies to be presented were those related to the Continental Europe Synchronous Area, the largest synchronous area in the world. Starting from the analysis of the Fast Reserve Unit, a pilot project by the Italian TSO Terna, a continental dissemination of this technology for fast primary regulation has been proposed. In addition to the provision of an original division scheme among the countries, the effects of this technology for a disturbance equal to the Reference

Incident and for that causing the System Split of the 08/01/2021 were evaluated. The results show how frequency parameters in 2040 can become comparable to the current ones with only 4000 MW of FRUs, suggesting the strategic relevance of the FFR service in future electric power systems.

In Chapter 4, the studies conducted on small islands were collected and examined, a topic that is very important to the research group at the University of Palermo, whose significant expertise has been built over the years. The island of Favignana, for example, has been the subject of studies for various aspects over the years, with the primary focus being on the integration of renewable sources. The study on Favignana was conducted in three different phases: first, the optimal energy mix was assessed to integrate renewable sources as much as possible without compromising stability. Subsequently, a feasibility study was conducted to verify the adequacy of the island's electrical system to accommodate the expected growth in electric mobility in the coming years. Building on the results of the first two phases, a study on the impact of V2G was conducted, identifying the minimum number of charging stations necessary to integrate 1 MW of photovoltaics into the electrical production park without jeopardising the stability of the system. The second case study related to small islands focused on the island of Gozo, the largest island in Malta. Despite being interconnected with Italy, Malta's electrical system exhibits all the characteristics that of a small island. Considering the results of several previous studies and data provided by the local TSO, Enemalta, a simulation study was conducted in which two large photovoltaic plants on the island were operated with Grid Forming control to provide frequency regulation. The results showed an improvement in frequency dynamics of up to 50% compared to the base case, suggesting that, in the near future, these types of services will not be the sole prerogative of High Voltage plants and that the distribution system will also be called upon to support the entire system through innovative services and controls.

Finally, the last chapter presented all the investigations related to the Sicilian electrical system. The study was conducted in within the framework of a research contract with the RSE research institute to assess the expansion of the Sicilian electrical system in future energy scenarios. Both static and dynamic simulations showed a system that will face challenges related to congestion of lines and

transformers and the reduction of inertia and primary reserve. The main cause of this can be attributed to the massive installation of renewable sources expected in 2030 and 2040. In this scenario, the provision of regulation services becomes crucial to avoid system collapses in the presence of severe disturbances. The developed control strategies have been evaluated under various disturbance and contingencies, such as sudden load changes, faults, and system splits. The results indicate an improved and faster system response, thereby minimizing the impact of disturbances on frequency stability. Noteworthy is the application of Grid Forming control for frequency control applications. The implemented schemes enable a decisive contribution to resolving emergency conditions in both strongly and weakly interconnected systems. However, differences exist in the behaviour of this control in different networks, particularly concerning the stability of the control in interconnected areas. As known, Grid-Forming control excels in weak networks, providing an independent reference for both frequency and voltage regardless of network conditions. In highly interconnected networks, there is a risk of instability associated with the possible mismatch between the Grid Forming voltage and the network voltage, leading to fluctuations in active power and potential overloads. The implemented cases have partially highlighted these differences, with good stability achieved in both the Maltese and Sicilian case studies. The reasons for this effect lie in the nature of the simulated energy scenarios: in the presence of a high penetration of renewable sources, the stiffness of the network has been, in fact, weakened, reducing the synchronization issues of the Grid Forming, which, in all simulated cases, showed no power fluctuations at steady-state.

The findings presented in this thesis underscore the significance of innovative control strategies in ensuring reliability of power systems undergoing significant transformations. The research outcomes not only advance academic knowledge but also offer practical insights for industry stakeholders and policymakers seeking to optimize frequency control.

Achieving the Zero Emissions target is not impossible, but it presupposes a radical change in the paradigms of all aspects of power systems management, starting with the way we produce, transport, distribute, and use the electrical energy.

Appendix 1

Power Systems Primary Control

The correct operation of a power system requires monitoring the frequency, power exchanges, and voltage at the nodes. Control of such complexity is performed using automatic control theory to accurately model the system. The control is carried out through two distinct regulation channels, the first one called "frequency-active power" (*f-P*), and the second one called "voltage-reactive power" (*V-Q*). This separation is considered appropriate and representative of reality due to the different response times of the two regulation channels. The second one, being primarily electrical, is much faster than the first, which is electro-mechanical in nature. It is possible to assert that:

- Static variations in active power ΔP only affect the phase angles of voltages (and thus active power flows), leaving their magnitudes (and thus reactive power flows) unchanged.
- Static variations in reactive power ΔQ only affect the magnitudes of voltages (and thus reactive power flows), leaving their phase angles (and thus active power flows) unchanged.

Indeed, for a line with impedance $\dot{Z} = R + jX$ where admittance can be neglected, connected to a load that consumes P_2 and Q_2 (resulting in a current I_2 and a phase φ), the voltage variation can be approximated as:

$$E_1 - E_2 = \overline{AB} \cong RI_2 \cos\varphi + XI_2 \sin\varphi = \frac{RP_2 + XQ_2}{E_2}$$

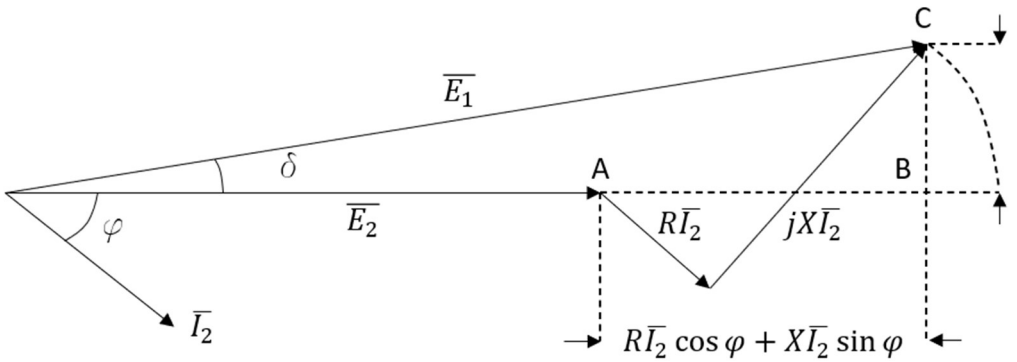

Figure A.1 Phase Diagram of Voltages.

The angle δ between the voltages $\overline{E_1}$ and $\overline{E_2}$ is:

$$\delta = \sin^{-1}\frac{\overline{BC}}{E_1}$$

Where:

$$\overline{BC} = \frac{XP_2 - RQ_2}{E_2}$$

Consequently:

$$\delta = \sin^{-1}\frac{XP_2 - RQ_2}{E_1 \cdot E_2}$$

In High Voltage Power systems, $X>>R$, so, accordingly to previous equations, it can be stated that:

$$\delta \cap P \qquad \Delta V \cap Q$$

The division of the two control channels can be considered correct when frequency variations occur in a quasi-static manner, meaning relatively small and rapid changes. Due to the high degree of interconnection of high-voltage systems, this approximation can be considered valid. This is why active power is regulated for frequency control.

Frequency is indeed linked to the rotational speed of alternators, which remains constant when a perfect balance between the active power generated and the power demanded by the grid, including load and losses, is achieved. This equilibrium is constantly disrupted due to the natural variability of the load, causing machines to either accelerate or decelerate depending on the circumstances. The purpose of frequency regulation in electrical networks is to automatically maintain the frequency at its nominal value, regardless of fluctuations in the load, and to keep the programmed exchanging power between areas fully consistent with provided values.

The variables involved in frequency regulation are divided into:

1. reference variables
    a. nominal frequency;
    b. programmed exchanged power;

2. controlled variables
    a. instantaneous frequency;
    b. instantaneous active power;
3. Disturb Variables
    a. Load variations;
    b. Line Faults;
    c. Generation faults;

A fundamental concept for frequency regulation is that of a control area, which refers to a group of loads and generators belonging to a well-defined geographic region and connected through the power lines. In the control area, it is assumed that frequency is a global quantity, meaning it has the same value at every point within the system. This assumption, which can be applied in the case of small, short-duration disturbances, is compatible with large interconnected high-voltage systems and allows the study of frequency transients with regulation using linear differential equations with constant coefficients that can be transformed using Laplace methods. In this way, it is possible to apply the theory of linear systems, leading to a system that can be modelled using block diagrams and transfer functions.

The load characteristic

Consider an assembly consisting of a prime mover coupled to an alternator feeding a load and assume that the opening of the turbine distributor is an independent variable. Referring to an initial equilibrium situation in which the generated power P_g equals the power demanded by the loads plus losses, let's assume the occurrence of a disturbance ΔP_D. Due to the disruption of equilibrium, the frequency of the system will change, and along with it, the power demanded by the load and the kinetic energy associated with rotating machines will vary as follows:

$$[P_g^0 + \Delta P_g] = [\Delta P_D] + [P_l^0 + l] + [\Delta P_a]$$

In the previous equation, the subscript "0" represents the value of the quantity in initial conditions. The term ΔP_a represents the "accelerating power" that is either absorbed or supplied by the machines depending on the situation. The power absorbed by the load depends on the frequency and is denoted as ΔP_l, which is

the change in load power consumption with respect to the frequency variation, while ΔP_D represents the change in power demanded by the load.

The accelerating power ΔP_a represent the variation in kinetic energy W_{kin} of the rotating masses, as:

$$\Delta P_a = \frac{d}{dt} W_{kin}$$

The kinetic energy varies with the angular speed ω as:

$$W_{kin} = \left[\frac{f(t)}{f_0}\right]^2 W_{kin}^0$$

With $\omega = 2\pi f$.

Since $f(t) = f_0 + \Delta f(t)$, if $\Delta f(t)$ is small, it is possible to assume that:

$$W_{kin} = \left[\frac{f_0 + \Delta f(t)}{f_0}\right]^2 W_{kin}^0 \cong \left[1 + \frac{2\Delta f(t)}{f_0}\right] W_{kin}^0$$

Combining the previous equations, it results:

$$\frac{d}{dt} W_{kin} = \frac{2W_{kin}^0}{f_0} \frac{d}{dt} \Delta f(t)$$

If we define the *inertia coefficient* $K = \frac{2W_{kin}^0}{f_0}$, we can conclude that:

$$\Delta P_a = K \frac{d}{dt} \Delta f(t)$$

The power requested by the loads varies depending on frequency. In general, the power absorbed by a group of loads can be defined as:

$$P_c(t) = P_c^0 \left[\frac{f(t)}{f_0}\right]^\alpha$$

With α a frequency-variation coefficient that is usually $\alpha \cong 1$.

Introducing finite elements and within the scope of small variations, the previous equation becomes:

$$\Delta P_c(t) = \alpha \frac{P_c^0}{f_0} \Delta f(t) = E_i \Delta f(t)$$

With E_i named as "*loads regulating energy*". This parameter express the variation in load demand with respect to the frequency, in figure A.2 it is reported the "*static characteristic of the load*". From this, it can be observed that the load provides a positive contribution to regulation: with a decrease (increase) in frequency, the load naturally responds by demanding less (more) power, thereby contributing to achieving a stable condition after a disturbance.

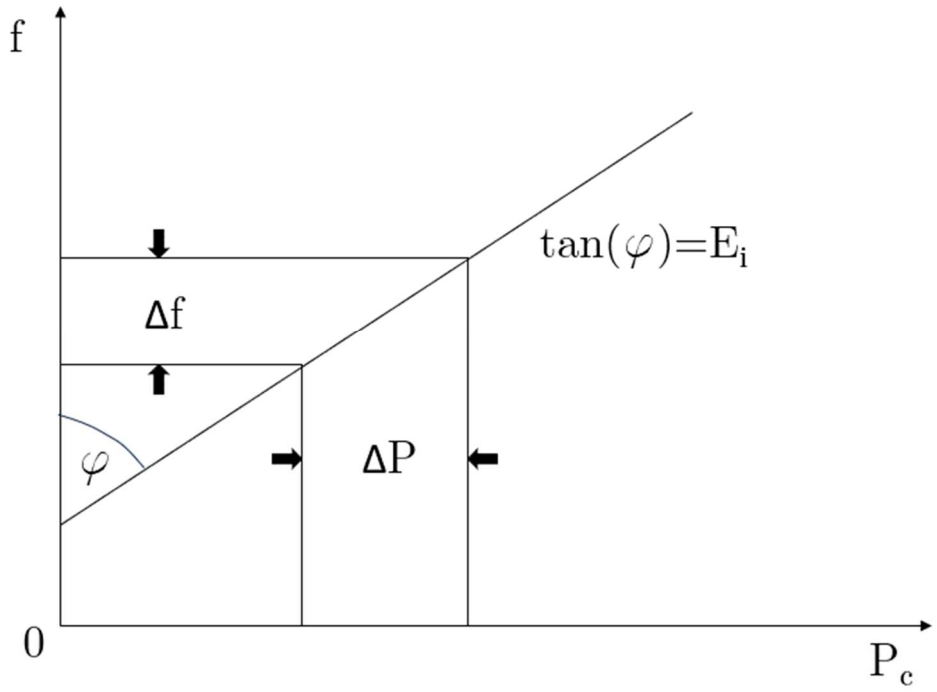

Figure A.2 Static Characteristic of the load

The term ΔP_g appearing on the left side of the equilibrium equation represents the dependence of the generated power on the opening degree of the turbine governor valve, considered as a variable independent at the moment. By substituting the now explicit terms into the equation, it can be obtained:

$$\Delta P_g(t) - \Delta P_D(t) = E_i \Delta f(t) + K \frac{d}{dt} \Delta f(t)$$

By Laplace-transforming:

$$\Delta P_g(s) - \Delta P_D(s) = \Delta F[E_i + sK]$$

Which can be re-written as:

$$\Delta F = \frac{E_i^{-1}}{1 + sK/E_i} \left[\Delta P_g(s) - \Delta P_D(s)\right]$$

By defining:

$$T_i = \frac{K}{E_i} = \frac{2W_{kin}^0}{\alpha P_c^0} = \frac{T_A}{\alpha}$$

It can be obtained:

$$\Delta F = \frac{E_i^{-1}}{1 + sT_i}\left[\Delta P_g(s) - \Delta P_D(s)\right]$$

The time constant $T_A = 2W_{kin}^0/P_c^0$ is called the "startup time" of the system consisting of the generator and its load. The final equation is represented by the block diagram shown in Figure A.3.

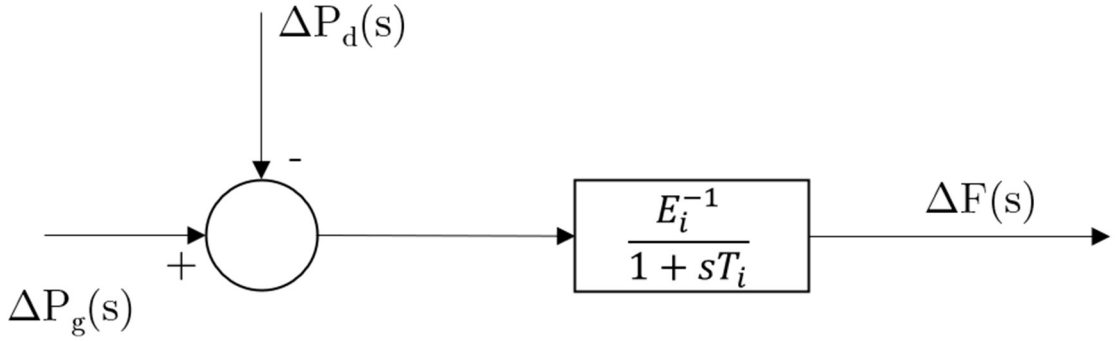

Figure A.3 Block Diagram of a plant made up by a load and a generator.

The Speed Regulator

The relationship expressing the behavior of the controller and the governor valve, along with their corresponding block diagram, is derived as shown in Figure A.5.

$$\Delta P_g = \Delta P_t = \frac{E_R}{1 + sT_R}\left[K'\Delta X_A - \Delta F\right]$$

where $'\Delta X_A$ is the position variation of the Round Per Minute Controller (RPM Controller) with respect to the initial one, assumed in this notation as “Point A”.

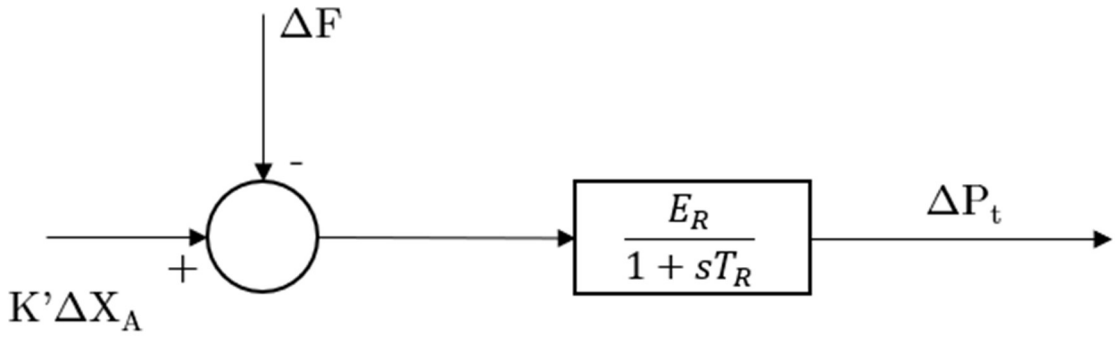

Figure A.5 Block Diagram of the Speed Regulator

From the block diagram in Figure A.5, it can be derived the steady-state relationship between frequency and power input to the turbine. Assuming no action on the RPM controller, meaning that the position of point A remains fixed ($\Delta X_A = 0$), then:

$$\Delta P_t = \frac{E_R}{1 + sT_R}[-\Delta F] = -\frac{E_R}{1 + sT_R}\Delta F$$

Applying the final value theorem to this relationship for a step change in frequency yields:

$$\Delta P_{t\,stat} = \lim_{t\to\infty}[\Delta P(t)] = \lim_{s\to 0}[s\Delta P_t] = \lim_{s\to 0}\left[s\frac{-E_R}{1 + sT_R}\Delta F\right] =$$

$$= -E_R \lim_{t\to\infty}[\Delta f(t)] = -E_R \Delta f_{stat}$$

When the frequency error $\Delta f(t)$ reaches a steady-state constant value Δf_{stat}, there is a corresponding constant change in power $\Delta P_{t\,stat}$.

$$\Delta P_{t\,stat} = -E_R \Delta f_{stat}$$

From this relationship, it is evident that changes in power input have an opposite sign to changes in frequency. The proportionality coefficient E_R has the dimensions of energy and is referred to as the "*regulating energy of the machine*". Indeed, the value of E_R depends on the characteristics of the controller and is measured in megawatts per hertz (MW/Hz). It quantifies the ability of the machine to respond to frequency variations and contribute to maintaining system stability. The previous relationship, when plotted in an *f-P* (frequency vs. active power) plane, traces a straight line with a slope of $-E_R$. This characteristic is known as the "*static characteristic of the machine*." From this characteristic, it

can be deduced that the higher the power demand from the user, the lower the speed of the machine, and consequently, the frequency.

It was previously assumed that the RPM controller was locked. Now, let's suppose that it can act, and let's consider the conditions of a system with predominant power ($\Delta F = 0$). By doing so, it can be written:

$$\Delta P_t = \frac{E_R}{1 + sT_R} K' \Delta X_A$$

Applying the final value theorem:

$$\Delta P_t = E_R K' \Delta X_A$$

From the previous equation, it can be deduced that a command ΔX_A on the RPM controller causes a translation of the static characteristic parallel to itself, Figure A.7. The purpose of the RPM controller is indeed to achieve static characteristics in which different speeds (and therefore frequencies) correspond to the same power level.

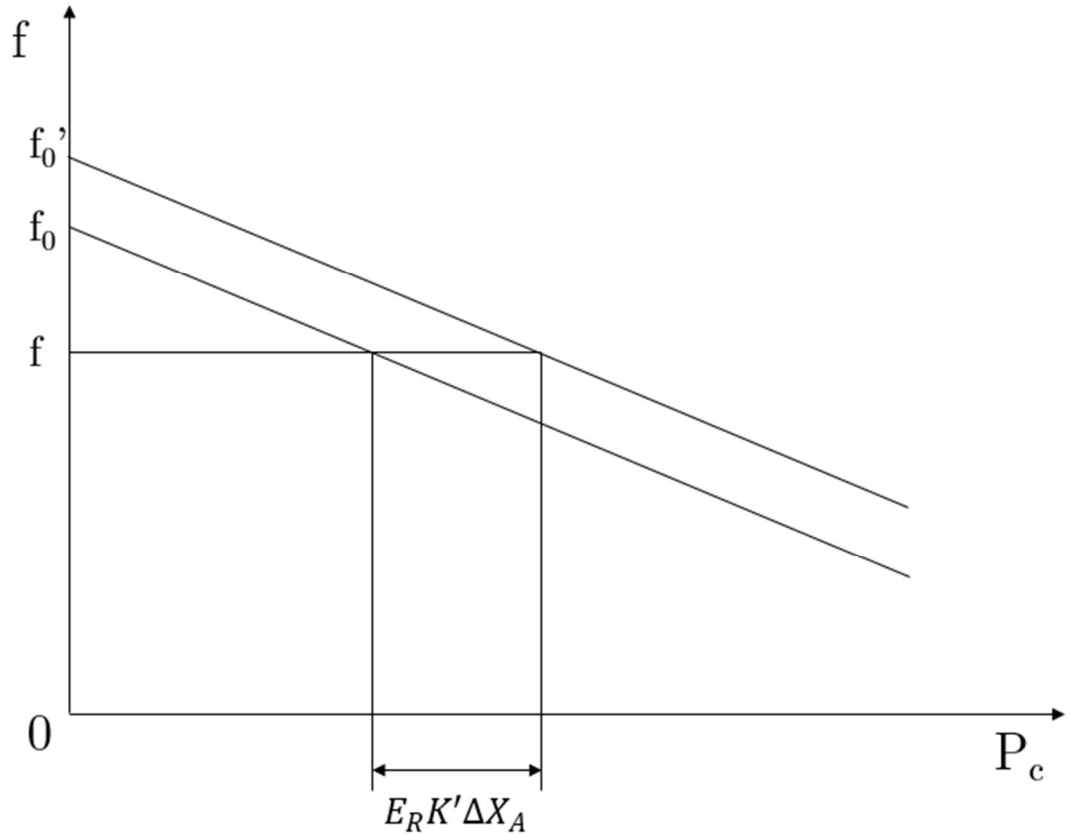

Figure A.7 Static Characteristic of the machine after an RPM controller action

Primary Control

In the two previous sections, the transfer functions of the speed controller and the plant consisting of a unit feeding a load were determined. Now, consider the combination of the plant and speed controller, assuming the RPM controller is kept locked. The corresponding block diagram is shown in Figure A.8, and it represents the result of the combination of the two previous diagrams.

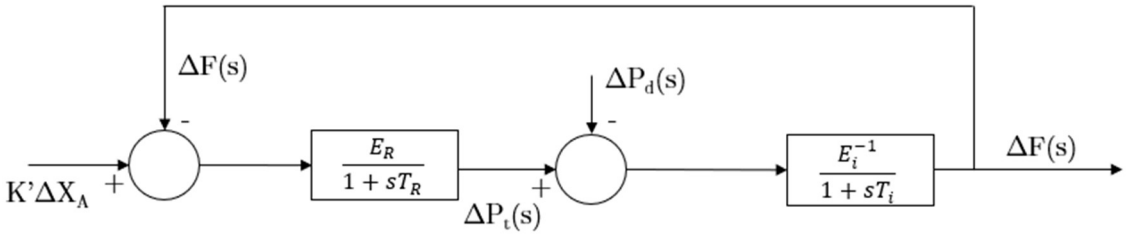

Figure A.8 Block Diagram of a controlled plant.

The system regulated in this way responds to load variations with frequency changes given by:

$$\Delta F\left[1+\frac{E_R}{1+sT_R}\cdot\frac{E_i^{-1}}{1+sT_i}\right]=\Delta P_D\cdot\frac{E_i^{-1}}{1+sT_i}$$

$$\Delta F\left[\frac{(1+sT_R)(1+sT_i)+E_R\cdot E_i^{-1}}{(1+sT_R)(1+sT_i)}\right]=\Delta P_D\cdot\frac{E_i^{-1}}{1+sT_i}$$

$$\Delta F=-\frac{(1+sT_R)}{E_i(1+sT_R)(1+sT_i)+E_R}\cdot\Delta P_D$$

The last equation constitutes the transfer function for the controlled machine-load system. Assuming there is a step change in the disturbance power ΔP_D, applying the final value theorem yields:

$$\Delta f=-\frac{\Delta P_D}{E_i+E_R}$$

Indeed, because E_R is much larger than E_i, the regulation of the machine allows for keeping the frequency deviation at much more limited values than what would have been achieved with an unregulated system.

The parameter $E_P=E_i+E_R$ is defined as the "*primary control energy*" of the system consisting of a machine and its load. The basic case of a single machine

can be extended to the control area, meaning an electrical power system that includes multiple generator machines and various loads. This concept of regulating energy is crucial in understanding and designing control systems for large-scale power grids. To analyse the control area, it is assumed that frequency is a global and unique parameter for all interconnected systems. In reality, there are phenomena of mutual oscillation among machines that are of crucial importance for the assessment of transient stability. However, given the slower dynamics considered for primary control, this approximation does not introduce significant errors and greatly simplifies the modelling of the problem. According to this assumption, different interconnected machines can be reduced to a single equivalent machine whose regulating energy is the sum of the various individual machine regulating energies. In particular:

- the term related to the variation in generated power will represent the sum of the power increments that the $''n''$ regulating machines inject into the system;
- the power disturbance ΔP_D will consider the overall load variation in the area;
- the change in absorbed power ΔP_C will consider the variation in power of all loads in relation to the altered supply frequency.
- the accelerating power ΔP_a will always be evaluated as $\frac{d}{dt} W_{kin}$.

In the case of a control area, we obtain:

$$\sum_{I=1}^{n} \Delta P_{ti} - \Delta P_D = \sum_{I=1}^{n} \Delta F \cdot [E_{ii} + sK_i] = \Delta F \cdot [E_{iT} + sK_T]$$

Where:

$$E_{iT} = \sum_{I=1}^{n} E_{ii} \quad ; \quad K_T = \sum_{I=1}^{n} K_i$$

The block diagram corresponding to the previous relationship is shown in Figure A.9. Note that the time constant $T_t = K_T \cdot E_{iT}^{-1}$ remains approximately the same as that of the individual machines because an increase in K_T corresponds to an increase in E_{iT}, thus keeping their ratio constant. The block diagram of the entire control area is shown in Figure A.10.

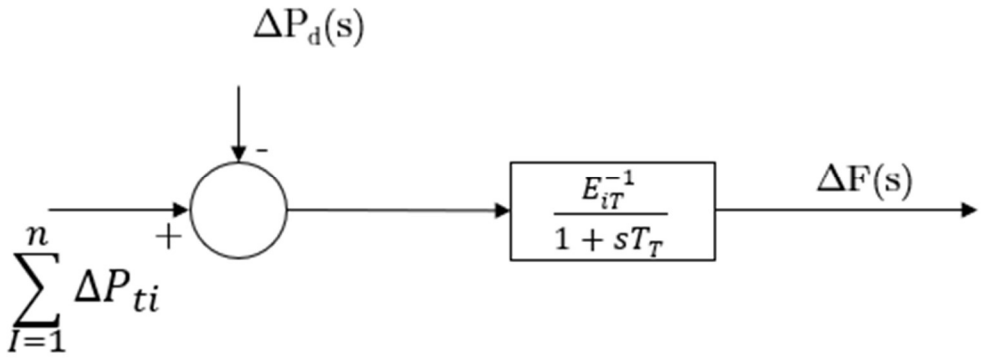

Figure A.9 Block Diagram of a power system

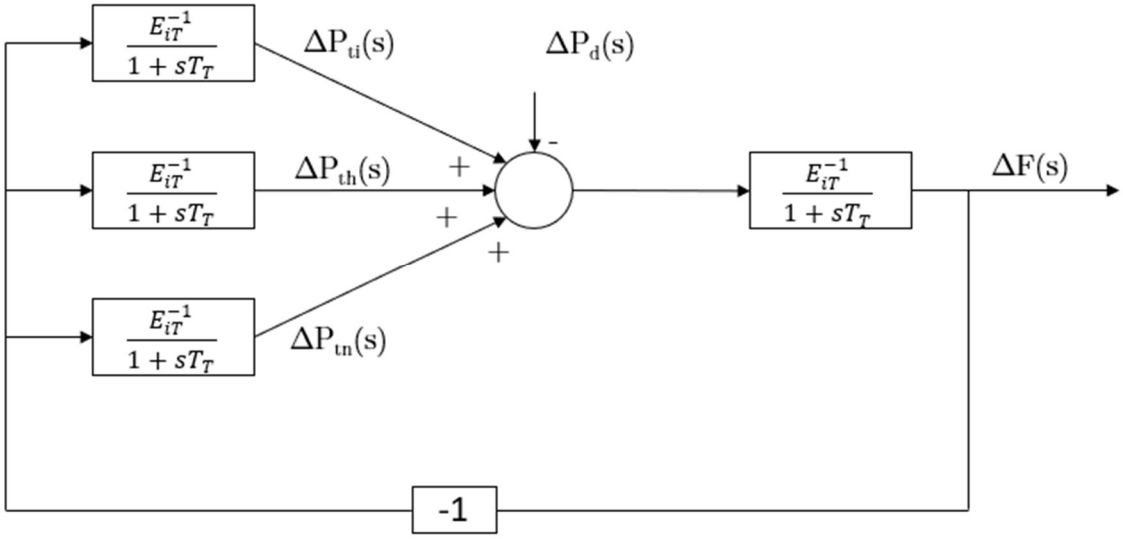

Figure A.10 Block Diagram of a multi-machine control area.

If we assume, for simplicity, that the time constants of the controllers are equal to each other, i.e.:

$$T_{R1} = T_{R2} = \cdots T_{Rh} = \cdots T_{Rn} = T_R$$

The transfer function of the entire control area can be expressed as:

$$\Delta F = -\frac{(1+sT_R)}{E_{iT}(1+sT_R)(1+sT_T)+E_T} \cdot \Delta P_D$$

At steady-state, after the application of a step disturbance, there will be a frequency deviation equal to:

$$\Delta f = -\frac{\Delta P_D}{E_{iT} + E_{RT}}$$

The parameter $E_{PT} = E_{iT} + E_{RT}$ is defined as the "*primary control energy of the control area*", it can be observed that the greater the number of machines participating in the regulation, the smaller the steady-state frequency deviation will be.

If it is intended to investigate the stability of the regulation, the characteristic equation in this case is given by:

$$E_{iT}(1 + sT_R)(1 + sT_T) + E_T = 0$$

For stability to be ensured, it is necessary for the roots to have a negative real part. Depending on the characteristic values ω_0 and ζ, there will be the presence of aperiodic or pseudo-periodic motion depending on whether the value of ζ is greater or less than 1.

Author's publications list

International Journal Articles

[JA.1] F. Massaro, R. Musca, A. Vasile, G. Zizzo, "A simulation study for assessing the impact of energy storage systems for Fast Reserve with additional synthetic inertia control on the Continental Europe synchronous area", Sustainable Energy Technologies and Assessments, Volume 53, Part D, 2022, 102763, ISSN 2213-1388, https://doi.org/10.1016/j.seta.2022.102763

[JA.2] R. Musca, A. Vasile, G. Zizzo, "Grid-forming converters. A critical review of pilot projects and demonstrators", Renewable and Sustainable Energy Reviews, Volume 165, 2022, 112551, ISSN 1364-0321, https://doi.org/10.1016/j.rser.2022.112551

[JA.3] M. L. Di Silvestre, M. G. Ippolito, E. Riva Sanseverino, G. Sciumè, A. Vasile, "Energy self-consumers and renewable energy communities in Italy: New actors of the electric power systems", Renewable and Sustainable Energy Reviews, Volume 151, 2021, 111565, ISSN 1364-0321, https://doi.org/10.1016/j.rser.2021.111565

Tech Reports on Power Systems

[TR.1] A. Barberi, R. Musca, E. Riva Sanseverino, A. Vasile, G. Zizzo, "Metodologie e analisi per la valutazione di espansione delle reti con nuovi collegamenti in DC - Attività 1: Analisi statiche e dinamiche di collegamenti HVDC - Rapporto tecnico Fasi 1 e 2" – RSE, Novembre 2022.

[TR.2] M. Beccali, M. Bonomolo, G. Ciulla, R. Colombarini, G. Leone, F. Martorana, L. Mineo, R. Musca, A. Piacentino, E. Telaretti, A. Vasile, G. Zizzo. "LA4.4 - Studio di fattibilità di soluzioni per l'efficientamento energetico delle Isole Minori", Accordo di Programma Ministero dello Sviluppo Economico PTR 2019/2021 – ENEA, Aprile 2021.

[TR.3] S. Favuzza, M. G. Ippolito, R. Musca, E. Telaretti, A. Vasile, G. Zizzo. "LA1.4 - Studio e sviluppo di scenari energetici per l'integrazione di reti AC/DC in MT/BT", Report RdS/PTR2020/001, Accordo di Programma Ministero dello Sviluppo Economico PTR 2019/2021 – ENEA, Ottobre 2020.

Conference Proceedings

[CP.1] A. Vasile, G. Zizzo, A. Micallef, C. S. Staines and J. Licari, "Simulation of Grid Forming PV Plants in the Medium Voltage Grid - A Maltese Case Study," 2023 AEIT International Annual Conference (AEIT), Rome, Italy, 2023, pp. 1-5, doi: 10.23919/AEIT60520.2023.10330391.

[CP.2] R. Musca, E. Riva Sanseverino, A. Vasile, G. Zizzo, A. Iaria, A. L'Abbate, L. Vitulano, "Power-Flow studies on the Future Electricity Grid of Sicily: Analysis of 2030 Scenario Cases," 2023 AEIT International Annual Conference (AEIT), Rome, Italy, 2023, pp. 1-6, doi: 10.23919/AEIT60520.2023.10330343.

[CP.3] R. Musca, E. Riva Sanseverino, A. Vasile, G. Zizzo, A. Iaria, A. L'Abbate, L. Vitulano, "Grid-Forming Operation of the HVDC Tyrrhenian Link-East for Improved Frequency Transients", AEIT HVDC International Conference, Roma, 25-26 maggio 2023.

[CP.4] D. Curto, V. Franzitta, A. Guercio, E. Riva Sanseverino, A. Vasile, G. Zizzo, " Assessing optimal energy mix and stability in the island of Favignana," 13th Mediterranean Conference on Power Generation, Transmission, Distribution and Energy Conversion (MEDPOWER 2022), La Valletta, Malta, 2022, pp. 1-6, doi: 10.1049/icp.2023.0030

[CP.5] P. Gallo, F. Massaro, E. Riva Sanseverino, S. Ruffino, G. Sciumè, A. Vasile, G. Zizzo, "A Test Bench for a Blockchain-based Management of Smart Prosumers' Flexibility," 2022 AEIT

International Annual Conference (AEIT), Rome, Italy, 2022, pp. 1-6, doi: 10.23919/AEIT56783.2022.9951781.

[CP.6] D. Curto, V. Franzitta, A. Guercio, R. Musca, A. Vasile and G. Zizzo, "Stability Analysis in a Vietnam Small Island for the Deployment of a Nearshore Wave Power Plant," 2022 Workshop on Blockchain for Renewables Integration (BLORIN), Palermo, Italy, 2022, pp. 236-241, doi: 10.1109/BLORIN54731.2022.10028639.

[CP.7] Q. Ali, M. L. Di Silvestre, G. L. Restifo, E. Riva Sanseverino, G. Sciumè, A. Vasile, G. Zizzo, "A Simulation Study for Assessing the Minimum Number of V2G Recharge Points in Favignana," 2022 IEEE International Conference on Environment and Electrical Engineering and 2022 IEEE Industrial and Commercial Power Systems Europe (EEEIC / I&CPS Europe), Prague, Czech Republic, 2022, pp. 1-6, doi: 10.1109/EEEIC/ICPSEurope54979.2022.9854609

[CP.8] M. L. Di Silvestre, P. Gallo, G. Restifo, E. R. Sanseverino, G. Sciumè and A. Vasile, "A Proposal for Customer Baseline Load Evaluation from Electricity Bills," 2022 IEEE 21st Mediterranean Electrotechnical Conference (MELECON), Palermo, Italy, 2022, pp. 1050-1055, doi: 10.1109/MELECON53508.2022.9843014.

[CP.9] M. L. Di Silvestre, R. Musca, E. R. Sanseverino, G. Sciumè, A. Vasile and G. Zizzo, "A Feasibility Study for the Transition to Electric Mobility in the Island of Favignana," 2021 IEEE International Conference on Environment and Electrical Engineering and 2021 IEEE Industrial and Commercial Power Systems Europe (EEEIC / I&CPS Europe), Bari, Italy, 2021, pp. 1-6, doi: 10.1109/EEEIC/ICPSEurope51590.2021.9584779.

[CP.10] V. Di Dio, G. Sciumè, G. Zizzo, R. Musca and A. Vasile, "Analysis of a Fast Reserve Unit Behaviour with Additional Modular Synthetic Inertia Control," 2021 IEEE 15th International Conference on Compatibility, Power Electronics and Power Engineering (CPE-POWERENG), Florence, Italy, 2021, pp. 1-6, doi: 10.1109/CPE-POWERENG50821.2021.9501206

References

[1] Brundtland, G.H. (1987) “Our Common Future”, World Commission on Environment and Development, Tech Report. Geneva, UN-Dokument A/42/427, available online: https://sustainabledevelopment.un.org/content/documents/5987our-common-future.pdf

[2] International Energy Agency (IEA), “CO2 Emissions in 2022”, Tech Report, 03/2023, available online: https://iea.blob.core.windows.net/assets/3c8fa115-35c4-4474-b237-1b00424c8844/CO2Emissionsin2022.pdf

[3] United Nations, “The Rio Conventions, The Interconnected Challenges of Climate Change, Desertification and Biodiversity Loss”, available online: https://unfccc.int/process-and-meetings/the-rio-conventions

[4] United Nations, “What is the Kyoto Protocol?”, available online: https://unfccc.int/kyoto_protocol

[5] United Nations, “The Paris Agreement”, available online: https://unfccc.int/process-and-meetings/the-paris-agreement

[6] European Commission, “European Green Deal”, available online: https://commission.europa.eu/strategy-and-policy/priorities-2019-2024/european-green-deal_it

[7] European Commission, “Fit for 55 Package”, available online: https://www.consilium.europa.eu/en/policies/green-deal/fit-for-55-the-eu-plan-for-a-green-transition/

[8] G. Pepermans, J. Driesen, D. Haeseldonckx, R. Belmans, W. D’haeseleer, “Distributed generation: definition, benefits and issues”, Energy Policy, Volume 33, Issue 6, 2005, Pages 787-798, ISSN 0301-4215.

[9] Talha Bin Nadeem, Mubashir Siddiqui, Muhammad Khalid, Muhammad Asif, Distributed energy systems: A review of classification, technologies, applications, and policies, Energy Strategy Reviews, Volume 48, 2023, 101096, ISSN 2211-467X.

[10] IRENA (2023), Renewable energy statistics 2023, International Renewable Energy Agency, Abu Dhabi., available online: https://www.irena.org/Publications/2023/Jul/Renewable-energy-statistics-2023

[11] IRENA (2018), “Global Energy Transformation, a Roadmap to 2050”, International renewable Energy Agency, Abu Dhabi, available online.

[12] European Network of Transmission System Operators for Electricity (ENTSO-E), official website: https://www.entsoe.eu/

[13] ENTSO-E, “Future System inertia”, Tech rep, 2015, available online: https://eepublicdownloads.entsoe.eu/clean-documents/Publications/SOC/Nordic/Nordic_report_Future_System_Inertia.pdf

[14] ENTSO-E, “Need for synthetic inertia (SI) for frequency regulation ENTSO-E guidance document for national implementation for network codes on grid connection”, Tech rep, 2018, available online: https://eepublicdownloads.entsoe.eu/clean-documents/Network%20codes%20documents/NC%20RfG/IGD_Need_for_Synthetic_Inertia_final.pdf

[15] ENTSO-E, “Inertia and Rate of Change of Frequency (RoCoF)”, Tech rep, 2020, available online: https://eepublicdownloads.entsoe.eu/clean-documents/SOC%20documents/Inertia%20and%20RoCoF_v17_clean.pdf

[16] ENTSO-E Vision, “A Power System for a Carbon Neutral Europe”, Tech rep, 2022, available online: https://eepublicdownloads.entsoe.eu/clean-documents/tyndp-documents/entso-e_Vision_2050_report_221006.pdf

[17] ENTSO-E, “P1 – Policy 1: Load-Frequency Control and Performance [C]”, Tech rep, available online: https://eepublicdownloads.entsoe.eu/clean-documents/pre2015/publications/entsoe/Operation_Handbook/Policy_1_final.pdf

[18] P. Kundur, Power System Stability and Control, new edition, McGraw-Hill Education, New York, USA, 1994.

[19] Pieter Tielens, Dirk Van Hertem, The relevance of inertia in power systems, Renewable and Sustainable Energy Reviews, Volume 55, 2016, Pages 999-1009, ISSN 1364-0321, https://doi.org/10.1016/j.rser.2015.11.016

[20] H. Alhelou, M.-E. Hamedani-Golshan, R. Zamani, E. Heydarian-Forushani, and P. Siano, “Challenges and Opportunities of Load Frequency Control in Conventional, Modern and Future Smart Power Systems: A Comprehensive Review,” Energies, vol. 11, no. 10, p. 2497, Sep. 2018, doi: 10.3390/en11102497
[21] Z. A. Obaid, L. M. Cipcigan, L. Abrahim and M. T. Muhssin, "Frequency control of future power systems: reviewing and evaluating challenges and new control methods," in Journal of Modern Power Systems and Clean Energy, vol. 7, no. 1, pp. 9-25, January 2019, doi: 10.1007/s40565-018-0441-1
[22] Yi Cheng, Rasoul Azizipanah-Abarghooee, Sadegh Azizi, Lei Ding, Vladimir Terzija, Smart frequency control in low inertia energy systems based on frequency response techniques: A review, Applied Energy, Volume 279, 2020, 115798, ISSN 0306-2619, https://doi.org/10.1016/j.apenergy.2020.115798
[23] Mrinal Ranjan, Ravi Shankar, A literature survey on load frequency control considering renewable energy integration in power system: Recent trends and future prospects, Journal of Energy Storage, Volume 45, 2022, 103717, ISSN 2352-152X, https://doi.org/10.1016/j.est.2021.103717
[24] Smart Energy Europe, “The smarten Map, Ancillary Services”, Tech Rep., 2022, available online: https://smarten.eu/wp-content/uploads/2022/12/the_smarten_map_2022_DIGITAL-2.pdf
[25] European Union, “Directive (EU) 2019/994 of the European Parliament and of the council of 5 June 2019 on common rules for the internal market for electricity and amending Directive 2012/27/EU”, Directive, 2019, available online: https://eur-lex.europa.eu/legal-content/EN/TXT/?uri=celex%3A32019L0944
[26] M. Fiorelli, D. Keles, F. Montana, G. L. Restifo, E. Riva Sanseverino, G. Zizzo, “Evaluation of the Administrative Phase-Out of Coal Power Plants on the Italian Electricity Market”, Energies, 2020, vol. 13, article 4596
[27] Terna S.p.A., “Regolamento recante i requisiti e le modalita` per la fornitura del servizio di regolazione ultra-rapida di frequenza - Progetto pilota ai sensi della delibera 300/2017/R/eel dell’Autorita` di regolazione per Energia reti e Ambiente” (Italian), 6 July 2020, available at: https://download.terna.it/terna/FastReserve_Allegato%203_Tecnico_8d76dc04c201b52.pdf
[28] ARERA, Deliberazione 200/20/R/EEL “Approvazione del regolamento predisposto da Terna s.p.a, ai sensi della deliberazione dell’Autorita` 300/2017/R/EEL relativo al progetto pilota per l’erogazione del servizio di regolazione ultra-rapida di frequenza” (Italian), Italy, 03 June 2020.
[29] Terna S.p.A, Stima delle ore di disponibilità per il servizio Fast Reserve per l’anno 2021 (Italian), 06 Nov. 2020, available at: https://download.terna.it/terna/Stima%20Ore%20di%20Disponibilit%C3%A0%202021_8d8824de1d29fa4.pdf
[30] Terna S.p.A, Progetto Pilota Fast Reserve – Esiti Asta (Italian), 10 Dec. 2020, available at: https://www.terna.it/it/sistema-elettrico/pubblicazioni/newsoperatori/dettaglio/esiti-asta-Fast-reserve
[31] ARERA, Deliberazione 574/2014/R/EEL, “ Disposizioni relative all’integrazione dei sistemi di accumulo di energia elettrica nel sistema elettrico nazionale” (Italian), Italy, 20 November 2014.
[32] Tamrakar U, Shrestha D, Maharjan M, Bhattarai BP, Hansen TM, Tonkoski R. virtual inertia, current trends and future directions. Applied Sciences 2017;7(7): 654.
[33] Z. Jietang, Q. Linan, R. Pestana, L. Fengkui, Y. Libin, Dynamic frequency support by photovoltaic generation with synthetic inertia and frequency droop control, 2017 IEEE Conference on Energy Internet and Energy System Integration (EI2), Beijing (China), 26-28 Nov. 2017
[34] Knap V, Chaudhary SK, Stroe DL, Swierczynski MJ, Craciun B-I, Teodorescu R. Sizing of an energy storage system for grid inertial response and primary frequency reserve. IEEE Trans Power Syst 2016;31(5):3447–56
[35] ENTSO-E. Initial Dynamic Model of Continental Europe. Available online: https://docstore.entsoe.eu/publications/systemoperations-reports/continental-europe/Initial-Dynamic-Model/Pages/default
[36] Busarello L, Musca R. Impact of high share of converter-interfaced generation on electromechanical oscillations in continental europe power system. IET Renew Power Gener 2021;14(19):3918–26.
[37] M. G. Ippolito, R. Musca, G. Zizzo, M. Bongiorno, Extension and Tuning of Virtual Synchronous Machine to Avoid Oscillatory Instability in Isolated Power Networks 12th AEIT International Annual Conference, Italy, 23 September 2020.

[38] ENTSO-E, Europe Power System 2040: completing the map & assessing the cost of non-grid, available at: https://docstore.entsoe.eu/Documents/TYNDP%20documents/TYNDP2018/european_power_system_2040.pdf
[39] ENTSO-E, Completing the map - Power system needs, available at: https://eepublicdownloads.entsoe.eu/tyndp-documents/IoSN2020/200810_IoSN2020mainreport_beforeconsultation.pdf
[40] ENTSO-E, Visualization Platform – Electricity Data, available at: https://tyndp.entsoe.eu/explore/visualise-system-needs
[41] ENTSO-E, Continental Europe Synchronous Area Framework Agreement, Annex 1: Policy on Load-Frequency Control and Reserves, Brussels, Belgium, April 2019, available at: https://eepublicdownloads.entsoe.eu/clean-documents/Publications/SOC/safa/1_-_Policy_on_Load-Frequency_Control_and_Reserves.pdf
[42] ENTSO-E, Statistical Factsheet, available at: https://www.entsoe.eu/publications/statistics-and-data/#statistical-factsheet
[43] ENTSO-E. Operation Handbook OpHB, Policy 1: Load-Frequency Control and Performance; Version 3.0; ENTSO-E: Brussels, Belgium, March 2009
[44] Commission Regulation (EU) 2017/2195 of 23 November 2017 establishing a guideline on electricity balancing, available at: https://eur-lex.europa.eu/legalcontent/EN/TXT/?uri=CELEX%3A32017R2195
[45] ENTSO-E. All CE TSOs Proposal for the Dimensioning Rules for FCR in Accordance with Article 153(2) of the Commission Regulation (EU) 2017/1485 of 2 August 2017 Establishing a Guideline on Electricity Transmission System Operation; ENTSO-E: Brussels, Belgium, August
[46] "Europe Beyond Coal: European Coal Plant Database, 10 Apr 2022", available at: https://beyond-coal.eu/database/
[47] ENTSO-E. System separation in the Continental Europe Synchronous Area on 8 January 2021—2nd update. Available online: https://www.entsoe.eu/news/2021/01/26/system-separation-in-the-continental-europe-synchronous-area-on-8-january-2021-2nd-update/
[48] Ippolito MG, Musca R, Zizzo G. Analysis and simulations of the primary frequency control during a system split in continental europe power system. Energies 2021; 14:1456
[49] D. Curto, V. Franzitta, M. Trapanese, and M. Cirrincione, "A Preliminary Energy Assessment to Improve the Energy Sustainability in the Small Islands of the Mediterranean Sea," J. Sustain. Dev. Energy, Water Environ. Syst., pp. 1–19, 2020.
[50] D. Curto, V. Franzitta, A. Viola, M. Cirrincione, A. Mohammadi, and A. Kumar, "A renewable energy mix to supply small islands. A comparative study applied to Balearic Islands and Fiji," J. Clean. Prod., p. 118356, Sep. 2019.
[51] Energy & Strategy Group, "Smart Mobility Report," 2020. Available: https://www.energystrategy.it/assets/files/SMR20webdef2910.pdf
[52] Ministero dello sviluppo economico, Decreto ministeriale 14 febbraio 2017 "Isole minori", ser. Repubblica Italiana. Gazzetta Ufficiale della Repubblica Italiana, 2017.
[53] V. L. Brano, M. Beccali, M. G. Ippolito, G. Ciulla, P. Finocchiaro, D. L. Cascia, G. Leone, and G. Zizzo, "Analisi delle tecnologie per la climatizzazione e sistemi ict applicati agli utenti finali delle isole minori non connesse alla rtn al fine di efficientare il sistema elettrico isolano", Tech Rep, 2015.
[54] A. Engler, C. Hardt, P. Strauss, M. Vandenbergh, Parallel operation of generators for stand-alone single-phase hybrid systems-first implementation of a new control technology (01 2001).
[55] K. Visscher, S. De Haan, Virtual synchronous machines (vsg's) for frequency stabilisation in future grids with a significant share of decentralized generation, in: CIRED Seminar 2008: SmartGrids for Distribution, 2008, pp. 1–4.
[56] L. Zhang, L. Harnefors, H.-P. Nee, Power-synchronization control of grid-connected voltage-source converters, IEEE Transactions on Power Systems 25 (2) (May 2010) 809–820. doi:10.1109/TPWRS.2009.2032231.
[57] L. Harnefors, M. Hinkkanen, U. Riaz, F. M. M. Rahman, L. Zhang, Robust analytic design of power-synchronization control, IEEE Transactions on Industrial Electronics 66 (8) (August 2019) 5810–5819

[58] Enemalta, Malta Energy Distribution, Official Website: https://www.enemalta.com.mt/.
[59] A. Micallef, C. Spiteri Staines, and A. Cassar, “Utility-Scale Storage Integration in the Maltese Medium-Voltage Distribution Network,” Energies, vol. 15, no. 8, p. 2724, Apr. 2022, doi: 10.3390/en15082724.
[60] PSI Neplan AG, SYMDEF, available online: https://www.neplan.ch/news/video-tutorial-symdef/?lang=de
[61] S. Favuzza, M. G. Ippolito, F. Massaro, G. Paternò, A. Puccio, “2015– 2020. Sicily and Italy as electricity hub in the Mediterranean area for the development of the European power grids interconnections”, 2015 EEE 5th International Conference on Power Engineering, Energy and Electrical Drives (POWERENG), Riga, Latvia, 2015, pp. 554-559, doi: 10.1109/PowerEng.2015.7266376.
[62] M. G. Ippolito, F. Massaro, M. Mustacciolo, “Application of Monte Carlo technique to evaluate the power injectable on electrical grid by wind farms”, 2008 43rd International Universities Power Engineering Conference, Padua, Italy, 2008, pp. 1-5, doi: 10.1109/UPEC.2008.4651537.
[63] M. G. Ippolito, F. Massaro, M. Mustacciolo, “Steady-state security analysis on the transmission grid for various scenarios of wind generation in Sicily”, 2009 International Conference on Clean Electrical Power, Capri, Italy, 2009, pp. 276-283, doi: 10.1109/ICCEP.2009.5212043.
[64] G. Filippone, M. G. Ippolito, F. Massaro, A. Puccio, “On the roadmap to supergrid in Sicily: LiDAR technology and HTLS conductors for uprating the 150 kV lines”, IEEE PES Innovative Smart Grid Technologies, Europe, Istanbul, Turkey, 2014, pp. 1-5, doi: 10.1109/ISGTEurope.2014.7028952.
[65] F. Massaro, M. Ippolito, G. Zizzo, G. Filippone, A. Puccio, “Methodologies for the Exploitation of Existing Energy Corridors. GIS Analysis and DTR Applications”, Energies, vol. 11, no. 4, p. 979, Apr. 2018, doi: 10.3390/en11040979.
[66] IEC, International Electrotechincal Vocabulary, available online: https://www.electropedia.org/iev/iev.nsf/index?openform&part=617
[67] Kaushal, A.; Van Hertem, D. “An Overview of Ancillary Services and HVDC Systems in European Context”. Energies 2019, 12, 3481. https://doi.org/10.3390/en12183481
[68] E. Ciapessoni, D. Cirio, A. Gatti and A. Pitto, "Renewable power integration in Sicily: Frequency stability issues and possible countermeasures," 2013 IREP Symposium Bulk Power System Dynamics and Control - IX Optimization, Security and Control of the Emerging Power Grid, Rethymno, Greece, 2013, pp. 1-7, doi: 10.1109/IREP.2013.6629350.
[69] G. M. Giannuzzi, F. Palone, M. Rebolini, J. Vassallo and R. Zaottini, "The Malta-Sicily EHV-AC interconnector," 8th Mediterranean Conference on Power Generation, Transmission, Distribution and Energy Conversion (MEDPOWER 2012), Cagliari, 2012, pp. 1-6, doi: 10.1049/cp.2012.2061.
[70] F. Del Pizzo et al., "Tyrrhenian Link: path towards a decarbonized electrical system," 2022 AEIT International Annual Conference (AEIT), Rome, Italy, 2022, pp. 1-6, doi: 10.23919/AEIT56783.2022.9951744.
[71] J. A. Adu et al., "Coordinated Inertial Response Provision by Wind Turbine Generators: Effect on Power System Small-Signal Stability of the Sicilian Network," 2022 IEEE International Conference on Environment and Electrical Engineering and 2022 IEEE Industrial and Commercial Power Systems Europe (EEEIC / I&CPS Europe), Prague, Czech Republic, 2022, pp. 1-6, doi: 10.1109/EEEIC/ICPSEurope54979.2022.9854616.
[72] A. Berizzi et al., "Stability analysis of the OSMOSE scenarios: main findings, problems, and solutions adopted," 2021 AEIT International Annual Conference (AEIT), Milan, Italy, 2021, pp. 1-6, doi: 10.23919/AEIT53387.2021.9626939.
[73] A. Derviskadic, A. Persico, E. Isabegovic, A. Thorslund, “Opportunities and Challenges in the Mediterranean Region with Grid Forming Control for HVDC Systems” , AEIT HVDC International Conference 2023, Rome, Italy, 2023
[74] J. A. Adu et al., “Power System Stability Analysis of the Sicilian Network in the 2050 OSMOSE Project Scenario,” Energies, vol. 15, no. 10, p. 3517, May 2022, doi: 10.3390/en15103517.
[75] Terna, “2023 Piani di sviluppo. Avanzamento dei piani di sviluppo precedenti. Avanzamento Centro Sud”, 2023.

[76] Terna, “Tyrrhenian Link: il doppio collegamento sottomarino tra Sicilia, Sardegna e Penisola”, Terna S.p.a., 2023, https://www.terna.it/it/progetti-territorio/progetti-incontri-territorio/Tyrrhenian-link
[77] R. Musca, E. Riva Sanseverino, G. Zizzo, and A. L’Abbate, “An Accurate Model for Steady-State and Dynamic Analysis of the Sicilian Network with HVDC Interconnections,” in the 17th International Conference on AC and DC Power Transmission (ACDC 2021), virtual event, 7-8 December 2021, pp. 188–192.
[78] R. Musca et al., "Grid-Forming Operation of the HVDC Tyrrhenian Link-East for Improved Frequency Transients," 2023 AEIT HVDC International Conference (AEIT HVDC), Rome, Italy, 2023, pp. 1-6, doi: 10.1109/AEITHVDC58550.2023.10179071.
[79] R. Musca, E. Riva Sanseverino, A. Vasile, G. Zizzo, A. Iaria, A. L’Abbate, L. Vitulano: “Power-flow studies on the Future Electricity Grid of Sicily: Analysis of 2030 Scenario Cases”, AEIT International Conference, 05 October 2023, Rome, Italy.
[80] Italian Ministry of Environment and Energy Security https://www.mase.gov.it/
[81] Terna, “Piano di Sviluppo 2023”, 2023 (in Italian). Available online: https://www.terna.it/it/sistema-elettrico/rete/piano-sviluppo-rete
[82] M. Gaeta, C. Nsangwe Businge, A. Gelmini, “Achieving Net Zero Emissions in Italy by 2050: Challenges and Opportunities”, Energies, vol. 15, no. 1, 2022, article 46.
[83] L. C. Vitulano, A. L'Abbate, S. D. Sessa, R. Calisti and F. Sanniti, "Assessment of technical and economic elements for HVAC-to-HVDC OHL conversion in Sicilian grid," 2023 AEIT HVDC International Conference (AEIT HVDC), Rome, Italy, 2023, pp. 1-6, doi: 10.1109/AEITHVDC58550.2023.10179050.
[84] L. Carmine Vitulano, S. Dambone Sessa, A. L’Abbate and R. Calisti, "HVAC-to-HVDC OHL conversion: a study case in the Sicilian transmission network," 2022 AEIT International Annual Conference (AEIT), Rome, Italy, 2022, pp. 1-6, doi: 10.23919/AEIT56783.2022.9951843.